DOE/BC/14883-T3
Distribution Category UC-122

SURFACTANT-ENHANCED ALKALINE FLOODING FOR LIGHT OIL RECOVERY

Final Report
1994-1995

By
Darsh T. Wasan

December 1995

Work Performed Under Contract No. DE-AC22-92BC14883

Prepared for
U.S. Department of Energy
Assistant Secretary for Fossil Energy

Jerry F. Casteel, Project Manager
Bartlesville Project Office
P.O. Box 1398
Bartlesville, OK 74005

Prepared by
Illinois Institute of Technology
10 West 33rd St.
Chicago, IL 60616

TABLE OF CONTENTS

LIST OF FIGURES

CHAPTER ONE

CHAPTER TWO

CHAPTER THREE

LIST OF TABLES

CHAPTER THREE

EXECUTIVE SUMMARY

In this report, we present the results of our experimental and theoretical studies in surfactant-enhanced alkaline flooding for light oil recovery. The overall objective of this work is to develop a very cost-effective method for formulating a successful surfactant-enhanced alkaline flood by appropriately choosing mixed alkalis which form inexpensive buffers to obtain the desired pH (between 8.5 and 12.0) for ultimate spontaneous emulsification and ultralow interfacial tension. In addition, we have (1) developed a theoretical interfacial activity model for determining equilibrium interfacial tension, (2) investigated the mechanisms for spontaneous emulsification, (3) developed a technique to monitor low water content in oil, and (4) developed a technique to study water-in-oil emulsion film properties, (5) investigated the effect of surfactant on the equilibrium and transient interfacial tension, (6) investigated the kinetics of oil removal from a silica surface, and (7) developed a theoretical interfacial activity model for determining equilibrium interfacial tension, accounting for added surfactant. The results of the studies conducted during the course of this project are summarized below.

Interfacial Activity Model

A new interfacial activity model which predicts equilibrium interfacial tension both qualitatively and quantitatively has been developed. The ultralow value of interfacial tension is shown to result from the simultaneous adsorption of ionized and unionized acid on the interface, and the lowering results from the formation of mixed micelles of ionized and unionized acid. This theoretical model can also be used to determine micellization parameters.

Interfacial Turbulence and Spontaneous Emulsification

Observation of roll cells indicates that the mechanism for spontaneous emulsification is interfacial turbulence. The effect of pH on roll cell formation is explained in terms of the concentration gradient of unionized acid in the oil phase, the sensitivity of interfacial tension to preformed surfactant concentration, and the rate of acid ionization. The added preformed surfactant creates an interfacial resistance to mass transfer, and it also makes the interface more rigid. It also makes the interfacial tension more sensitive to the ionized and unionized acid. It is shown that interfacial turbulence is a necessary but not sufficient condition for spontaneous emulsification. Low interfacial tension is also a necessary condition for spontaneous emulsification, if the rotational velocity of the cell is too slow for emulsion snap-off. In other words, there is a trade-off between interfacial tension and rotational velocity. This study shows that reacting alkali/acidic oil systems are ideal for investigating interfacial turbulence and to test theories, because roll cell size, rate of amplification, rate of reaction, etc. can be controlled by controlling the pH, unionized acid concentration, ionic strength, added preformed surfactant concentration and type, etc. In addition, interfacial turbulence appears to improve penetration of an aqueous solution between an oil and solid surface leading to oil removal from the solid surface.

Low Water Content determination

Simple exact solutions to the microwave interferometric transmission equations have been derived, thus allowing determination of complex dielectric constant without time consuming iterative procedures. Moisture levels are shown to be detectable with an accuracy of about 0.5

volume percent water content using microwave interferometric dielectrometry. The ease of obtaining the data, the noninvasivity of the measurement technique, and the rapidity with which results are obtainable makes low water content determination using dielectrometry highly desirable in comparison to a wet technique such as Karl Fisher titration.

Demulsification of Water-In-Crude Oil Emulsions

A new technique has been developed for the study of the film properties governing the water-in-crude oil emulsion film stability. With the technique, the film properties in the presence of demulsifiers were measured and the factors governing the rate of film thinning and its stability of the water-in-crude oil emulsion film have been discussed. The performance of three differently blended oil soluble demulsifiers on the water separation from the emulsions and the emulsion film rheology have been studied. It has been found that there is a direct correlation between the demulsifier performance and the rheology of water/crude oil/water emulsion film in the presence of the demulsifier. Also, to improve the demulsifier efficiency, the demulsifier components need to create a low emulsion film elasticity (dilational film modulus), higher film diffusivity and low film tension.

The effect of added surfactant in alkali/acidic oil systems

An experimental investigation of the buffered surfactant-enhanced alkaline flooding system chemistry was undertaken to determine the influence of various species present on interfacial tension as a function of pH and ionic strength. Phase behavior tests that monitor the extent of emulsification are sufficient to determine the region of low interfacial tension. Optimization of interfacial tension by adjustment of the ionic strength alone may not necessarily provide the lowest interfacial tension under the best conditions. The pH should be

simultaneously optimized along with ionic strength to allow better control over attainment of low interfacial tension. The dominant mechanism by which added surfactant aids in the reduction of interfacial tension is the formation of mixed micelles with the ionized acid. Although added surfactant partitioning from the influence of the unionized acid and ionic strength will affect interfacial behavior, the formation of mixed micelles plays a dominant role. Middle phase formation is possible with a low acid oil using a petroleum sulfonate at a proper pH and ionic strength.

Fluid-solid interaction: optical imaging by differential and common interferometry

A new experimental technique has been developed and used to determine the three-phase contact angle and to study the three-phase contact angle kinetics using common and differential interferometry. It has been found that for most systems studied, the contact angle increases with time until the crude oil droplet separates from the silica surface. The addition of surfactant causes the kinetics of separation to be slower. With smaller drops, the three-phase contact angle reaches its equilibrium value faster. It was also observed that water penetrates between the crude oil and silica surface to form a water film which helps the crude oil to separate from the silica surface.

Interactions in acidic oil/Alkaline-surfactant solutions: Theoretical Studies

This chapter describes predictive models developed for computing the interfacial tension of a system chosen to model acidic light crude oil in contact with alkaline solution of a surfactant. The bulk phase concentrations and specific adsorptions of the various surface active components are computed based on the pseudo-phase separation theory and the mass action model for mixed micelle formation. Non-ideality due to mixing of two types of surface active components, namely the generated soap and the added surfactant, is modeled by the regular solution approximation. The model was used to analyze experimental data where the sodium ion concentration was kept constant by the addition of NaCl. The increase in the number of micelles

with alkali concentration causes the actual sodium ion concentration to decrease. Its effect on the electrostatic contribution to the surface pressure is examined in this model. The model also accounts for surfactant partitioning into the oil phase.

Porous Media Dielectric Properties

The dielectric properties of porous media are shown to be predicted adequately by treating it as an O/W type dispersion of sand grains in water. Dielectric measurements of emulsion flow in porous media show that dielectric techniques may be applied to determine emulsion characteristics in porous media. The experimental observations were confirmed by theoretical analysis.

The dielectric properties of porous media are shown to be predicted adequately by treating it as an O/W type dispersion of sand grains in water. Serious discrepancies between Beer-Lambert's rule and the effective medium model predictions are noted. The frequency invariant dielectric modulus at 20% rock porosity suggests viability of lower frequency measurements. Porous rock characteristics at much greater depth of field can, therefore, be obtained since there is much less attenuation at lower frequencies. The lower limit of usable frequency will be governed by salinity considerations.

Effect of Demulsifier on Interfacial and Film Rheological Properties and Stability of Water-in-Crude Oil Emulsions

Demulsifiers commonly used for crude oil demulsification are inevitably polymeric in nature, often tending toward high molecular weight (10,000 - 50,000). High molecular weight

has often been seen to increase performance. High molecular weight, however, means low diffusivity, which, in the absence of other variables, should mean lower dynamic interfacial activity and poor performance. Obviously other variables must complicate this picture, especially in systems as varied and complex as crude oil emulsions. The work presented, however, is valuable in that it demonstrates the important role that rapidly diffusing, low molecular weight components of demulsifiers likely play in demulsification, i.e., maintaining a low dynamic interfacial tension during film drainage. Indeed, low molecular weight (<10,000) components are present in virtually all "high molecular weight" components commonly used in the oilfield to a significant extent.

The novel experimental technique demonstrated in this chapter, in particular those used in studying the rheology of crude oil films, are particularly useful in modeling events leading to coalescence in oilfield emulsions. Additional work is underway to better understand the role in demulsification of high molecular weight demulsifier fractions. Empirical observations from field testing indicate that such fractions often times are necessary to obtain good performance.

PRACTICAL APPLICATIONS

1. The use of dielectric techniques to characterize emulsions in porous media has applications in monitoring emulsions as they flow through the core.
2. A new theoretical model for prediction of interfacial tension has been developed, which can be incorporated into a chemical flood predictor model for prediction of flood performance.
3. A new instrument has been developed for measuring thin liquid film rheological properties, which have direct one-to-one correlation with emulsion stability.

PUBLICATIONS

1. Rudin, J. and Wasan, D.T., "Mechanisms for Lowering of Interfacial Tension in Alkali/Acidic Oil Systems: Effect of Added Surfactant," *Ind. Eng. Chem. Res.*, **31**, 1899 (1992).
2. Rudin, J. and Wasan, D.T., "Mechanisms for Lowering of Interfacial Tension in Alkali/Acidic Oil Systems: 1. Experimental Studies," *Colloids and Surfaces*, **68**, 67 (1992).
3. Rudin, J. and Wasan, D.T., "Mechanisms for Lowering of Interfacial Tension in Alkali/Acidic Oil Systems: 2. Theoretical Studies," *Colloids and Surfaces*, **68**, 81 (1992).
4. Borwankar, R.P., Lobo, L.A., and Wasan, D.T., "Emulsion Stability-Kinetics of Flocculation and Coalescence," *Colloids and Surfaces*, **69**, 135 (1992).
5. Rudin, J. and Wasan, D.T., "Interfacial Turbulence and Spontaneous Emulsification in Alkali/Acidic Oil Systems," *Chem. Eng. Sci.*, **48**, 2225 (1993).
6. Lobo, L. and Wasan, D.T., "Mechanisms of Aqueous foam Stability in the Presence of Emulsified Non-Aqueous Phase Liquids: Structure and Stability of the Pseudoemulsion Films," *Langmuir*, **9**, 1668 (1993).
7. Rudin, J. and Wasan, D.T., "Low water content Determination Using Microwave Interferometric Dielectrometry," *J. Colloid and Interface Sci.*, in press (1994).
8. "The Effect of Added Surfactant on Interfacial Tension and Spontaneous Emulsification in Alkali/Acidic Oil Systems", Rudin, J., Bernard, C., and Wasan, D.T., *Industrial and Engineering Chemistry Research*, **33**, 1150-1158 (1994).
9. "Oscillatory Deep Channel Interfacial Rheometer," Nagarajan, R. and D.T. Wasan, *Rev. of Scientific Instruments*, **65**, 2675 (1994).
10. "Coalescence of Single Drops at a Liquid-Liquid Interface in the Presence of Surfactants/Polymers," Aderangi, N. and D.T. Wasan, *Chemical Engineering Comm.*, **132**, 207 (1995).
11. "A Controlled Drop Tensiometer for Measuring Dynamic Interfacial Tension and Film Tension," Nagarajan, R., Koczo, K., Erdos, E., and D.T. Wasan, *A.I.Ch.E. Journal*, **41**, 915 (1995).

12. "Study of Dynamic Interfacial Mechanisms For Demulsification of Water-in-Oil Emulsions," Kim, Y.H., D.T. Wasan, and P.J. Breen, *Colloids and Surfaces*, **95**, 235 (1995).

13. "Automatic Apparatus for Measuring Interfacial and Film Tension Under Static and Dynamic Conditions," Soos, J.M., K. Koczo, E. Erdos and D.T. Wasan, *Rev. of Scientific Instruments*, **65**, 3555 (1994).

14. "Effects of Surfactant on Multiple Stepwise Coalescence of Single Drops at Liquid-Liquid Interfaces," Nikolov, A. and D.T. Wasan, *I&EC Research*, **34**, 3653 (1995).

ACCOMPLISHMENTS

ACADEMIC AND PROFESSIONAL HONORS:

- 1995 - Clarkson University, **Robert Gilpin Memorial Lectureship Award**
- 1994 - Case Western Reserve University, **Jacob J. Bikerman Distinguished Lecturer**
- 1993 - Appointed Editor-in-Chief, *Journal of Colloid and Interface Science.*
- 1991 - Chemical Engineering Division of American Society for Engineering Education **3M Lectureship Award** for Outstanding Contributions to Fundamental Chemical Engineering Theory and Practice.
- 1991 - Syracuse University, **Donald Gage Stevens Distinguished Lectureship Award**
- 1990 - **Asen Zlatarov National Award** for Chemical Sciences for research publications in "Ordered Microstructures in Thin Liquid Films," Bulgarian Academy of Sciences.
- 1990 - University of California at Berkeley, **Phoebe Apperson Hearst Distinguished Lecturer.**

Chapter 1

Porous Medium Dielectric Properties

INTRODUCTION

Microwave attenuation measurements have been extensively used in monitoring the saturation of Berea sandstone cores in laboratory core flood experiments using transmission interferometric techniques. The results are usually interpreted in terms of a simple mixing rule such as Beer-Lambert rule. The technique works only for simple calibrated systems. In the absence of calibration data and for emulsified systems the technique fails. We show, in the first part of this chapter, that better accuracy in data interpretation is possible by the use of effective medium theories. In the second part of this chapter, we explore the feasibility of employing dielectric techniques to characterize emulsions in porous media.

COREFLOOD EXPERIMENTS

A computer controlled absorption instrument, shown in Figure 1-1, was developed in our laboratory for the automated measurement of oil/water saturation in laboratory models of porous media. It consists of a PDP-11/10 mini computer, two constant rate pumps, a differential pressure transducer, an automated fraction collector, and a microwave adsorption analyzer. The components of the measuring device are the microwave focused lens horns, one of them transmitting and the other receiving. The attenuation data has been interpreted to date under the assumption that when microwave radiation travels through a homogeneous medium, the power intensity of the beam is reduced according to Beer-Lambert's rule. Microwave energy is considered to be absorbed exclusively by the water molecules. Other model components such as oil, gas, consolidated rock, and epoxy paint are considered nearly transparent compared with water. Thus, the total absorption is a direct function of the number of water molecules in the

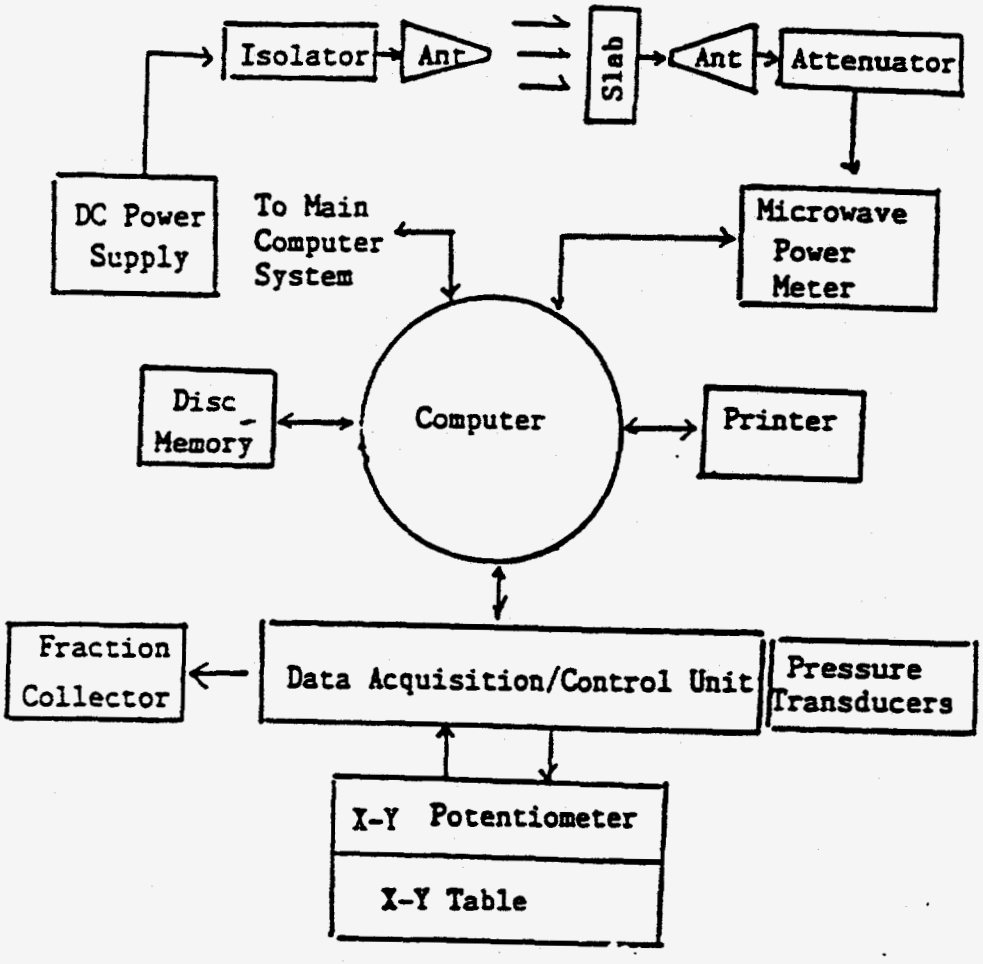

Figure 1-1. Schematic Diagram of Core Flooding Apparatus

beam path and is described by Beer Lambert's rule:

$$\frac{I_t}{I_i}=A=\exp(-K_aCh) \tag{1-1}$$

where I_t is the radiation emerging from the sample, I_i is the radiation intensity incident on the sample, K_a is the molar absorption coefficient, C is the concentration of the absorber, h is the thickness of the sample, and A is the absorbance. Water saturation is obtained from the logarithmic ratio of the microwave signal.

The serious limitation in this approach is that it treats the porous medium, which is a dispersion of sand grains in brine, as a simple mixture. The porous medium is better modelled as a dispersion of sand grains. For a spherical dispersion of sand grains, the dielectric behavior of the porous medium can be described by Hanai's model as

$$\frac{(\varepsilon_1-\varepsilon_2)^3}{(\varepsilon_1-\varepsilon_m)^3}\left(\frac{\varepsilon_m}{\varepsilon_2}\right)=\frac{1}{(1-\phi)^3} \tag{1-2}$$

This formula is applicable to non-spherical dispersions that possess self similarity. The experimental measurements, obtained from reference 1, for a model porous media of fused glass beads in various solvents, is shown in Figure 1-2.

As can be seen from the figure, the comparison between the measured values of the dielectric constant and the theoretical predictions of the effective medium theory is very good. Experimental measurements of the dielectric properties of dry Berea sandstone core were made at 23.45 GHz during the course of this study. The phase shift variation with pathlength is shown in Figure 1-3. The measured value of the permittivity compared with the effective medium theory to within 8%. The deviation from Beer-Lambert's mixing rule was substantially much

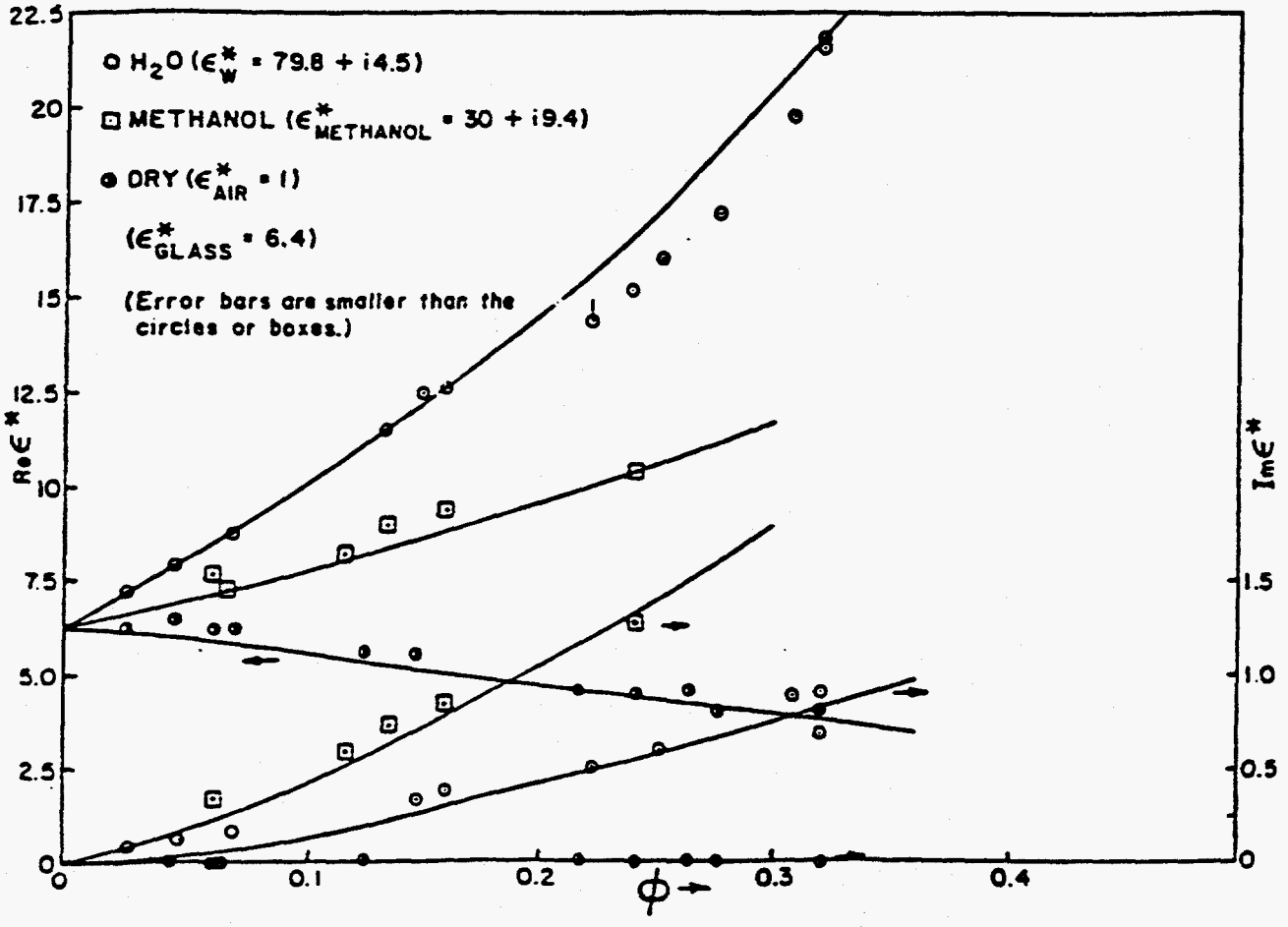

Figure 1-2. Comparison of Experimental Data with Effective Medium Theory for Model Porous Medium of Fused Glass Beads with various Solvents

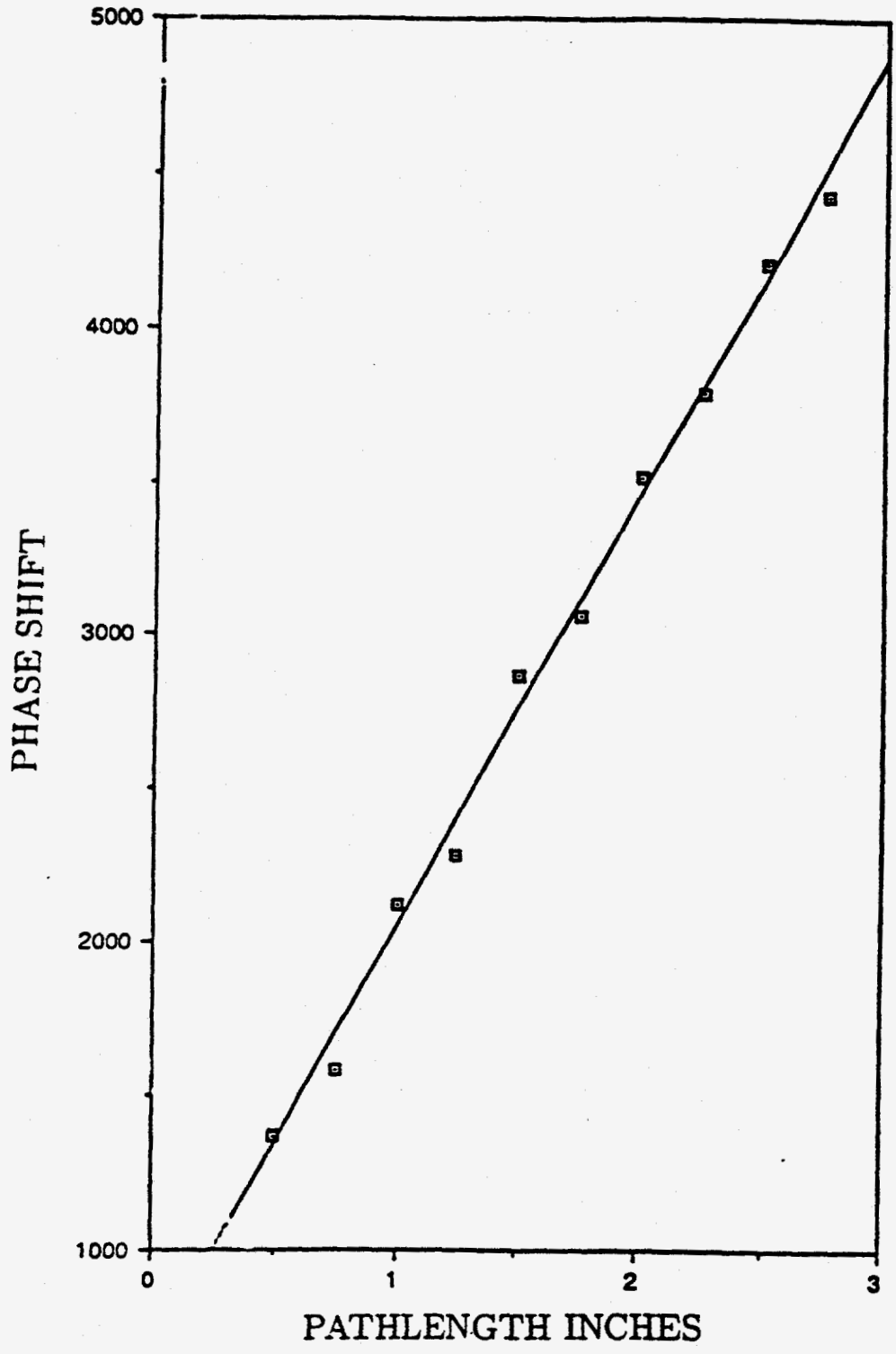

Figure 1-3. Dry Core Variable Pathlength Phase Shift Data at 23.45 GHz.

higher at 26%. Thus the effective medium theory which treats the porous medium as an O/W type dispersion appears to be valid in predicting porous medium dielectric characteristics.

The choice of an effective medium theory will depend on the rock characteristics of the formation. For a rock made up of randomly shaped grains, the model developed would be appropriate, while for rocks that posses self similarity, the Hanai equation would apply. The practical consequences of using Beer-Lambert rule instead of the effective medium models is illustrated in Figure 1-4 for an O/W type dispersion. As can be seen from the figure, theoretical calculation using Beer's law will tend to overpredict the amount of water present, especially at high water saturations. The loss factor plotted in Figure 1-4 is directly proportional to the measured attenuation for a constant size core. Earlier core flooding experiments gave good results as they were calibrated to the porosity by material balance.

RESULTS AND DISCUSSION

An accurate way to interpret microwave dielectric data to determine porous media saturation characteristics is to use an effective medium theory, with ε' and ε'' computed by phase and attenuation measurements. The dielectric modulus for a water saturated Berea sandstone core with 20% porosity is shown in Figure 1-5.

It is important to note from Figure 1-5 that the modulus of the system is frequency invariant over a wide range of frequencies. This result has the important implication that low frequency data is adequate for determining the saturation characteristics and is especially significant for insitu monitoring of porous medium in oil fields. The porous medium is akin to

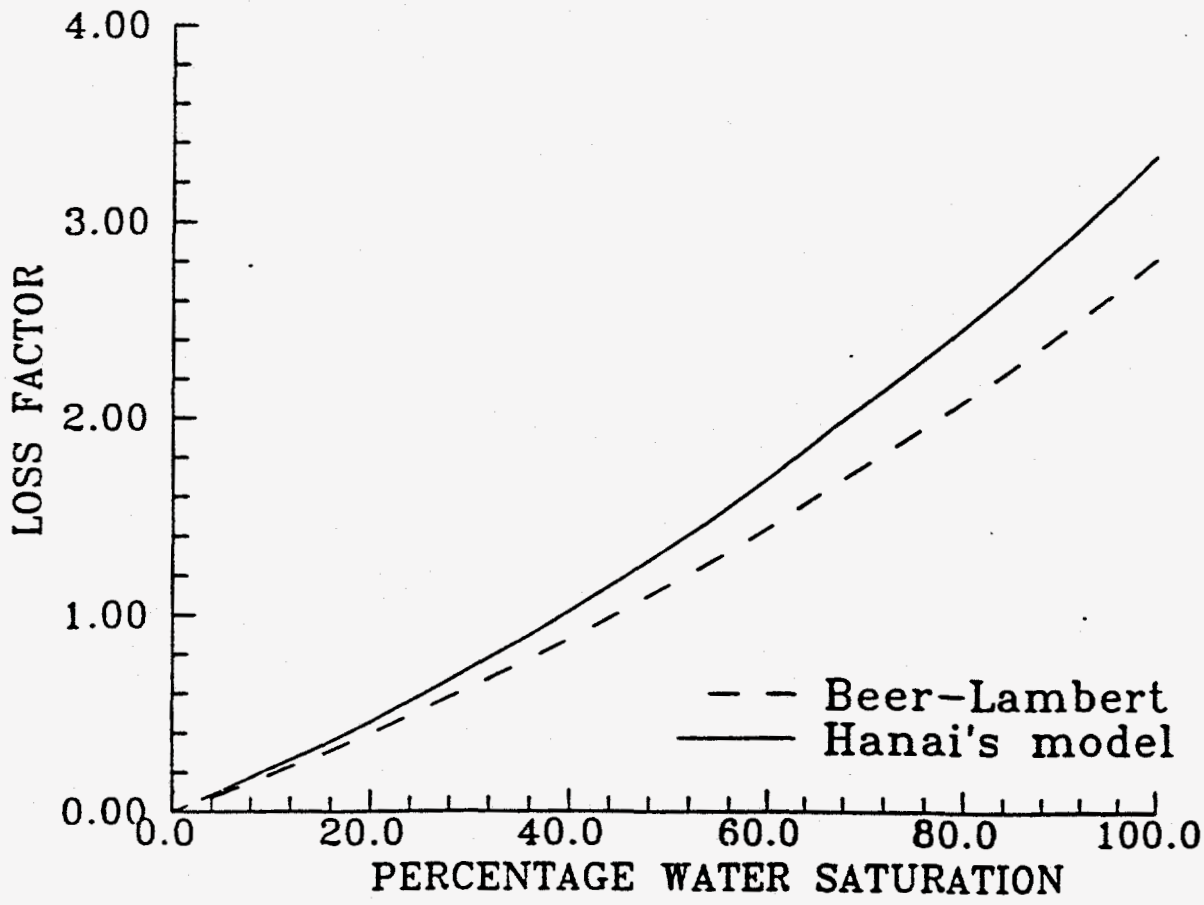

Figure 1-4. Comparison of Beer Lambert Law with Effective Medium Models for an O/W type Dispersion at 23.45 GHz.

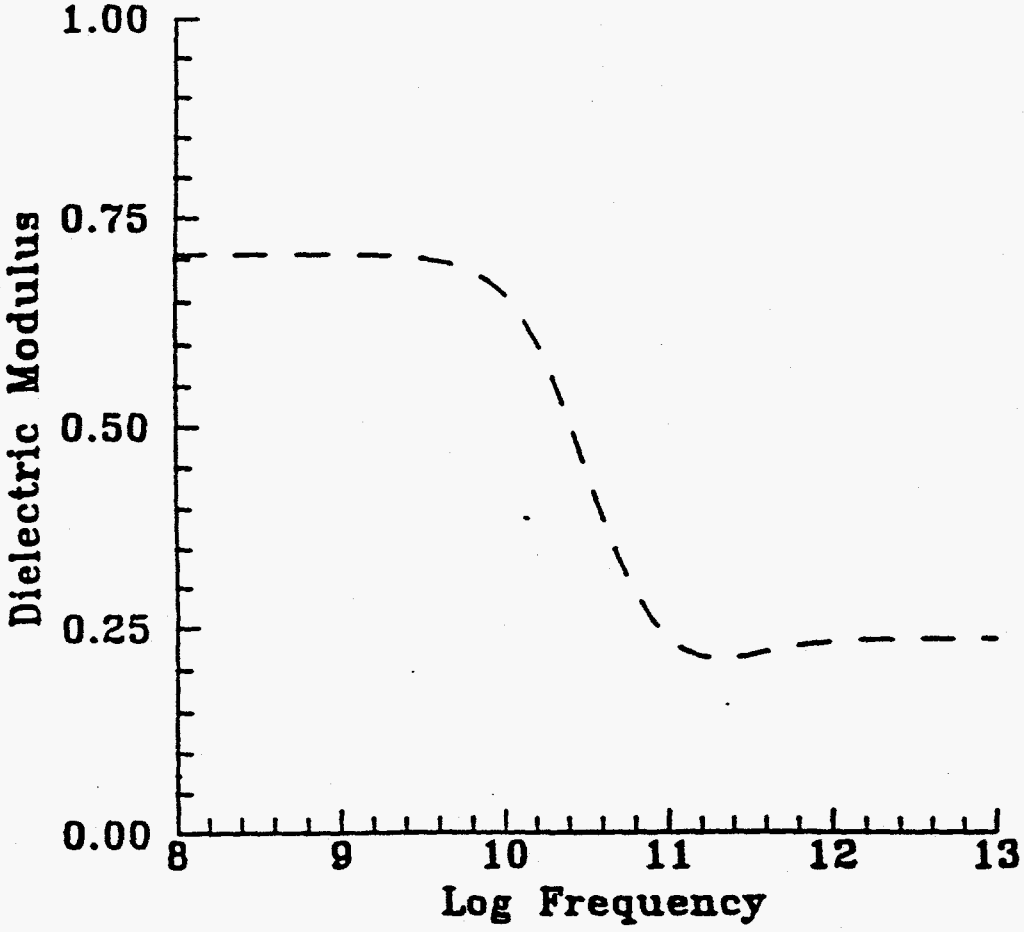

Figure 1-5. Frequency Invariant Modulus Plot of the Dielectric Modulus of Berea Sandstone Porous Medium at 20% Porosity

an oil-in-water emulsion system and low frequency microwave techniques are preferable since there is considerably less attenuation at low microwave frequencies. Porous rock characteristics at much greater depths can, therefore, be obtained by a single frequency measurement of the dielectric constant. The lower limit of the usable frequency will be governed by salinity considerations. The dielectric data of O/W type systems, including porous media, from several sources at various frequencies in the microwave region is represented as a dielectric modulus in Figure 1-6. The data spans virtually the entire range of dispersed phase volume fractions and compares favorably with the dielectric modulus of O/W emulsion systems obtained from our model computations.

Brine Conductivity

The conductivity of the porous medium increases with increasing salt concentration. The conductivity contribution to the global complex permittivity takes on the form of an imaginary quantity, which is an additional term to the imaginary part of the dipolar-type relaxation permittivity. The total permittivity of a substance can be written as

$$\varepsilon^*(f)=\varepsilon'(f)-i\varepsilon''_T(f) \tag{1-3}$$

where

$$\varepsilon''_T=\varepsilon''(f)+\varepsilon''_C \tag{1-4}$$

Therefore

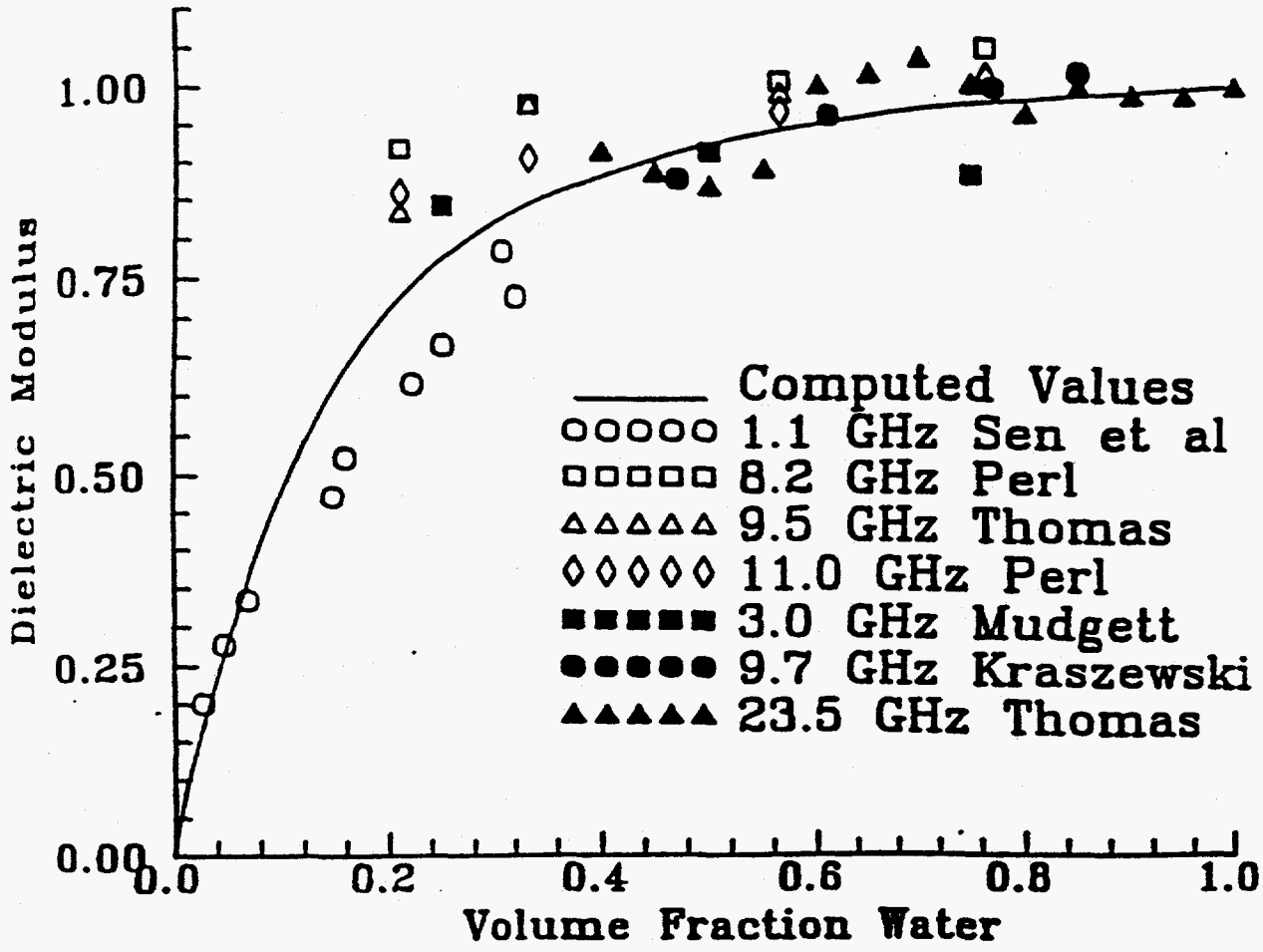

Figure 1-6. Frequency Invariant Modulus Plot of the Dielectric Modulus of O/W Type Dispersions using Effective Medium Theory

$$\varepsilon^*(f)=\varepsilon'(f)-i\varepsilon''_R(f)-i\frac{\sigma}{2\pi\varepsilon_0 f} \qquad (1\text{-}5)$$

ε''_T denotes the total absorption coefficient, ε''_R being the contribution of dipolar type relaxation processes, and ε''_C the contribution of conduction phenomena. It can be seen from the equation that the conduction absorption term is preponderant at low frequencies while its contribution can become negligible at high frequencies. If the steady conductivity is large enough, a wide overlapping of relaxation and conduction can occur, which complicates the interpretation of complex permittivity measurements.

Clearly, as brine concentration increases, higher frequency measurements will be necessary to determine saturation profiles.

Grain shape

The size of sandstone grains constituting the formation will not affect the dielectric properties of the porous media. The effect of grain shape can be considerable, especially when the grains are platey and have preferential orientations. The effect of grain shape on the dielectric properties of a water saturated berea sandstone core with 20% porosity is illustrated in Figures 1-7 to 1-9. A shape factor of 0 will correspond to platey grains oriented perpendicular to the measurement direction. A shape factor of 1 represents platey grains parallel to the measurement direction. All other grain shapes and configurations will fall in between. A spherical dispersion will have an L factor of 0.33. The frequency dependent effects of grain shape on the dielectric properties of the water saturated core is represented by the Debye and Cole Cole plots in Figures 1-10 to 1-12.

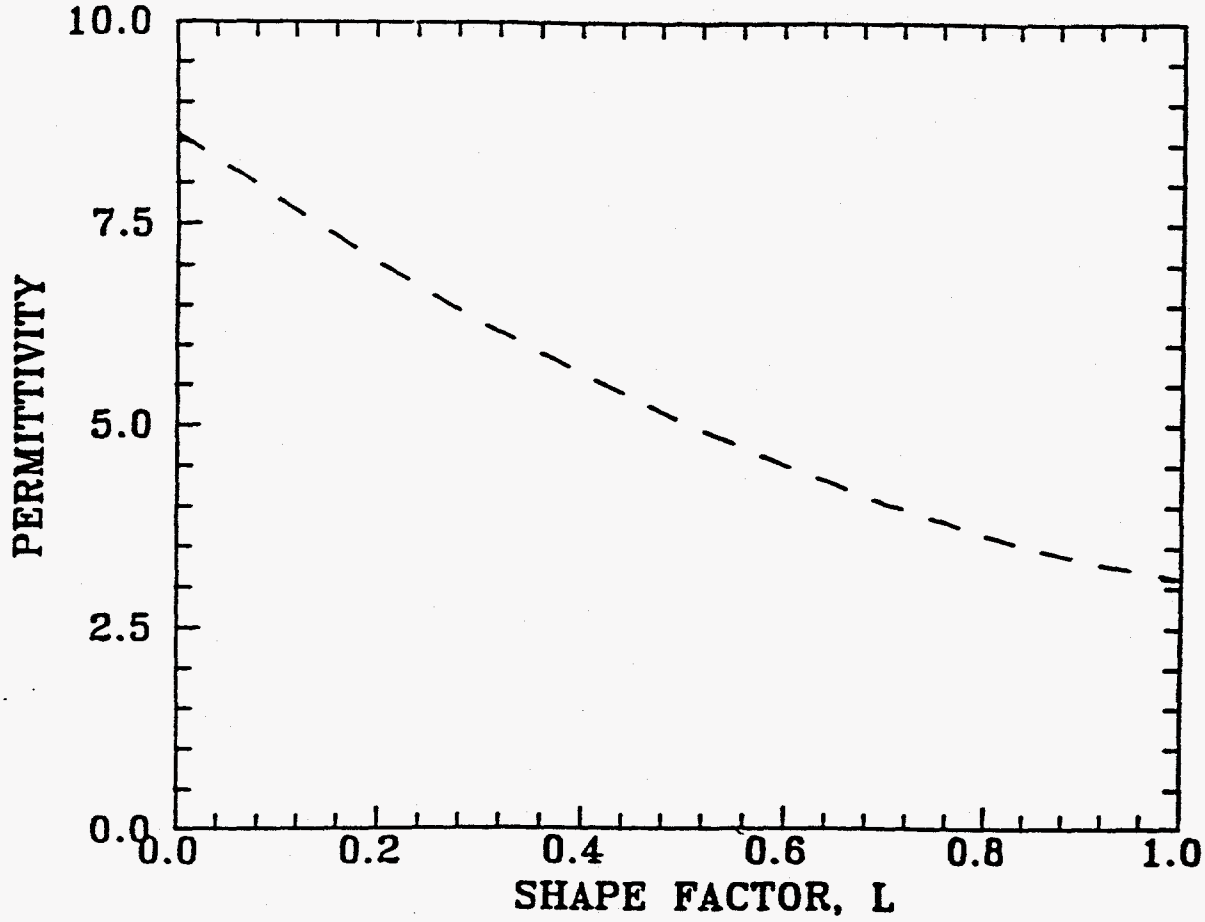

Figure 1-7. Effect of Grain Shape on the Permittivity of Water Saturated Berea Sandstone Core with a 20% Porosity

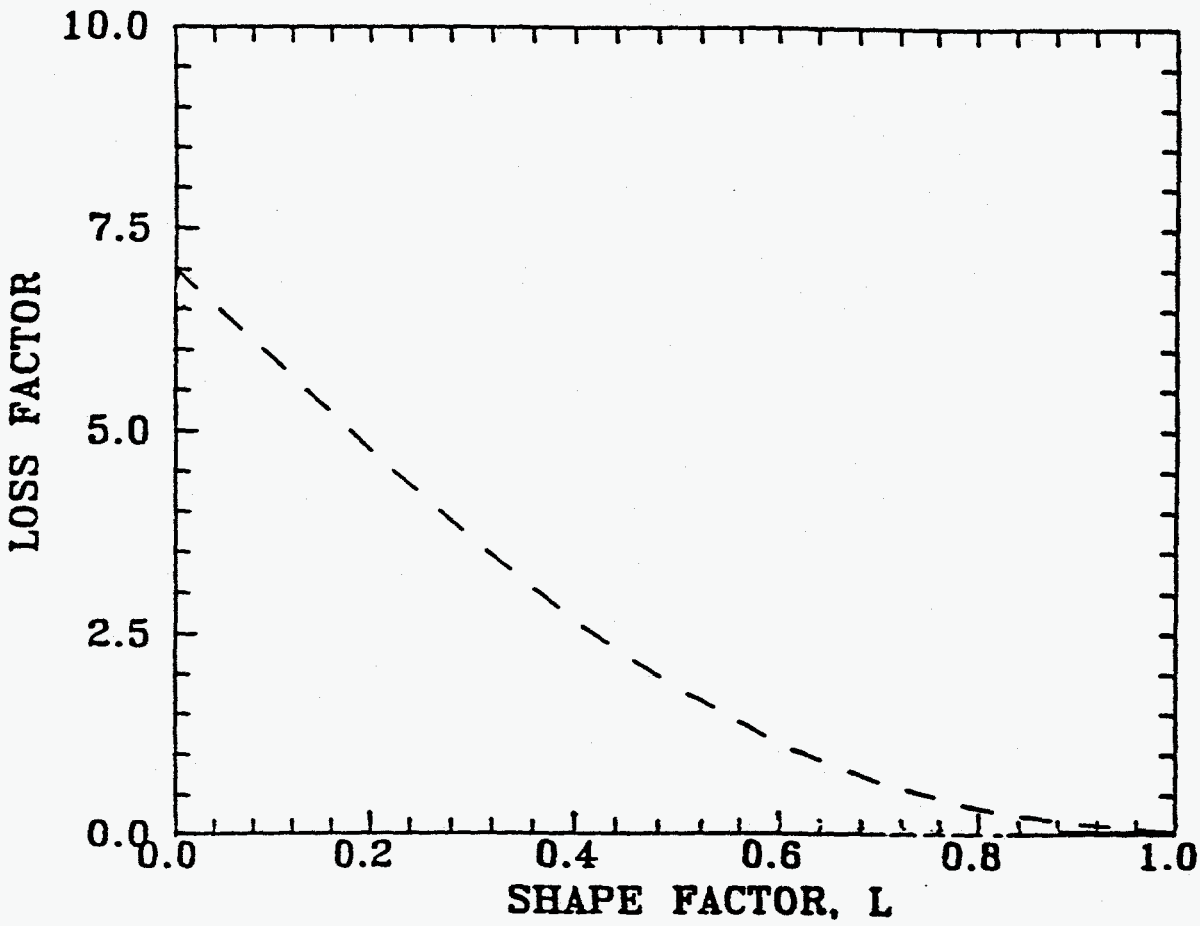

Figure 1-8. Effect of Grain Shape on the Loss Factor of Water Saturated Berea Sandstone Core with a 20% Porosity

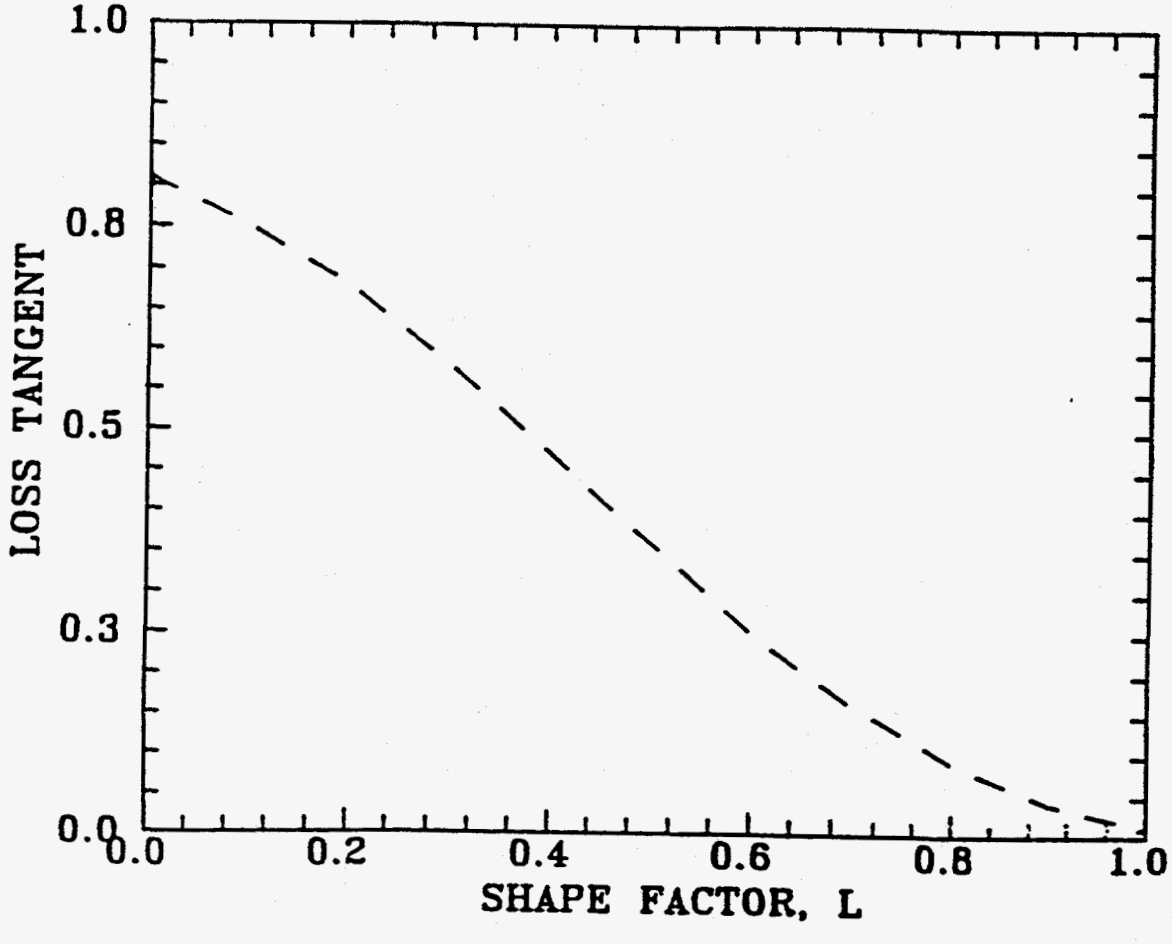

Figure 1-9. Effect of Grain Shape on the Loss Tangent of Water Saturated Berea Sandstone Core with a 20% Porosity

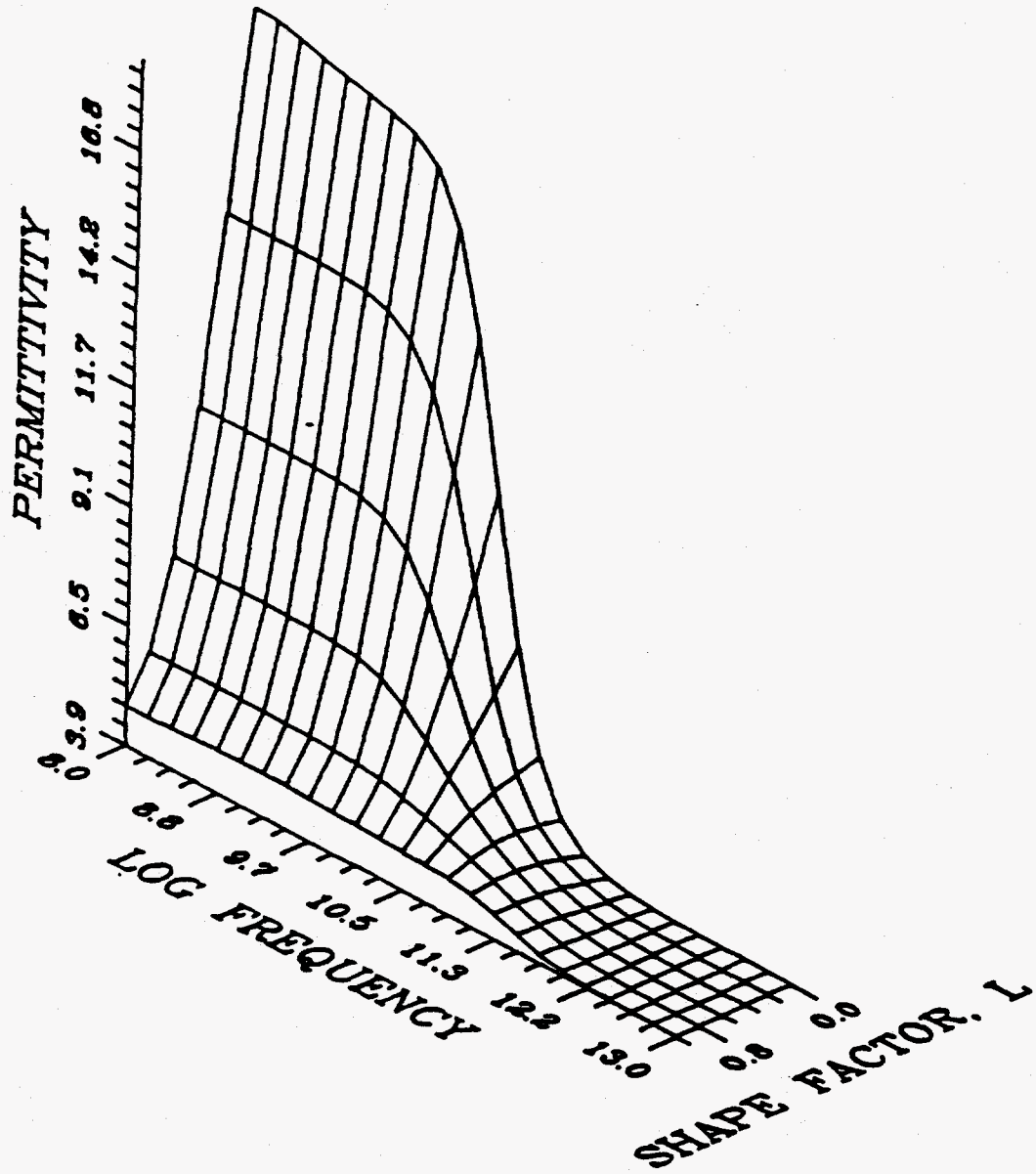

Figure 1-10. Debye Plot of Permittivity Variation with Grain Shape for Water Saturated Berea Sandstone Core with a 20% Porosity

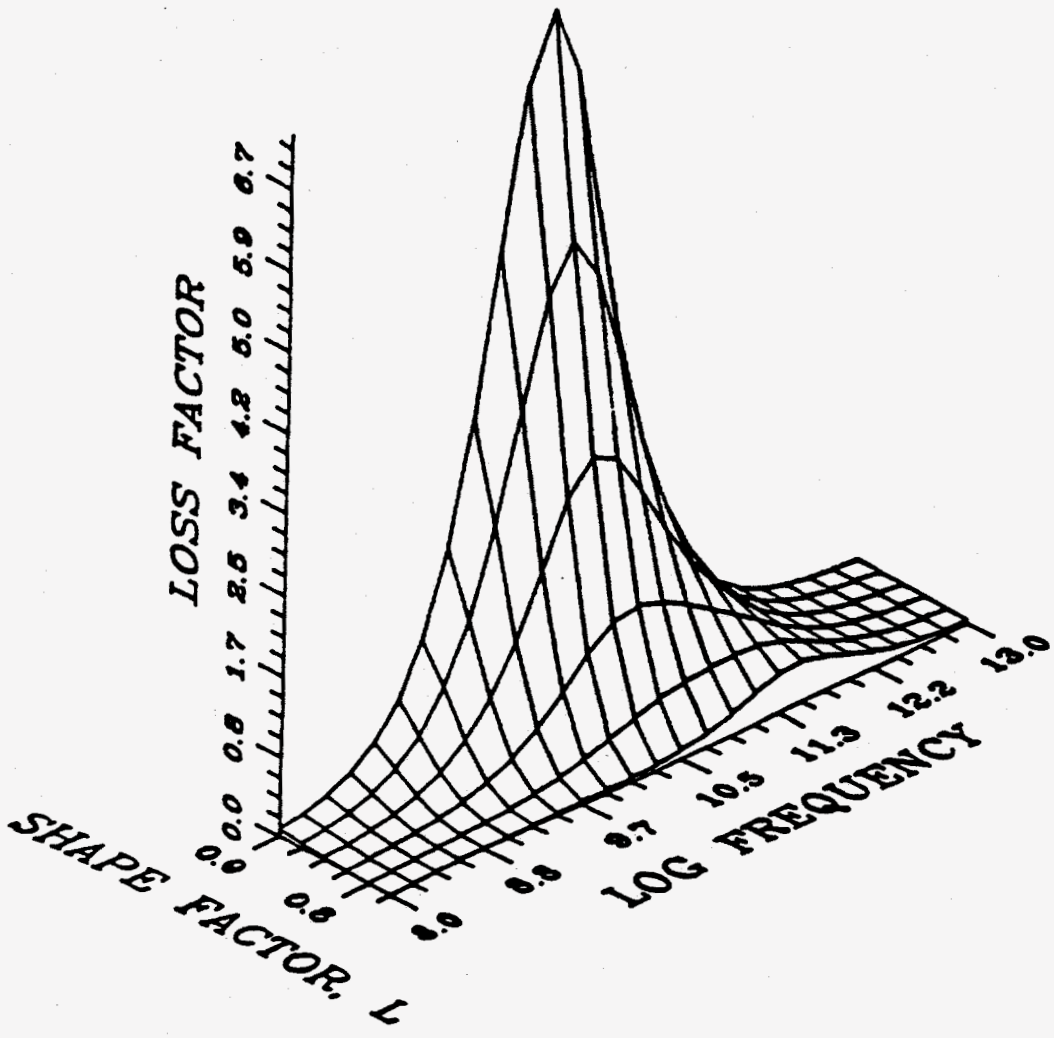

Figure 1-11. Debye Plot of Loss Factor Variation with Grain Shape for Water Saturated Berea Sandstone Core with a 20% Porosity

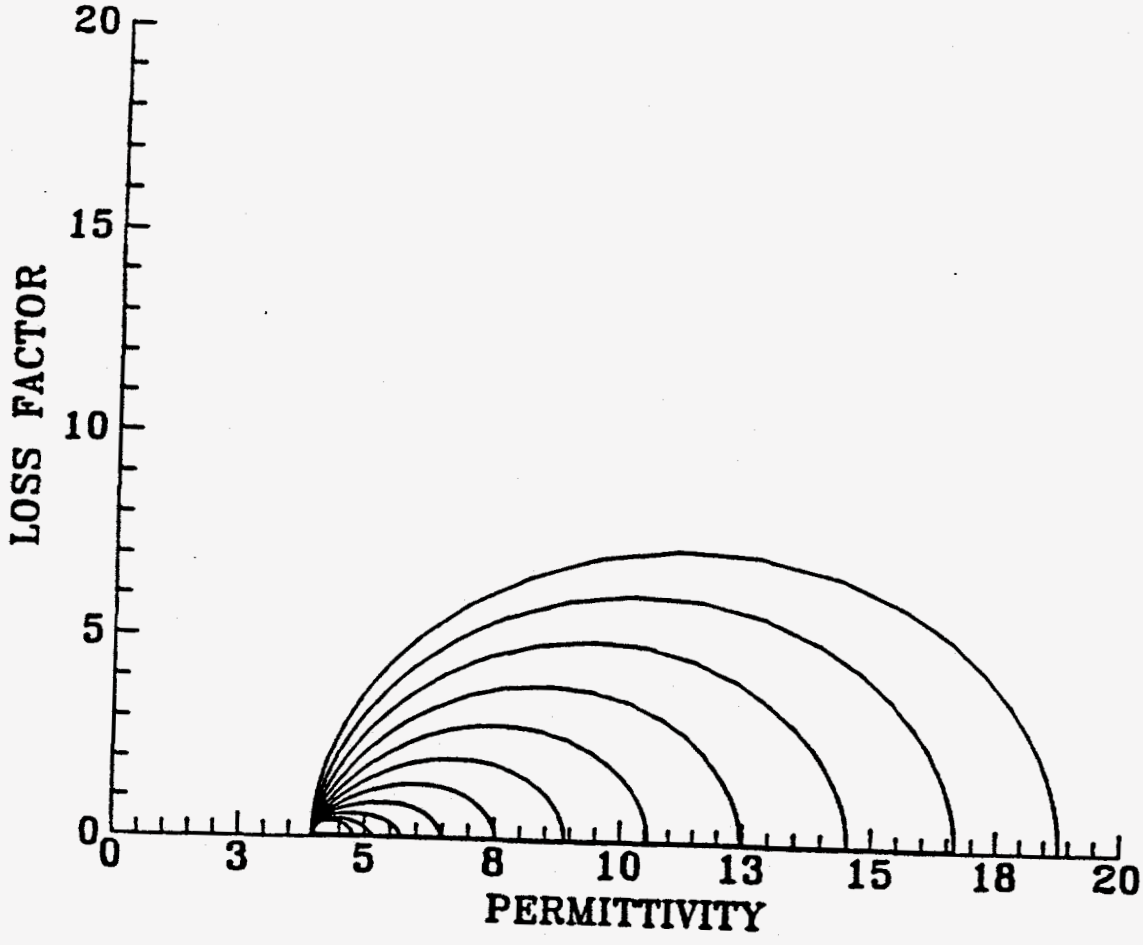

Figure 1-12. Cole-Cole Plots of Water Saturated Berea Sandstone Core with a 20% Porosity as a Function of Grain Shape.

EMULSIONS IN POROUS MEDIA

The problem of characterizing emulsions in porous media is very important in enhanced oil recovery applications. This is usually accomplished by externally added or insitu generated surfactants that sweep the oil out of the reservoir. Emulsification of the trapped oil is one of the mechanisms of recovery. The ability to detect emulsions in the porous medium is therefore crucial to designing profitable flood systems. The capability of microwave dielectric techniques to detect emulsions in porous medium is demonstrated by mathematical modelling and by experiments.

Modelling of emulsions in porous media

The system of emulsions in porous media will correspond to the situation when there are 3 macrophases dispersed in each other, such as occur in multiple emulsion systems. One approach that can be taken is to express its total dielectric constant by iterating or combining formulas valid for binary systems. For instance, a double spherical dispersion-type system having two different phases 1a and 1b, characterized respectively by ε^a_1 and ε^b_1 can be considered as a dispersion of 1a spherical particles embedded in a continuous medium characterized by ε^2, or alternatively, as a dispersion of 1b spherical particles in a continuous medium characterized by ε^2. Both procedures do not in all cases yield the same answer. The modelling of such systems will be examined in the context of emulsion flow in porous media.

In the modelling of a bicontinuous structure such as a porous medium, the first question to be asked is whether a water saturated core should be treated as an oil-in-water emulsion or a water-in-oil type dispersion. The experimental data of Sen (1981) suggests that the answer to

this question is to treat the rock grains as being dispersed in water. We could therefore model the ternary system of emulsions in porous media by successive iteration of two binary systems. The effective dielectric constant of the emulsions could be determined from Hanai's model for two phase dispersions. The rock grains could then be treated as being dispersed in a fluid of dielectric constant being equal to the effective dielectric constant of the emulsions. the dielectric constant of this binary mixture could again be computed by Hanai's model. However for rock formations with little or no clay content, the dielectric constant of the rock grains will be comparable to the dielectric constant of oil. Therefore, an O/W emulsion system in porous media can in effect be modelled as a dual dispersion of sand grains and oil in water. Similarly, a W/O emulsion in porous media can be regarded as a dual dispersion of water and sand grains in oil. This approach implies that a 50% emulsion of O/W in a porous medium with a 20% porosity will be similar to a 90% O/W type dispersion. A 50% W/O emulsion, on the other hand, will be similar to a 10% W/O type dispersion. We can, therefore, expect differences in the dielectric behavior of the two systems. The computed results for the two emulsion systems with dispersed phase volume fractions of upto 60%, in a berea sandstone core with a 20% porosity shown in Figures 1-13 to 1-15 clearly demonstrated the differences. In Figure 1-16, we compare the computed loss tangent values of the two emulsions with a system containing equivalent proportions of unemulsified constituents. The differences in emulsified and unemulsified systems indicated that dielectric properties may be used to determine not only the emulsion type and composition, but also to ascertain if emulsification occurs at all.

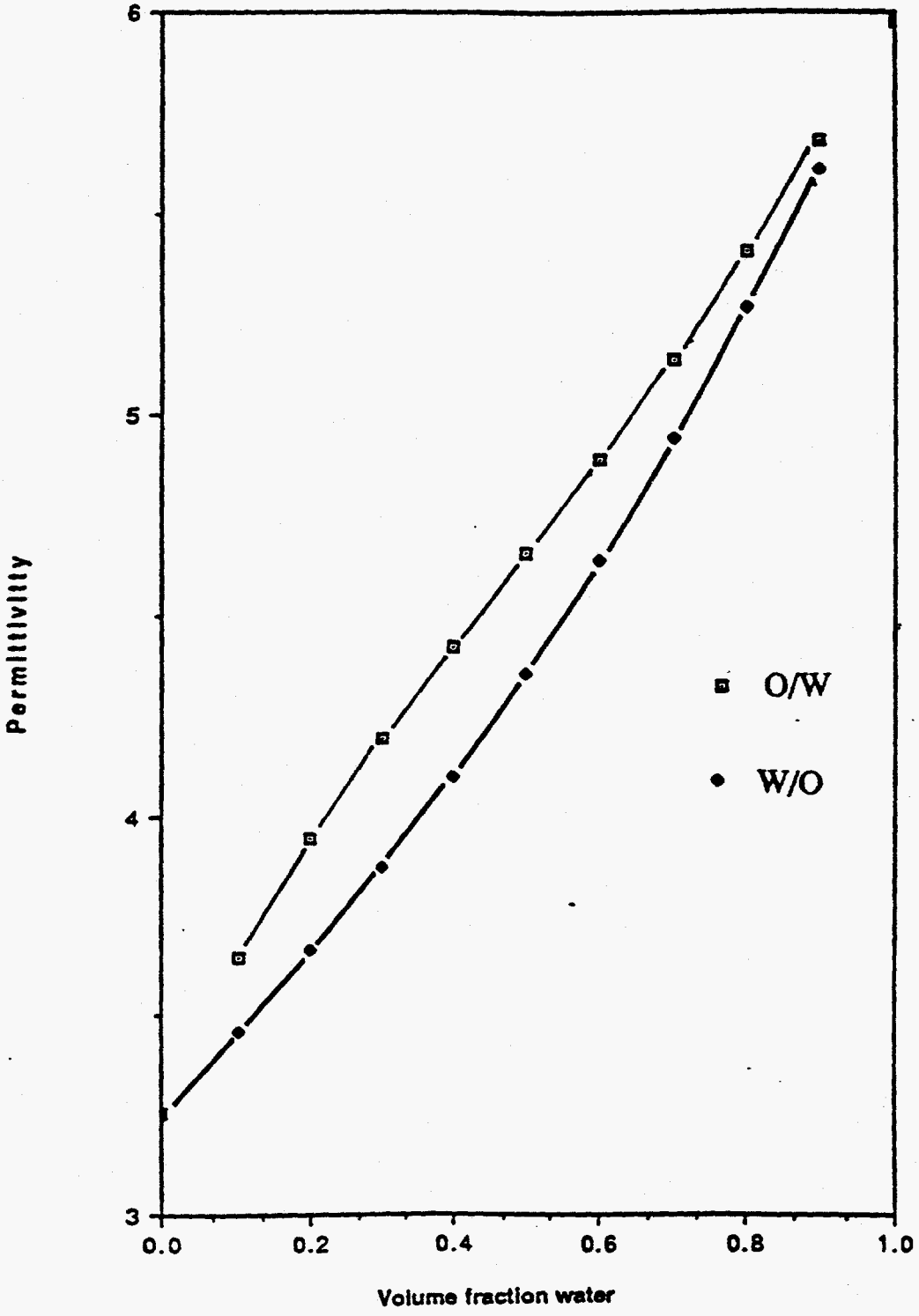

Figure 1-13. Computed Permittivity values at 23.45 GHz for O/W and W/O emulsions inside Berea Sandstone Core with a 20% Porosity

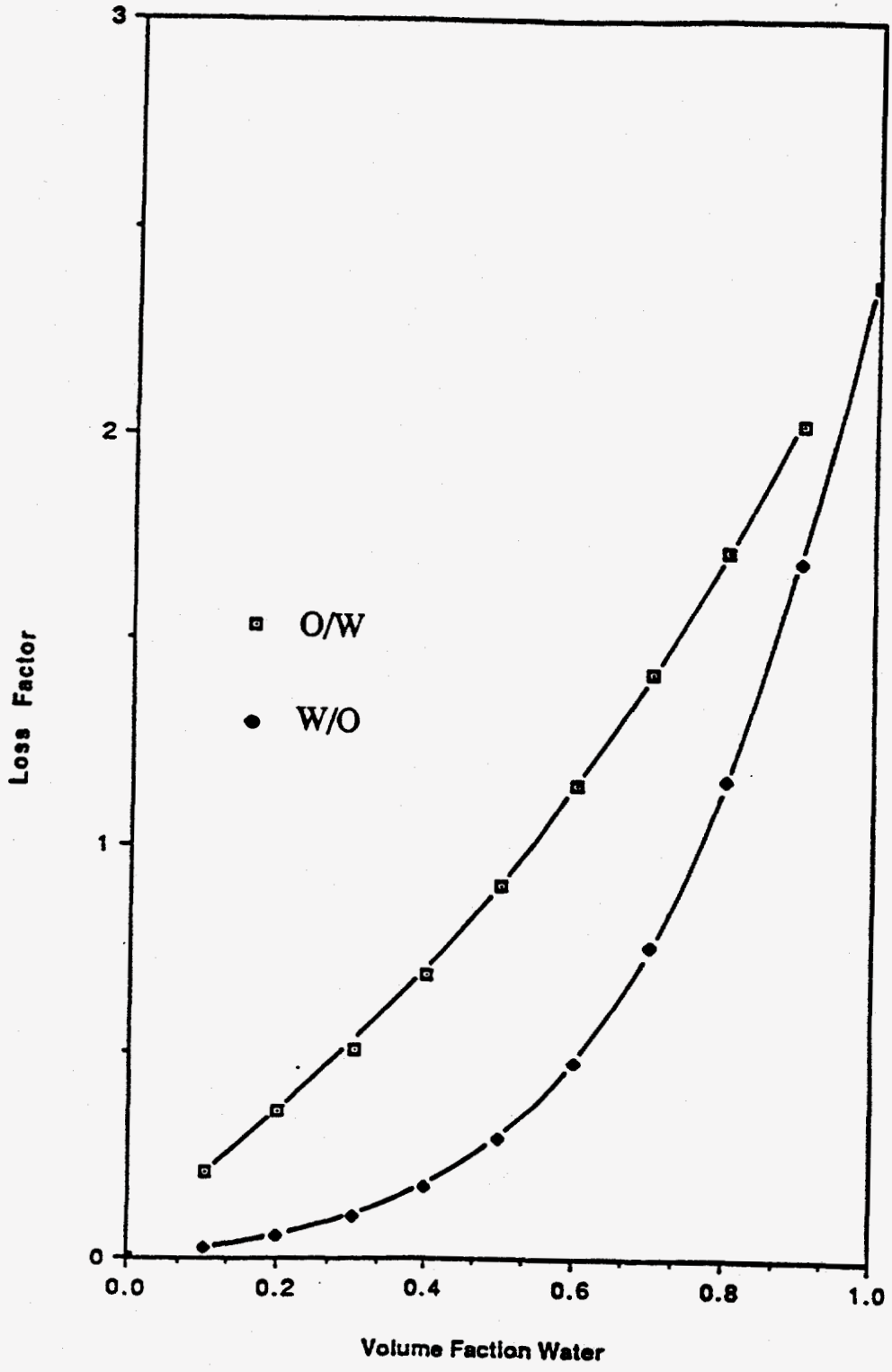

Figure 1-14. Computed Loss Factor values at 23.45 GHz for O/W and W/O emulsions inside Berea Sandstone Core with a 20% Porosity

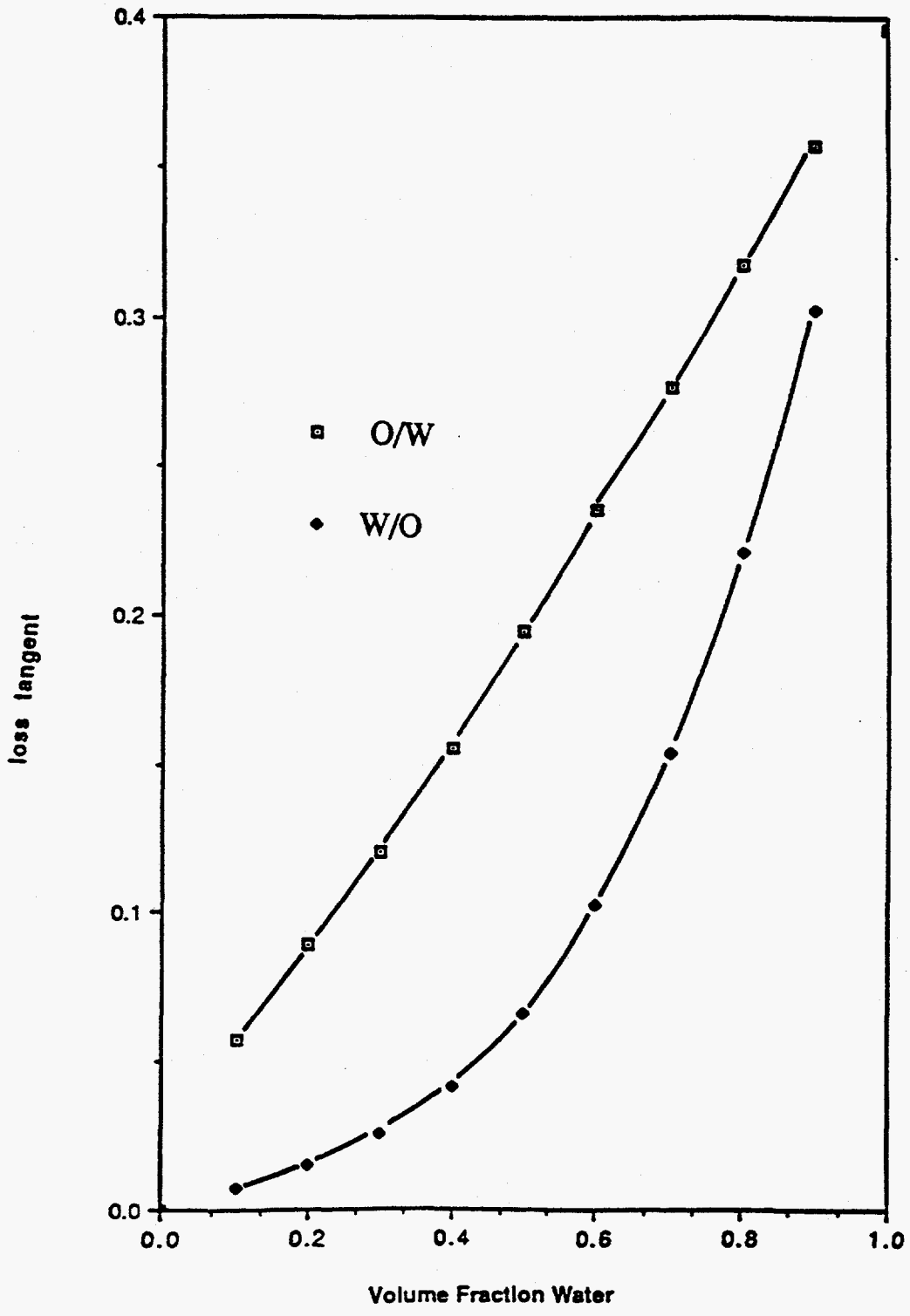

Figure 1-15. Computed Loss Tangent values at 23.45 GHz for O/W and W/O emulsions inside Berea Sandstone Core with a 20% Porosity

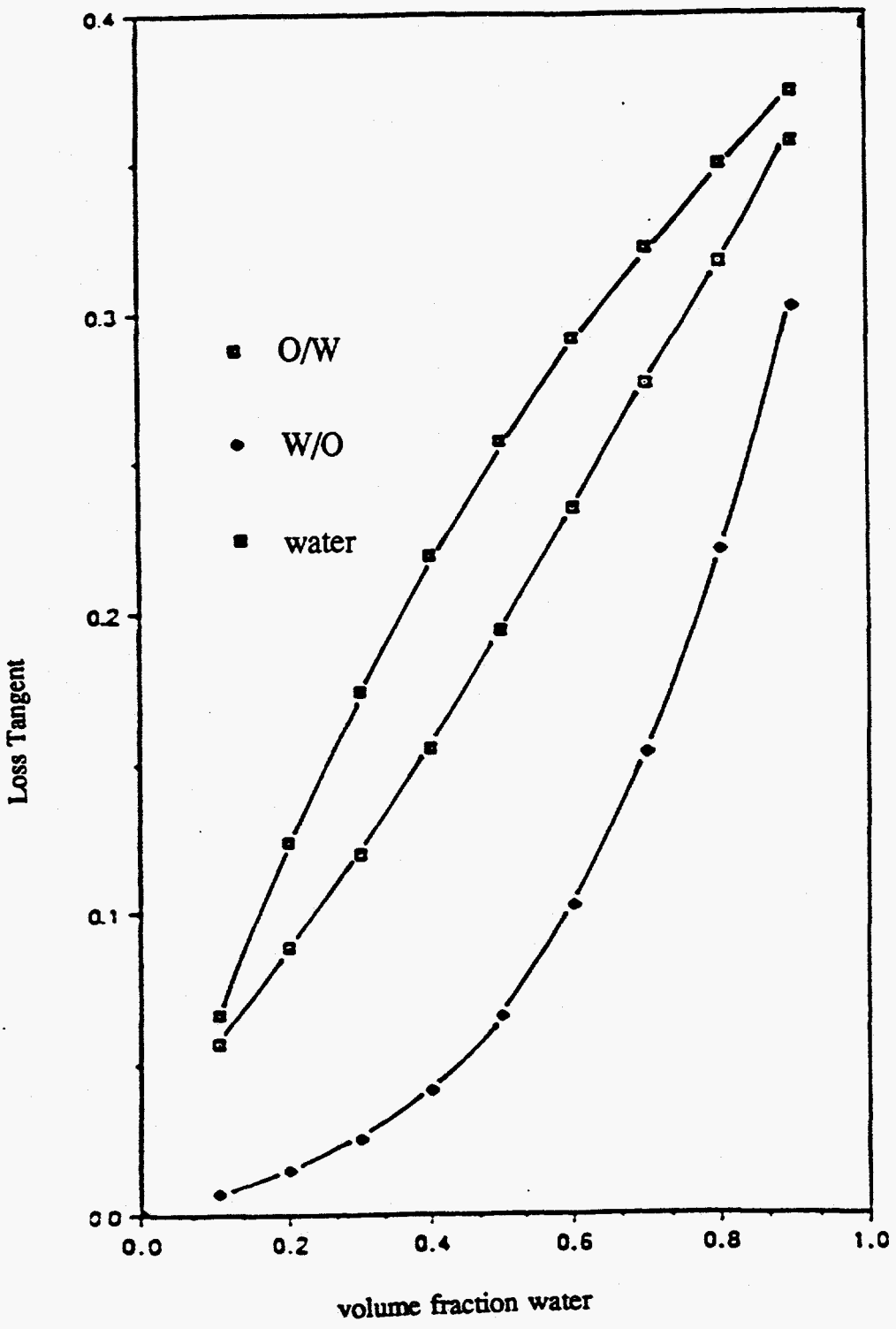

Figure 1-16. Computed Loss Tangent values at 23.45 GHz for Emulsified and Unemulsified Oil and Water Systems inside Berea Sandstone Core with a 20% Porosity

MICROVISUALIZATION EXPERIMENTS

Microwave dielectric experiments were undertaken to demonstrate the feasibility of characterizing emulsions in porous media. To ensure that there was no accumulation of the emulsions in the Berea sandstone core in the course of the experiments, the effluent and influent concentrations of the emulsions were measured. In addition, definitive assurance was sought by visualizing the flow of emulsions in an etched glass microporous media. The average size of the pores were matched with that of the berea sandstone core used and was about 150 microns. The average size of the emulsions used was about 5 microns. The etched glass models were made by asphalt coating the glass piece covered by a silk screen. The asphalt partially covered the glass piece exposing the silk screen patterns on the glass piece. The glass piece was then immersed in hydrofluoric acid, which etched the exposed areas of the glass. The glass piece was cleaned to remove the acid and treated with organic solvents to remove the asphalt. The etched glass piece was then covered with a cover glass piece, after grooves were cut on both glass pieces to allow for inflow and outflow, and the pieces fused by overnight heating in a furnace set at a temperature of 1200 ^{o}F.

O/W and W/O emulsions of different concentrations were made visualizable by dyeing the dispersed phase and pumped through the model at low flow rates of 1 ft/day. The flow patterns were observed through a microscope and a vidiograph made. The results clearly show that there was no accumulation of the emulsions in the porous medium. Occasionally, there was breakup of large emulsion drops into smaller drops at bifurcations. Since the size of the emulsions has no bearing on the dielectric properties of macroemulsions, this is not expected to affect the results. The dielectrically determined concentrations of the emulsions should, therefore,

provide accurate values.

EMULSION CORE FLOOD EXPERIMENTS

Two inch square berea sandstone pieces were prepared by coating them with resin. The ends were covered with plexiglass pieces with holes drilled to allow for inflow and outflow. W/O emulsions of varying concentrations were first prepared and characterized dielectrically. Water was pumped into the core at a flow rate of 1 ft/day and the dielectric constant monitored. After breakthrough, five pore volumes of the continuous phase was pumped through to ensure complete saturation. The lowest concentrations of the emulsion was then pumped through the core. The effluent concentrations were then monitored by a cavity resonance dielectrometer. A schematic diagram of the experimental setup is shown in Figure 1-17.

When the effluent concentrations matched the influent concentrations, steady state flow conditions were considered to prevail and the dielectric constant of the emulsions in the porous media recorded. The next higher concentration of emulsion was pumped through the core and the procedure repeated. For W/O emulsions, the berea sandstone core is first flooded with oil and five pore volumes of oil pumped through. To facilitate oil wetting of the core, the oil filled core was left untouched for a week. About five pore volumes of oil was pumped through before W/O emulsions were introduced.

Results and discussion

The experimentally measured value of the dielectric loss tangent is shown in Figure 1-18. Differences in the dielectric properties of the two emulsion systems are clearly observed. The

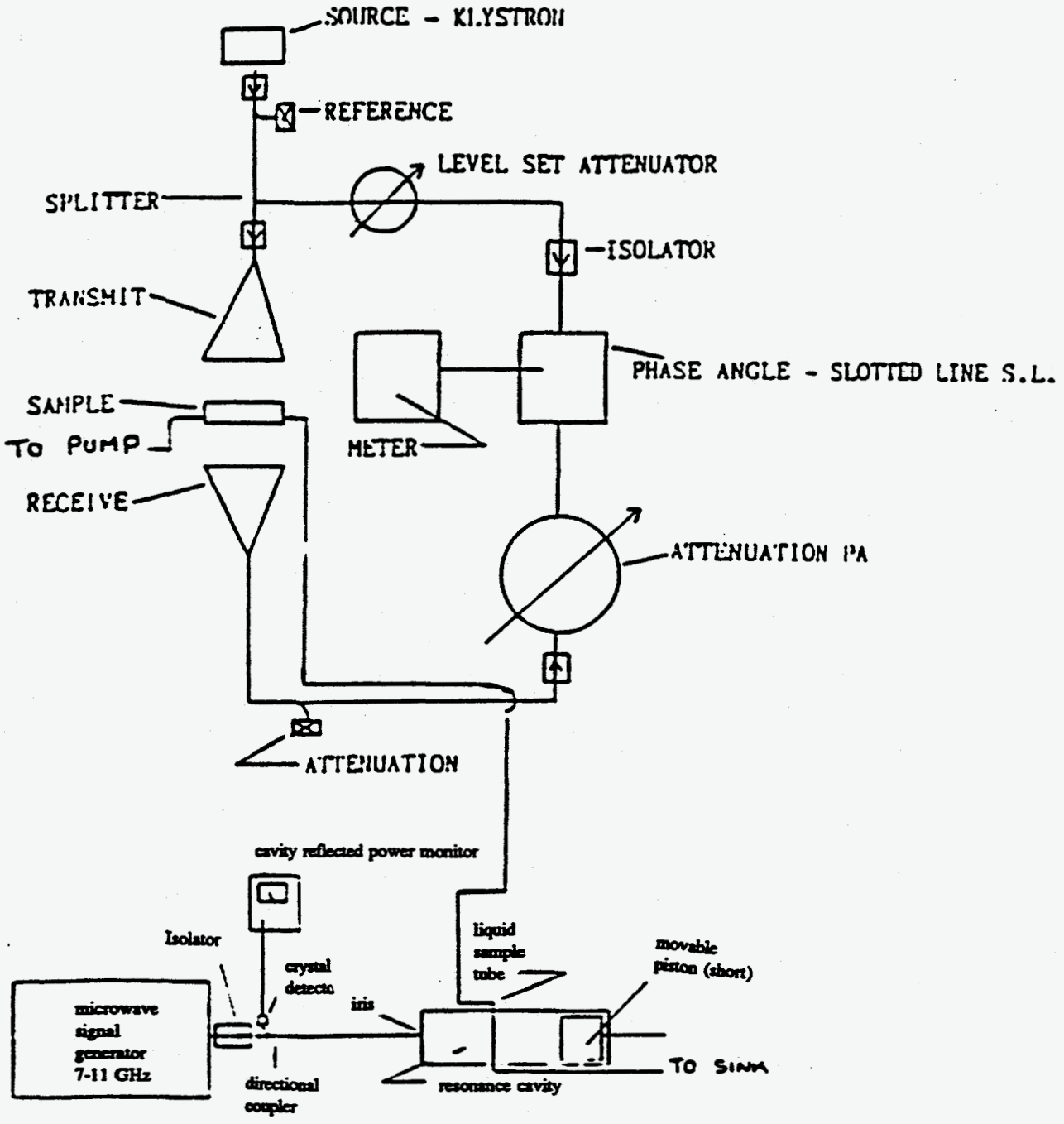

Figure 1-17. Schematic of Emulsion Core Flood Experiments with Emulsion Dielectric Behavior inside Porous Media Measured by Interference Dielectometer at 23.45 GHz and the Effluent Concentration Monitored by a Cavity Resonance Dielectrometer

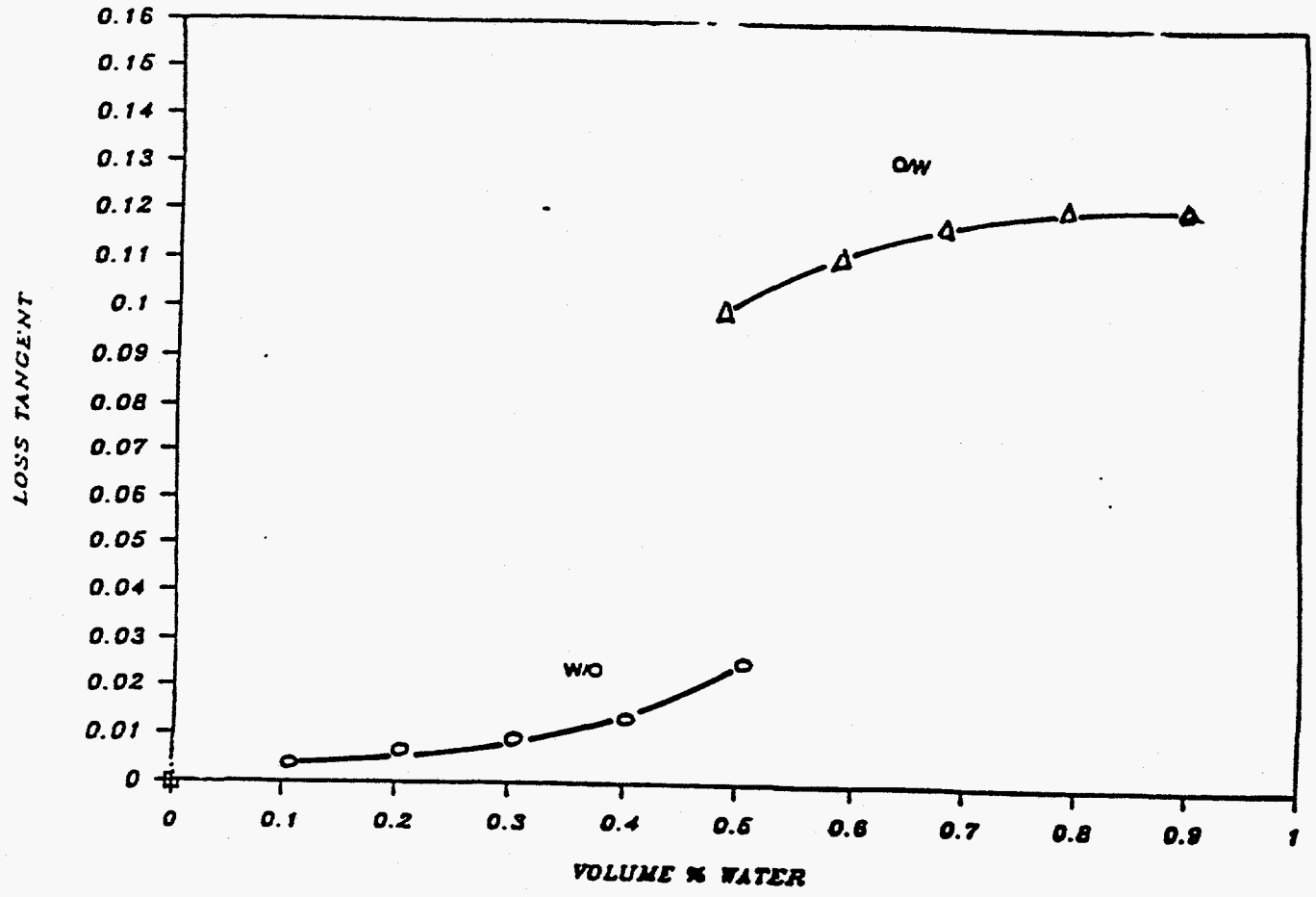

Figure 1-18. Experimentally Measured Loss Tangent Values at 23.45 GHz for Emulsions Inside Porous Media at 20% Rock Porosity

loss tangent of O/W emulsions in the core is considerably higher than the loss tangent of W/O emulsions, at all concentrations without any overlap for dispersed phase concentrations of upto 60%.

Analogous to the definition of the Dielectric modulus of emulsions outside the porous medium we can define a Dielectric Modulus P_{pore} for emulsions inside the porous medium as follows:

$$P_{pore} = \frac{loss\ tangent\ of\ emulsions}{loss\ tangent\ of\ water\ saturated\ core} \qquad (1\text{-}6)$$

This would allow for the comparison of dielectric data obtained at different frequencies for emulsion dielectric data inside porous medium. The computed P_{pore} results are shown in Figure 1-19 as a function of volume fraction water. The differences in the dielectric characteristics of the two emulsion types are clearly defined in the plot.

Both the experimental and theoretical values clearly establish the feasibility of determining emulsion characteristics by dielectric measurements in the microwave region.

SUMMARY

1. The dielectric properties of porous media are shown to be predicted adequately by treating it as an O/W type dispersion of sand grains in water. Serious discrepancies between Beer-Lambert's rule and the effective medium model predictions are noted. The frequency invariant dielectric modulus at 20% rock porosity suggests viability of lower frequency measurements. Porous rock characteristics at much greater depths of field can,

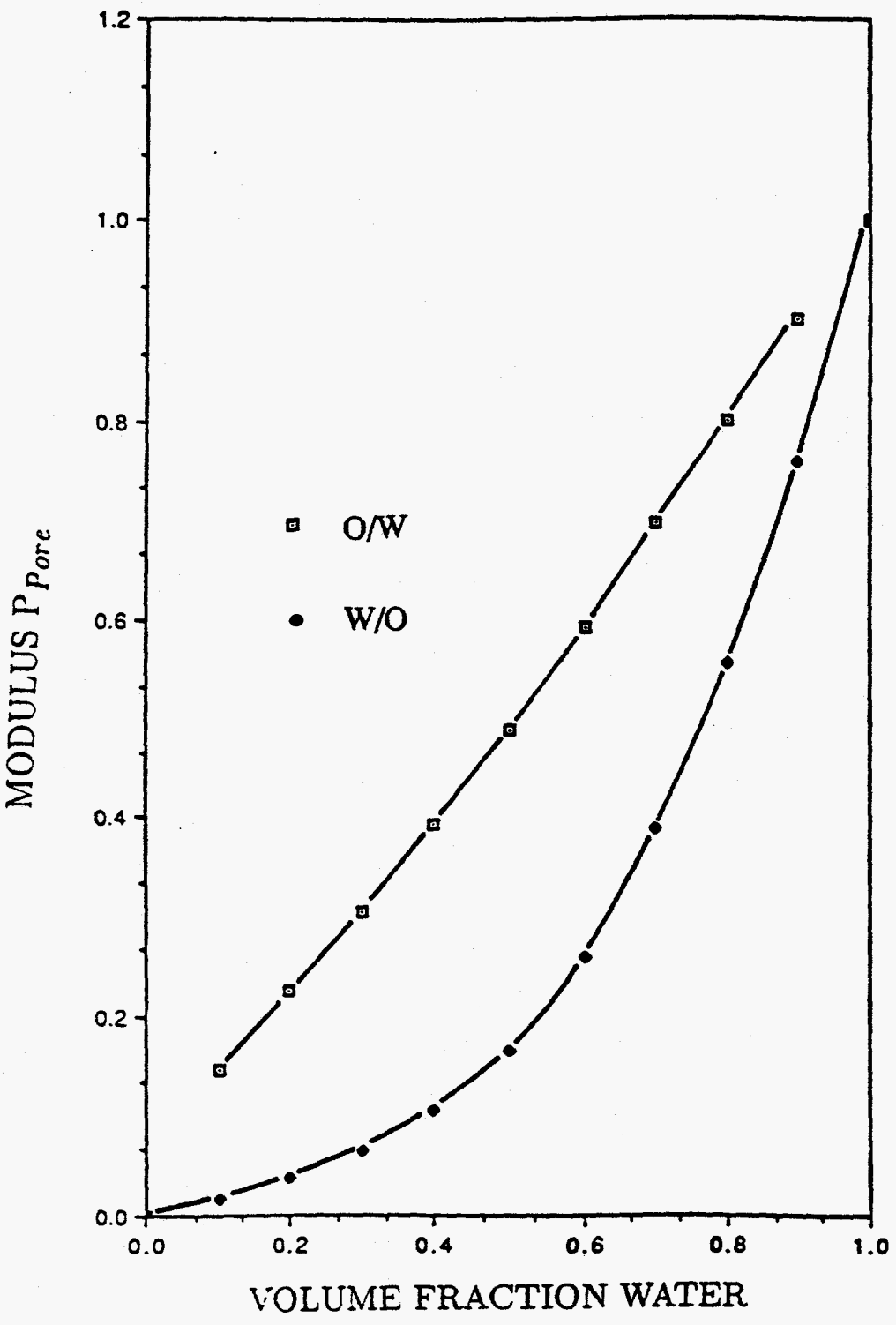

Figure 1-19. Computed Frequency Invariant Dielectric Modulus P_{pore} for O/W and W/O Emulsions inside Berea Sandstone Core with a 20% Porosity

therefore, be obtained since there is much less attenuation at lower frequencies. The lower limit of usable frequency will be governed by salinity considerations. The effect of grain shapes on dielectric properties were examined analytically.

2. Microvisualization experiments and dielectric measurements of emulsion flow in porous media show that dielectric techniques may be applied to determine emulsion characteristics in porous media. The experimental observations were confirmed by theoretical analysis.

REFERENCES

1. Sen, P.N., Scala, C., and Cohen, M.H., *GeoPhysics*, **46**, 781 (1981).
2. Perl, J.P., Bussey, H.E., and Wasan, D.T., *J. Colloid and Interface Sci.*, **108**, 528 (1985).
3. Thomas, C., Perl, J.P., and Wasan, D.T., *J. Colloid and Interface Sci.*, **139**, 1 (1990).
4. Mudgett, R.E., Wang, D.I.C., and Goldblith, S.A., *J. Food Sci.*, **39**, 632 (1974).
5. Kraszewski, A., Kulinski, S., Matuszewski, M., *J. Appl. Phys.*, **47**, 1275 (1976).

Chapter 2

Interfacial Activity Model for Soap/Acid/Surfactant Systems

Introduction

The variation of interfacial tension between an acidic oil and an alkaline solution with pH of the aqueous phase, at constant counterion concentration has been experimentally observed and modelled by Rudin and Wasan (1992). One of the most interesting observations they made was that though an initial pH of around 10.75 is sufficient to generate enough soap (for their model system of oleic acid in decane) for its concentration in the aqueous phase to reach its cmc the minima in interfacial tension (IFT) occurs at an initial aqueous phase pH of about 11.5. This post cmc minima in IFT is unexpected.

In the actual process of enhanced oil recovery a preformed surfactant is added to the alkaline aqueous solution which is called the flood, in order to obtain low oil/water interfacial tension. The purpose of this work was to study the effect of the presence of soap and preformed surfactant on the oil/water IFT. IFT in oil water systems can be reduced due to adsorption of surface active molecules at the interface, increase in activity of the surfactant or solvent molecules in the bulk and the ionization of the surface active adsorbed molecules. The primary objective of this study was to investigate interactions between the natural surfactants (acid) and added surfactant at the oil water interface and in mixed micelles.

Experimental

An oil phase and an aqueous phase were prepared modeling an acidic crude oil and alkaline flood solution. The phases were brought in contact and equilibrated by gentle mixing over an extended period of time (months). The phases were separated after equilibration and the oil/water interfacial tension was measured by the spinning drop technique. The pH of the

aqueous phase was measured prior to oil/water contact using a calomel ion selective electrode. The pH of the aqueous phase was also measured after equilibration.

The oil phase was prepared by dissolving oleic acid, acquired from Sigma chemical company contained in sealed brown glass vials and stored at 0 ^{o}C until use in Decane which was also obtained from Sigma Chemical company. The phase was mixed using a acid cleaned teflon stirrer and kept away from sunlight. The aqueous phases were prepared by dissolving Sodium Dodecyl Benzene Sulphonate in deionized water (conductivity < 10^{-6} semens). Sodium hydroxide and Sodium chloride, obtained from Fisher Scientific, reagent grade, were dissolved in the aqueous phase to obtained desired pH and ionic strength. The total added sodium ion concentration from NaCl and NaOH was kept constant at 0.1 M or 0.171 M. Solutions were prepared by dilutions from the concentrate wherever possible. If salts had to be weighed they were correct within 10^{-4} g.

The aqueous phase was placed in 25 ml glass vials. The pH of the phase was measured, and an equal volume of oil phase introduced gently. The vials were sealed with Teflon. The seal was broken after 2 months and the oil and aqueous phase were separated. The pH of the aqueous phase was measured followed by oil/water IFT. Each IFT measurement was preceded by acid cleaning (at least overnight) followed by repeated DI water rinsing (few hours) of the capillary. The pH probe was rinsed in DI water prior to each measurement and 2 point calibrated before each measurement.

Data and Discussion

The measured IFT for different initial pH of the oil water system in which the acid

concentration was constant at 0.02 M, the total added counterion concentration was constant at 0.1 M and the total added surfactant concentration was 0.1 wt % is shown in Figure 2-1. Figure 2-2 shows the variation of equilibrium pH with initial pH for the same system. It can be seen that the IFT goes through a minima with initial pH. The minima occurs at the aqueous phase initial pH of 11.7. The pH of the aqueous phase at the point of IFT minima is about 9.2.

Figure 2-3 shows the variation of measured IFT with initial pH for two different systems. The only difference in the two systems is the initial surfactant concentration (0.05 wt % and 0.1 wt %). It is observed that the minima in IFT is lowered when the surfactant concentration is reduced to 0.05 wt %. The initial pH for minima drops to 11.5 for the lower surfactant case, but the equilibrium pH for minima are very similar for the 2 systems (about 9.2) as read from Figure 2-4. The interfacial tension at the point of IFT minima for no added surfactant reported by Rudin and Wasan is much lower (less than 0.1 dyn/cm).

The effect of total counterion concentration on the IFT variation over pH of the water phase is shown in Figure 2-5. The two systems are identical except for the total Na+ concentration which are 0.1 M and 0.171 M. The IFTs for the 0.171 M system appear to be slightly lower but are very similar. But the equilibrium pH curves for the two systems shown in Figure 2-6 are different. The equilibrium pH at the IFT minima is lowered to 9 from 9.2 when the counterion concentration is increased to 0.171 M from 0.1 M.

The effect of initial acid concentration in the oil phase on the IFT variation over pH is shown in Figure 2-7. The two curves are for systems which only differ by the total acid concentration (0.02 and 0.0067 M). The minimum IFT is lower for higher acid concentration. The minima occurs at a lower initial pH when the acid concentration is lower. However from

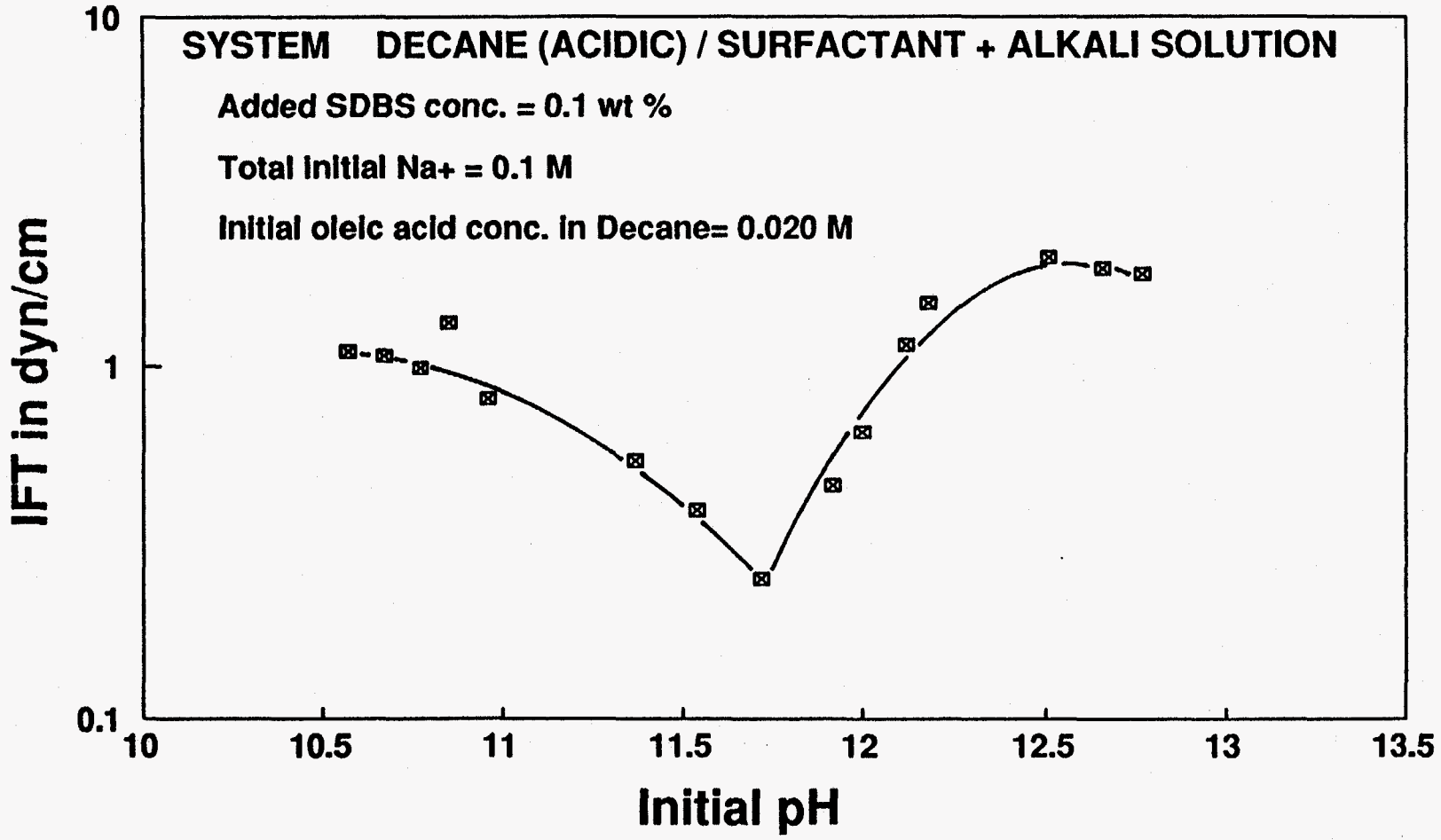

Figure 2-1. Experimentally Determined Variation in IFT with Initial pH of the Aqueous Phase

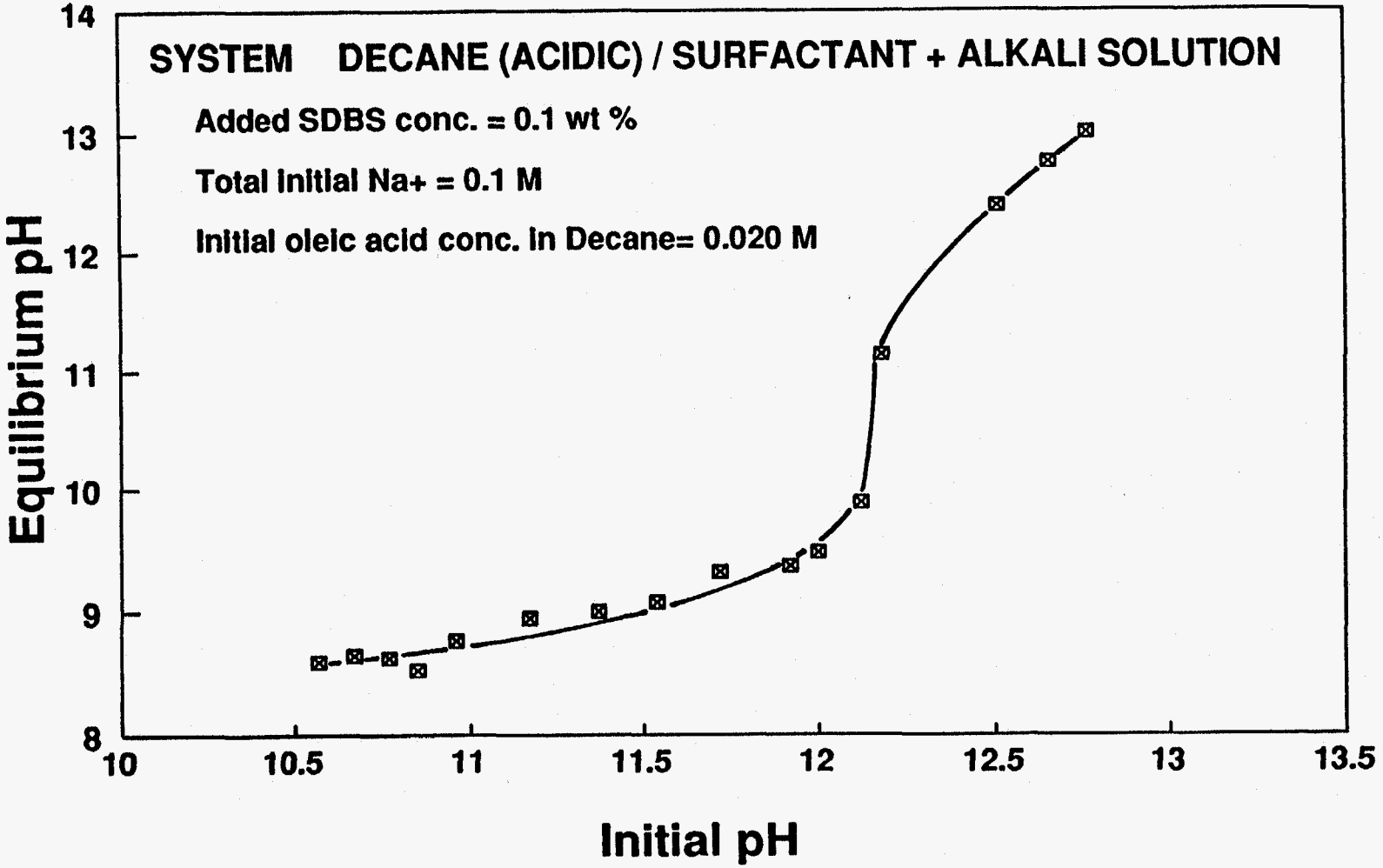

Figure 2-2. Experimentally Determined Variation in Equilibrium pH with Initial pH of the Aqueous Phase

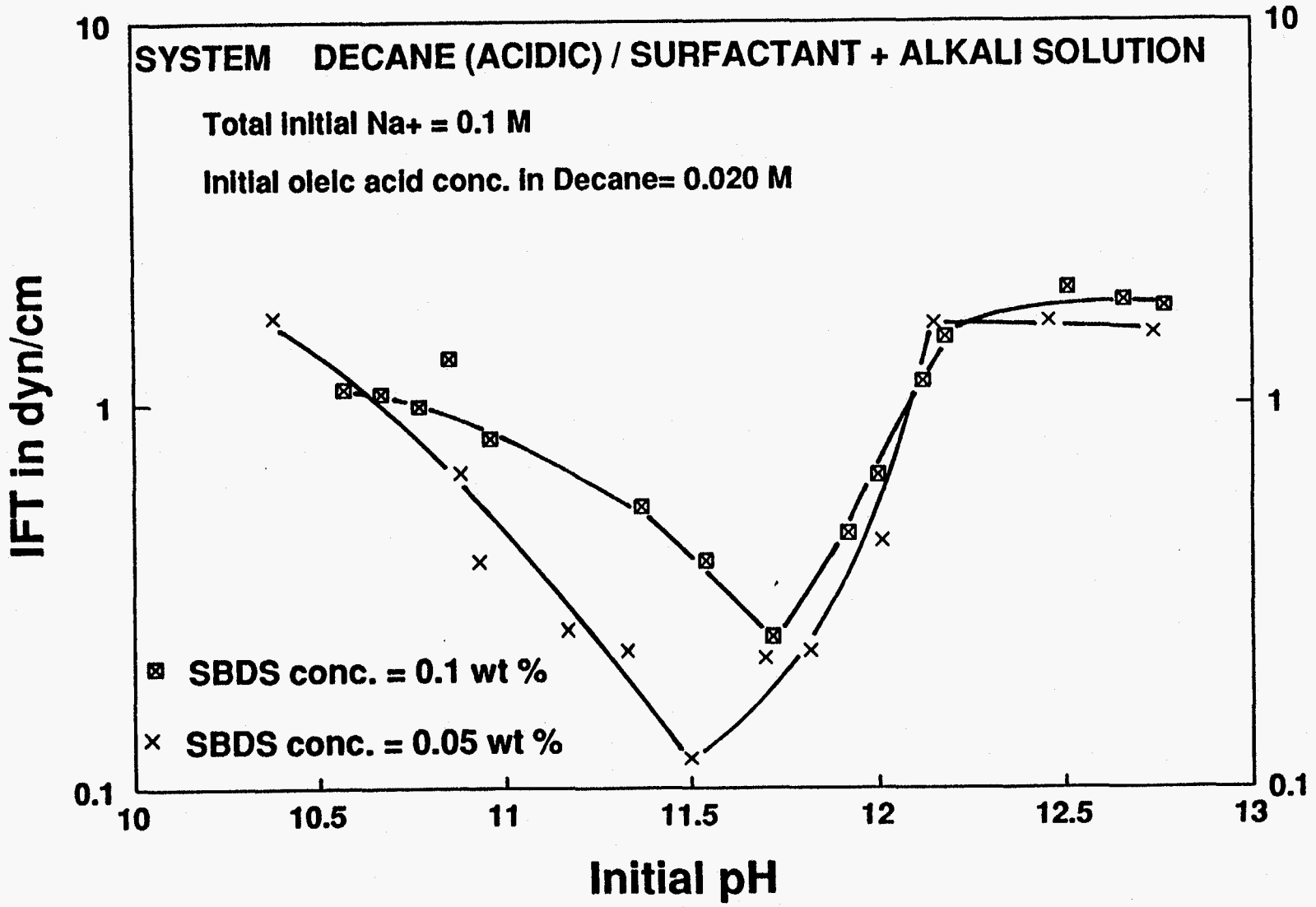

Figure 2-3. Experimentally Determined Effect of Surfactant Concentration on the Variation of IFT Over pH of the Aqueous Phase

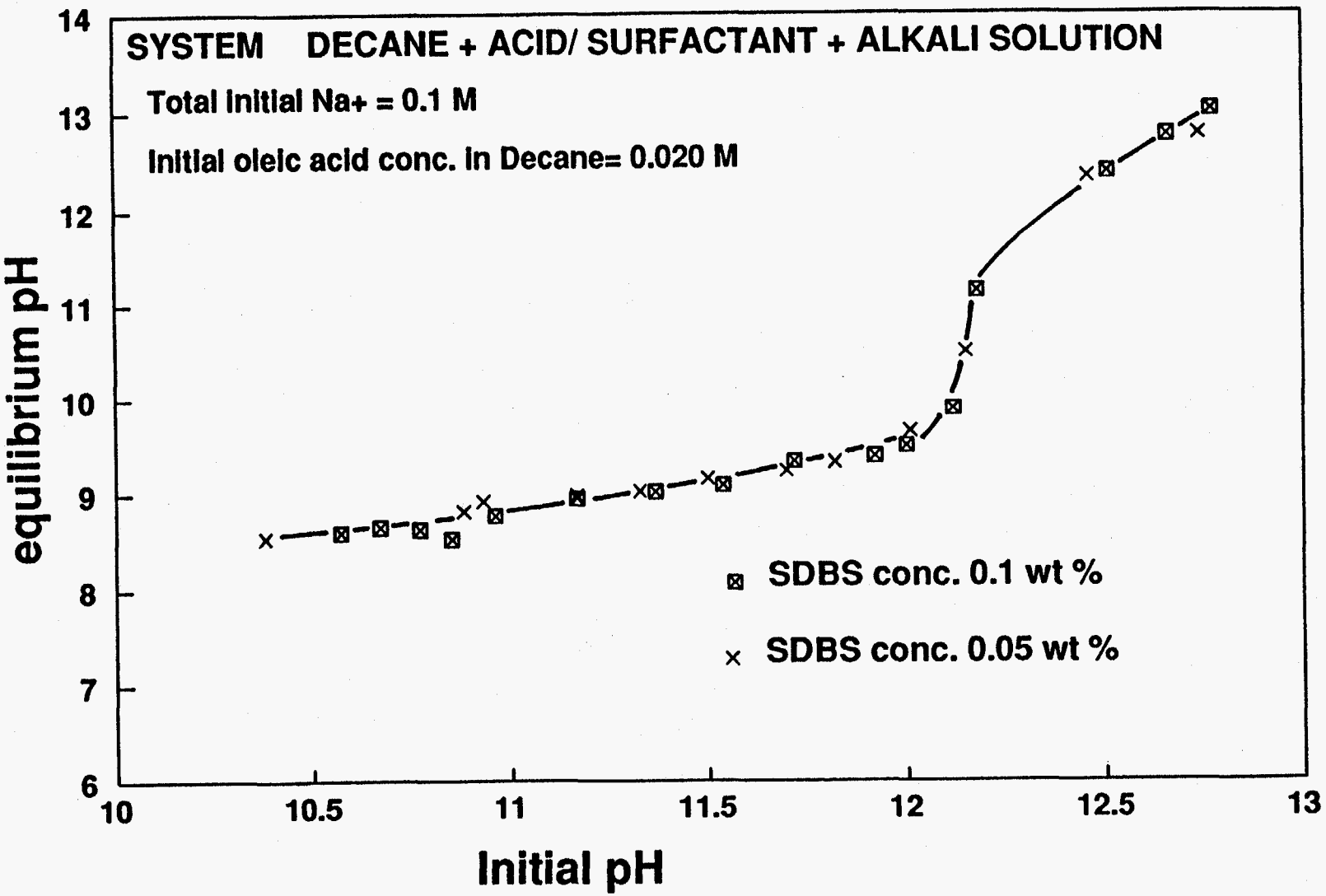

Figure 2-4. Experimentally Determined Effect of Surfactant Concentration on the Variation of Equilibrium pH Over Initial pH of the Aqueous Phase

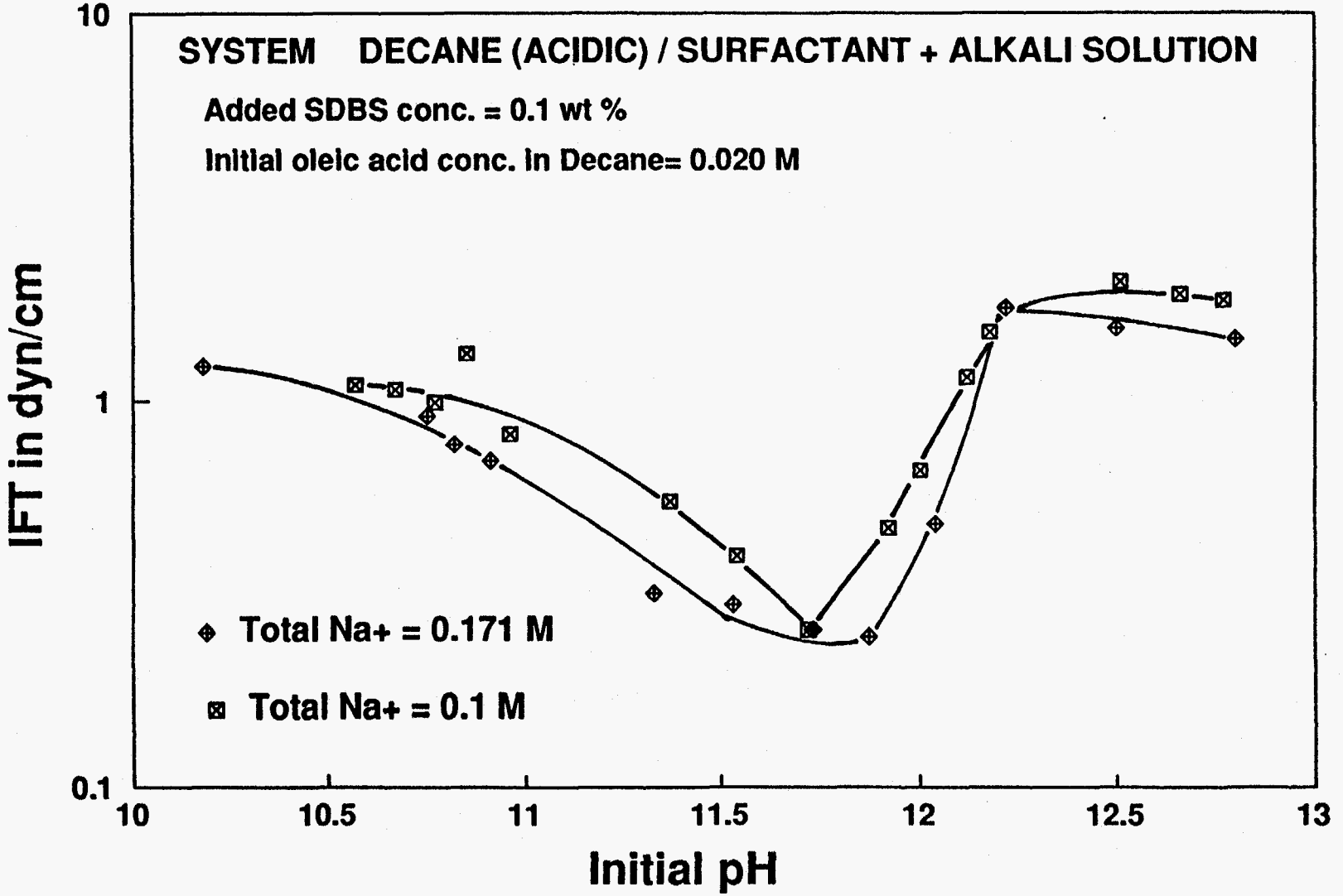

Figure 2-5. Experimentally Determined Effect of Counterion Concentration on the Variation of IFT Over Initial pH of the Aqueous Phase

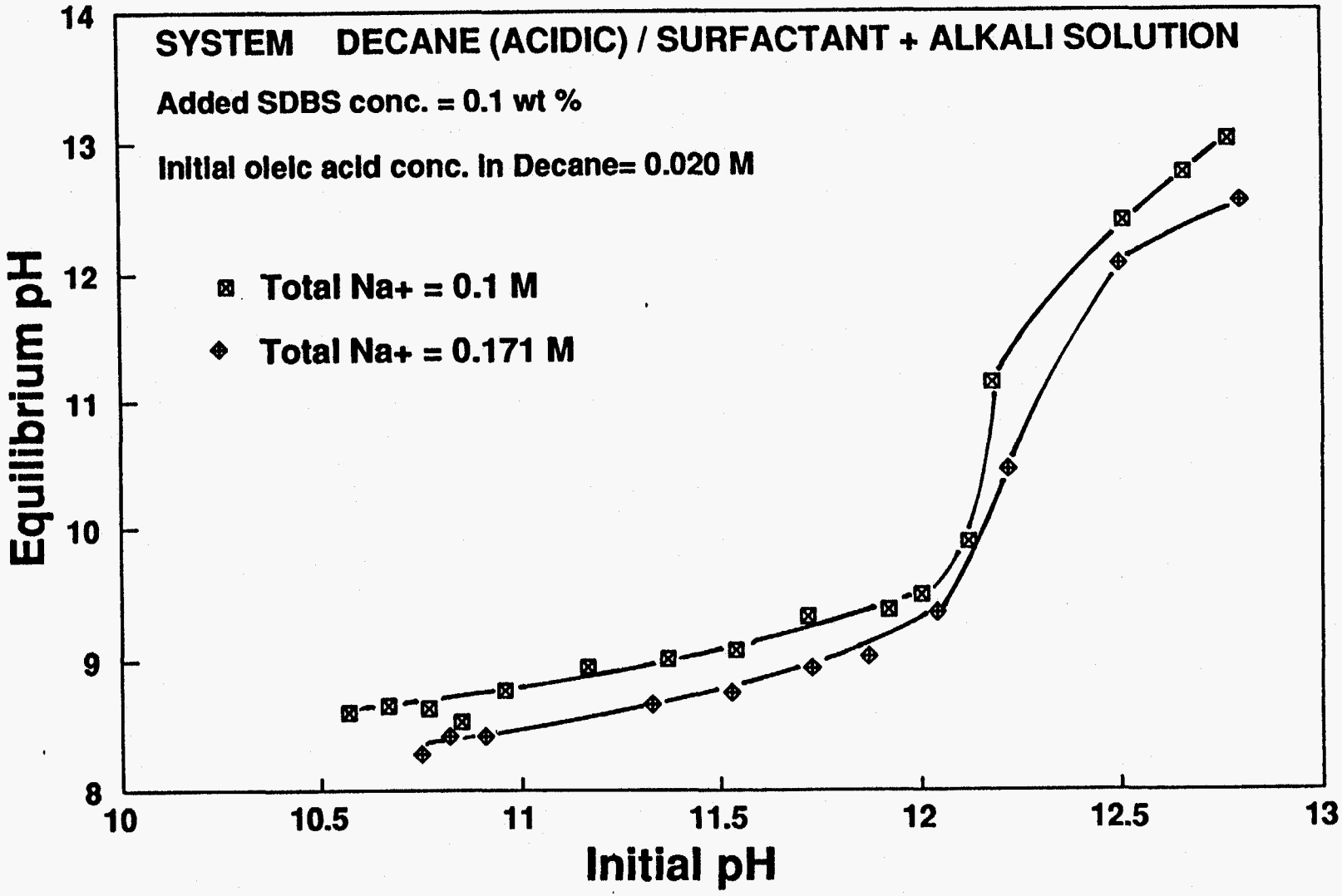

Figure 2-6. Experimentally Determined Effect of Counterion Concentration on the Variation of Equilibrium pH Over Initial pH of the Aqueous Phase

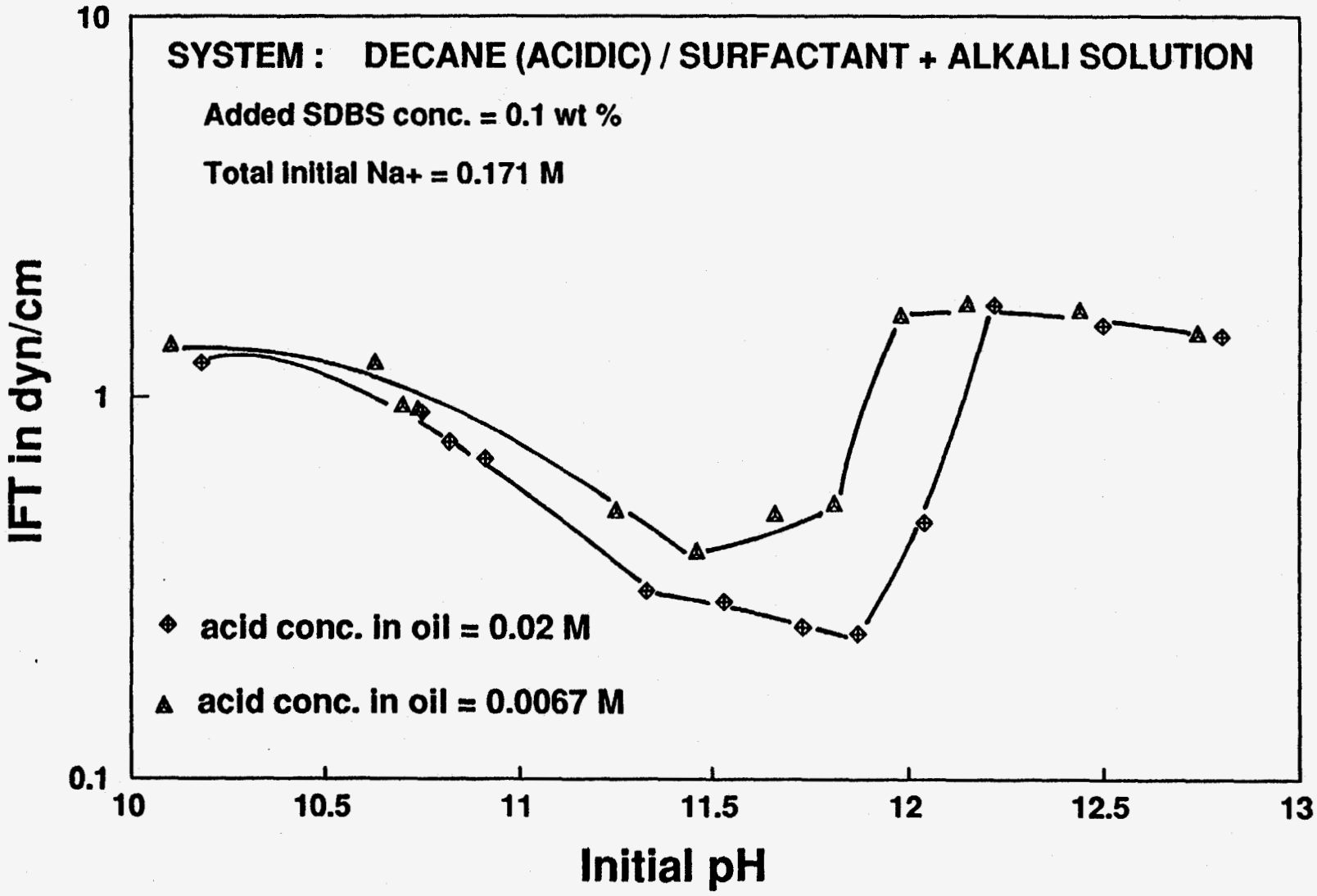

Figure 2-7. Experimentally Determined Effect of Acid Concentration on the Variation of IFT Over Initial pH of the Aqueous Phase

Figure 2-8 we clearly see that the pH of the aqueous phase in equilibrium with the minimum IFT system is about 9 for both systems.

Based on experimental data only we can venture the following. The pH of the aqueous phase at the IFT minima does not change with either the surfactant concentration in water or the acid concentration in the oil. However the total counterion concentration does produce a shift in this pH from 9.2 to 9 as Na^+ increases from 0.1 M to 0.171 M.

Equilibrium Model

The ionized acid plays a major role in lowering of interfacial tension to ultralow values in alkali/acidic oil systems. The interfacial tension goes through a minimum with pH of the aqueous phase. This minima is observed even when a preformed surfactant is added to the system. The purpose of this study is to develop a comprehensive model to account for the presence of the added surfactant and the interaction between the added, generated surfactant (soap) and unionized acid on the interfacial tension. Figure 2-9 shows the system chemistry which occurs when an acidic oil is contacted with an alkaline solution of a surfactant.

Adsorption Model

A model for mixed monolayers has been proposed by Holland (1986). This model accounts for the non-ideality of mixing and has been shown to predict the deviation from ideality observed in surface tensions of non-ionic surfactant mixtures for different compositions of the mixture. In this study we will develop an interfacial model which will account for the deviations from ideality in the interfacial monolayer formed by three surface active compounds, namely the

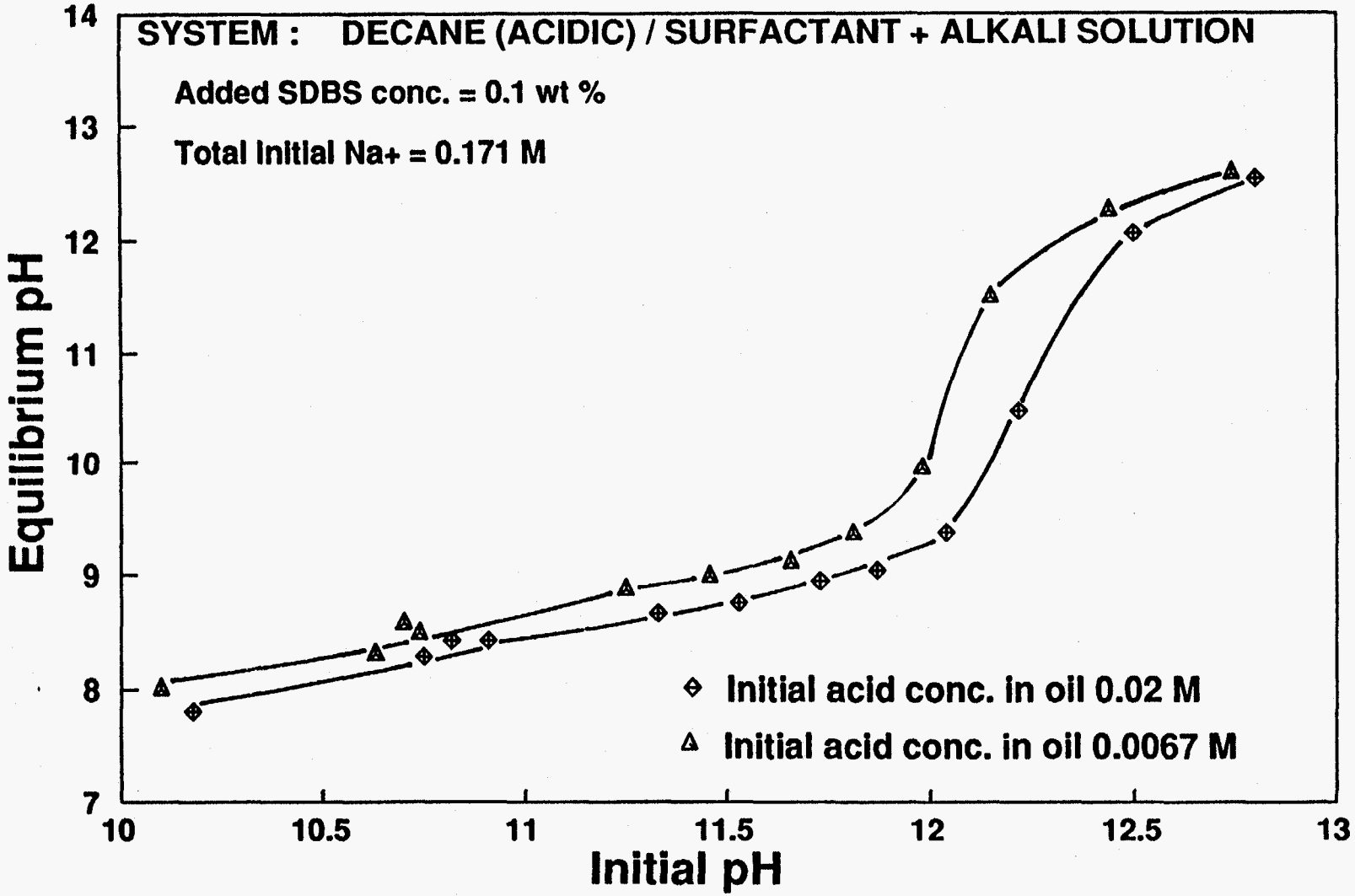

Figure 2-8. Experimentally Determined Effect of Acid Concentration on the Variation of Equilibrium pH Over Initial pH of the Aqueous Phase

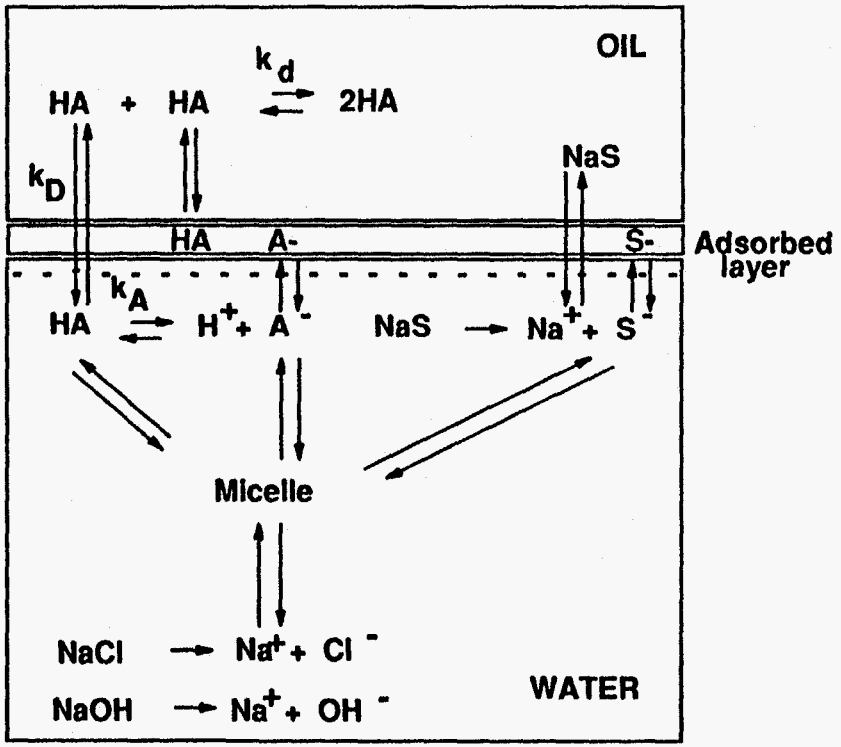

Figure 2-9. System Chemistry

acid, soap and the preformed surfactant, two of which are nonionic.

The approach adopted by Holland and others amounts to using the ideas used in solution thermodynamics. Surface excess free energy, partial molar surface excess energy and surface activity coefficients are defined in a manner analogous to that used in solution thermodynamics. For an ideal mixed monolayer, the surface activity coefficient is unity. The surface activity coefficient quantifies the energy of interaction between each component with the other components of the system. If the interaction is attractive there is a lowering of the total energy of the monolayer due to mixing which gives an activity coefficient of less than unity and the area per molecule is lowered. This amounts to a negative deviation from ideality. If the interaction is repulsive we have a positive deviation from ideality. The total energy of the monolayer increases due to mixing and the surface activity coefficient is greater than unity and the area per molecule is higher.

A quantitative expression for activity coefficient is obtained by considering the free energy change due to mixing per mole of adsorbed surfactant molecules in a monolayer. The surface excess free energy of a mole of adsorbed mixture is the difference between the free energy of a mole in an ideal mixed monolayer and that in an actual mixed monolayer. This excess free energy change per mole of mixture is usually expressed as a function of the mole fraction of the mixture components and a dimensionless interaction energy discussed in Prausnitz.

$$\frac{G^E}{RT} = \beta_{SA}\, x_S x_A + \beta_{SH}\, x_S x_{HA} + \beta_{AH}\, x_A x_{HA} \qquad (2\text{-}1)$$

The above amounts to assuming that the mixed monolayer is regular. The regular solution

theory has been applied to estimate the surface activity coefficients for mixed monolayers (Rosen, 1982). The regular solution approximation may be applied since two of the main components of the mixture, the soap and surfactant, are both anionic and the number of possible configurations should not change significantly due to mixing. The partial molar surface free energy, g^E_A, is the difference in free energy associated with a mole of A in an actual adsorbed monolayer and a mole of A in an ideal mixed monolayer.

$$g^{E,s}{}_A = g^{act}{}_{A,mix} - g^{ideal}{}_{A,mix} = RT \ln x_A^s \gamma_A^s - RT \ln x_A{}^s = RT \ln \gamma_A{}^s \quad (2\text{-}2)$$

Since the energy change due to mixing for a mole of A in a mixture (g) and a mole of mixture (G) are related by

$$\frac{\partial(nG^E)}{\partial n_A} = g^E{}_A \quad (3\text{-}3)$$

where moles of all other components in the mixture are constant, we get the following expression for the surface activity coefficients of component A in the mixture.

$$\ln \gamma_A^S = \beta_{AB}^S x_B^2 + \beta_{AC}^S x_C^2 + (\beta_{AB}^S + \beta_{AC}^S - \beta_{BC}^S) x_B x_C \quad (2\text{-}4)$$

where β^Ss are dimensionless binary interaction energy parameters.

The Davies type adsorption equations, Davies & Rideal (1963), can be used to obtain the specific adsorptions of all the surface active compounds. Since the bulk concentrations are

known from the system chemistry, we get 3 equations in as many variables. The variables here are the moles per unit area of the interface of the unionized acid, the ionized acid and the surfactant. Due to the highly non-linear nature of these equations, variable elimination was not attempted and they were solved iteratively on a micro-computer using a Newton Raphson type convergence technique. The kinetic and electrical contributions to surface pressure were computed from these variables. The equilibrium IFT was computed based on the equation of state (for the adsorbed layer) approach (Ramakrishnan, 1985). The computed surface pressure is subtracted from the IFT for the clean interface to get the final IFT. In the following equations n_S refers to the moles of surfactant per unit area of the interface at equilibrium, while n_A and n_{HA} refer to the moles per unit area of the ionized and unionized acid at the interface.

$$n_A - d_A c_A (1-f) \exp\left[\frac{W_A - RT\ln\gamma_A^s - \psi_o F z_A}{RT}\right] = 0 \qquad (2\text{-}5)$$

or $g_1(n_A, n_{HA}, n_S) = 0$, where W_A is the energy released due to adsorption of a mole of A- to an ideal oil water interface from water, d_A is the length of the surfactant in the aqueous phase and f is the fractional surface covered. The fractional surface covered is arrived at in the following manner. Adamson (1982) and Ramakrishnan & Wasan (1985) expressed the area per molecule in the ideal mixed monolayer as the mole fraction weighted sum of the individual areas. Since the specific adsorption is the reciprocal of the area per mole we get

$$f = \frac{n_A}{n_{A,max}} + \frac{n_S}{n_{S,max}} + \frac{n_{HA}}{n_{HA,max}} \qquad (2\text{-}6)$$

If the monolayer is non-deal we get

$$\frac{n_{soap} + n_{acid} + n_{surf}}{n_{\max,mixed}} = \gamma^{S}_{acid}\frac{n_{acid}}{n_{acid,\max}} + \gamma^{S}_{soap}\frac{n_{soap}}{n_{soap,\max}} + \gamma^{S}_{surf}\frac{n_{surf}}{n_{surf,\max}} \qquad (2\text{-}7)$$

The adsorption of the acid from the oil phase is quantified by,

$$n_{HA} - d_{HA}\, c_{HA}\, (1-f)\, \exp\left[\frac{W_{HA} - RT\, \ln\gamma^{s}_{HA}}{RT}\right] = 0 \qquad (2\text{-}8)$$

or $g_2(n_A,n_{HA},n_S) = 0$ where W_{HA} is the energy released due to the adsorption of a mole of acid to an ideal oil-water interface from the bulk oil and d_{HA} is the length of the acid in the oil phase. The adsorption of surfactant from the aqueous phase is quantified by,

$$n_S - d_S\, c_S\, (1-f)\, \exp\left[\frac{W_S - RT\ln\gamma^{s}_{S} - \psi_o F z_s}{RT}\right] = 0 \qquad (2\text{-}9)$$

or $g_3(n_A,n_{HA},n_S) = 0$, where W_S is the energy released due to adsorption of a mole of surfactant at an ideal oil water interface from the bulk aqueous phase and d_S is the length of the surfactant in the aqueous phase.

Solution Technique

These adsorption equations were solved for the three variables n_A, n_S and n_{HA} using a

modified Newton-Raphson type scheme. Iterations were stopped when all the variable values from two successive steps agreed upto 5 significant digits.

$$\begin{bmatrix} n_A^{n+1} \\ n_S^{n+1} \\ n_{HA}^{n+1} \end{bmatrix} = \begin{bmatrix} n_A^{n} \\ n_S^{n} \\ n_{HA}^{n} \end{bmatrix} + \begin{bmatrix} \frac{\partial g_1}{\partial n_A} & \frac{\partial g_1}{\partial n_S} & \frac{\partial g_1}{\partial n_{HA}} \\ \frac{\partial g_2}{\partial n_A} & \frac{\partial g_2}{\partial n_A} & \frac{\partial g_2}{\partial n_{HA}} \\ \frac{\partial g_3}{\partial n_A} & \frac{\partial g_3}{\partial n_S} & \frac{\partial g_3}{\partial n_{HA}} \end{bmatrix}^{-1} \times \begin{bmatrix} -g_1^{\,n} \\ -g_2^{\,n} \\ -g_3^{\,n} \end{bmatrix} \qquad (2\text{-}10)$$

The fractional surface covered and the resulting surface pressure were computed based on the values of specific adsorptions.

(2-11)

The kinetic contribution to the surface pressure is given by (Frumpkin, 1925).

$$\pi_K = RT\, n_{\max} \ln (1-f)$$
$$\text{where} \quad n_{\max} = \frac{n_A + n_S + n_{HA}}{f} \qquad (2\text{-}12)$$

The electrical contribution to the surface pressure accounts for the repulsion in the adsorbed monolayer of ionic surfactants (Ramakrishnan, 1985).

$$\pi_E = \frac{4RT}{F}\sqrt{2RT\varepsilon_m c_{Na}}\left[\cosh\left(\frac{F\psi(0)}{2RT}\right) - 1\right] \qquad (2\text{-}13)$$

where,

$$\psi(0) = -\frac{2RT}{F}\sinh^{-1}\left[\frac{(n_A+n_S)F}{\sqrt{8\varepsilon_m RTc_{Na}}}\right] \qquad (2\text{-}14)$$

Model for System Chemistry

It has been shown that oleic acid dimerizes in the oil phase (Mukherjee 1965). At equilibrium the following relation holds

$$c_{2HA} = k_d\, c_{HA}^2 \qquad (2\text{-}15)$$

where c_{HA} is the concentration of the acid in the oil phase and c_{2HA} is the conc. of the dimer in the oil and k_d is the dimerization reaction equilibrium constant.

The distribution of the acid between the oil and the aqueous phase may be approximated by the distribution coefficient since the concentration of the acid in the aqueous phase is very low. The partitioning can be written as

$$c_{HA} = k_D\, c_{HA,w} \qquad (2\text{-}16)$$

where k_D is the partition coefficient and $c_{HA,w}$ is the concentration of the acid in the aqueous phase.

The dissociation of the acid in water may be quantified by

$$k_A c_{HA,w} = c_{H+} c_{A-} \tag{2-17}$$

The water dissociation constant gives,

$$k_W = c_{OH-} c_{H+} \tag{2-18}$$

It has been shown by Chan & Shah, 1980, and later by Granet et al that sodium salts of the surfactant as well as the acid tends to partition into the oil phase due to the high salt concentration in the aqueous phase. This partitioning can be quantified in the following manner,

$$S- + Na = NaS_o,$$

$$\mu^o_{NaS,oil} + RT \ln a_{NaS,oil} = \mu^o_{Na+} + RT \ln a_{Na+} + \mu^o_{S-} + RT \ln a_{S-}$$

$$\exp\left[\frac{\Delta G^o}{RT}\right] = \frac{C_{Na} C_S \gamma_{Na} \gamma_S}{C_{NaS,o}} \tag{2-19}$$

The oil phase is assumed ideal. The partitioning of the sodium salts of the soap may also occur and can be quantified in the above manner to give

$$\mu^{o}_{NaA,oil} + RT \ln a_{NaA,oil} = \mu^{o}_{Na+} + RT \ln a_{Na+} + \mu^{o}_{A-} + RT \ln a_{A-}$$

$$\exp\left[\frac{\mu^{o}_{NaA,oil} - \mu^{o}_{Na+} - \mu^{o}_{A-}}{RT}\right] = \frac{C_{Na} C_{A} \gamma_{Na} \gamma_{A}}{C_{NaA,o}} \qquad (2\text{-}20)$$

Several researchers have experimentally studied the minima observed in oil/water IFT, with salinity of the aqueous phase (Granet et. al. 1990, Chan and Shah 1980). The effect of electrolyte concentration of the aqueous phase on the IFT between oil and water is known. However, a comprehensive quantitative model which accounts for all the observed phenomena is lacking. Increasing the electrolyte concentration of the aqueous phase beyond 0.1 M may cause the bulk activity of the other dissolved species to increase. This increases the interfacial adsorption of the generated soap as shown by Rosen (1988). Further increase in the electrolyte concentration in the aqueous phase causes its activity to increase and the surfactants are "salted out" of the aqueous phase. If the sodium salts of the surface active anions are oil soluble, they diffuse into the oil phase. The net effect of salting out may be an increase in IFT. Presence of high concentrations of electrolyte also cause separation of the surfactant monomers into the micellar phase at lower concentrations (Rosen 1988) as well as the formation of larger micelles.

For an accurate prediction of bulk, surface and oil phase concentrations of surfactants we need to estimate the activity coefficients of the surface active anions in the presence of a high electrolyte concentration. Several models such as those proposed by Guggenhiem (1955), (1967) and later by Bromley (1973), and Pitzer (1979) for estimating the activity coefficient of dissolved ions in aqueous solutions are available. The equation proposed by Guggenhiem is of the form

$$\ln\gamma_{A^-} = \frac{-B\sqrt{I}}{1+\sqrt{I}} + \sum_{cations} \beta_{Cations-A} C_{Cations} \qquad (2\text{-}21)$$

where I is the ionic strength of the aqueous phase and B is a constant. ß is a binary interaction energy parameter for each cation anion pair of the aqueous phase. These binary interaction energy parameters for the aqueous phase have not been estimated for surface active anions. These need to be estimated by fitting the experimental data to accurately describe surfactant partitioning between the oil and water phases.

At equilibrium the initial acid in the oil phase is distributed as acid remaining in the oil, dimer in oil, ionized acid in water, ionized acid in the micelles, unionized acid in the water and unionized acid in the micelles. The amount of species at the interface is negligible. A material balance gives,

$$c_{HA,i} = c_{HA} + 2c_{2HA} + \frac{c_{HA,w}}{V_R} + \frac{c_{A-}}{V_R} + \frac{M_A}{V_o} + \frac{M_{HA}}{V_o} \qquad (2\text{-}22)$$

where $c_{HA,i}$ is the conc. of acid initially present in the oil, V_R is the ratio of the volume of the oil and water phases, M_A is the moles of ionized acid in the micellar phase.

Material balance on Na+ gives

$$c_{s,i} + c_1 + c_2 = c_{Na+} + V_R C_{NaS,o} + \frac{(1-\alpha)M}{V_w} \qquad (2\text{-}23)$$

where $c_{s,i}$ is the added surfactant conc., c_1 is the concentration of the added NaOH, M is the total moles in the micellar phase, V_w is the volume of the water phase and α is the fraction of counterion binding to the micellar surface.

A material balance on the added surfactant gives,

$$c_{Si} = c_{S-} + \frac{M_S}{V_w} + V_R c_{NaS,o} \qquad (2\text{-}24)$$

Where M_S is the moles of surfactant in the micellar phase.

Overall neutrality imposes the following charge balance,

$$c_{Na+} + c_{H+} = c_{OH-} + c_2 + c_{S-} + c_{A-} + \frac{\alpha M}{V_w} \qquad (2\text{-}25)$$

Mixed micellization - Pseudo phase separation approach

The pseudo-phase separation model (PSM), Stainsby & Alexander, 1950, holds the following view of micellization. Adding surfactant to aqueous phase causes its bulk concentration to increase till a critical concentration of surfactant is reached. Addition of surfactant beyond this critical concentration causes the formation of surfactant micelles. All the surfactant added after the critical concentration does not increase the critical concentration, but forms micelles. This critical concentration is called the critical micellization concentration (cmc). The surface and interfacial tension (IFT) depends on the extent of adsorption, bulk phase activities of the surfactant and solvent molecules. Thus no further lowering of IFT that can be achieved by a single surfactant beyond its cmc.

The PSM approach has been applied to non-ionic surfactant mixtures by Holland & Rubingh, 1983. Kamrath et al, 1983, have applied the phase separation approach to model mixed cmcs of ionic surfactants having a common counterion, in the presence of a salt of the same. Their model though developed with a generic mixing model, showed some variation in the values of the micellar interaction parameter, when the regular solution approximation was used to model mixing in the micellar phase.

Micelles are present in the alkaline flood solution at equilibrium with an acidic oil. When no surfactant is added to the flood, these micelles are made up of ionized and unionized acid, partitioned from the oil phase. When surfactant is also present, the micelles are expected to contain surfactant monomers in addition to the above two. Since the PSM approach views micelles as a separate phase, all the thermodynamic relationships applicable to phase equilibria can be applied to micellization. This model strictly applies when micellar

aggregates are very large, since the finite aggregation number of micelles is not accounted for in this model. In the system being studied, micelles are expected to be very large because of the high counterion concentration. Non-ideality arises due the interaction between the different surface active molecules in the micelle. Rosen & Hua (1982) have shown that the observed "synergistic" lowering of IFT in mixtures of surfactants beyond that possible by either component alone, is due to the difference in the interaction of the surfactants in the mixed monolayer and mixed micelles. The concept of surfactants mixing ideally and non-ideally apply to the micelles as well and has been discussed by Holland et. al. (1983) and Hall et. al. (1985).

At equilibrium in a system containing a single surfactant species at a conc. above its cmc,

$$\mu_i^M = \mu_i^0 + RT \ln cmc_i^P \qquad (2\text{-}26)$$

The superscript M refers to the variables in the micellar phase. μ_i is the chemical potential of the surfactant in the bulk solution, μ_i^0 is the chemical potential of i, at a standard state, R is the universal gas constant, T is the temperature and cmc_i^P is the concentration of i in the bulk in the presence of pure micelles.

By definition the activity coefficient of a compound in a mixture is the fugacity of the compound from the mixture divided by the fugacity of the compound from an ideal mixture of identical composition. Adopting the above definition for a micelle we get

$$\mu_i^M = \mu_i^{M,pure} + RT \ln \frac{\gamma_i^M x_i^M f_i^{M,pure}}{f_i^{M,pure}} \qquad (2\text{-}27)$$

The chemical potential of i in the bulk in the mixed system is given by

$$\mu_i = \mu_i^0 + RT \ln c_i \gamma_i \qquad (2\text{-}28)$$

At equilibrium between the surfactant monomer and the surfactant in the micelle we get,

$$\mu_i^0 + RT \ln c_i \gamma_i = \mu_i^0 + RT \ln cmc_i^p + RT \ln x_i^M \gamma_i^M \qquad (2\text{-}29)$$

Thus the pseudo-phase separation model for micellization applied to the formation of mixed micelles gives

$$c_A = \frac{cmc_A \, x^M{}_A \, \gamma^M{}_A}{\gamma_A} \qquad (2\text{-}30)$$

where the subscripts denote the component, and the superscript denotes the phase (no superscript denotes the aqueous phase). The standard state of a micelle is defined as the pure micelle of a surfactant in an aqueous solution containing only the surfactant at its cmc. Equations for the formation of mixed micelles of non-ionic surfactants without added electrolyte have been discussed by Holland et. al. (1983). For the surfactant in aqueous

solution the standard state is the infinitely dilute solution of the surfactant.

Cmcs in mixed surfactant systems have shown considerable deviation from ideality. Mixtures of fluorocarbon-hydrocarbon surfactants are known to show positive deviations from ideality, Mukherjee & Yang, 1976. Mixtures of anionic and cationic surfactants have shown negative deviations from ideality, Zhao et al, 1980. More recently the regular solution approximation has been applied to the micellar phase by Kamrath and Frances, 1983. Applying the regular solution approximation to the micellar phase, we obtain

$$\gamma_S^M = \exp\left[\beta_{SA}x_A^2 + \beta_{SH}x_{HA}^2 + (\beta_{SA}+\beta_{SH}-\beta_{AH})\,x_A x_{HA}\right]$$
$$\gamma_A^M = \exp\left[\beta_{SA}x_S^2 + \beta_{AH}x_{HA}^2 + (\beta_{SA}+\beta_{AH}-\beta_{SH})\,x_S x_{HA}\right] \qquad (2\text{-}31)$$

where ßs are constants analogous to the constants in the Margules two suffix equation and quantify an overall interaction between the compounds in the mixed micelle. The ß's are dimensionless because they are estimates of free energy change due to mixing per mole, divided by the product RT.

The sparingly soluble unionized acid in the aqueous phase tends to partition into the micellar phase. The distribution of the unionized acid between the bulk water and the micellar phase can be represented by the Boltzman's distribution law.

$$c_{HA,w} = c^M \frac{c_{HA}^M}{c^M} \exp[-\frac{\Delta G}{RT}] = c^M x_{HA}^M \exp[\frac{-\Delta G}{RT}] \qquad (2\text{-}32)$$

Where c^M is the molar conc. of the micellar phase, $c_{HA}{}^M$ is the concentration of acid in the micellar phase and G is the free energy change of a mole of acid moving between the bulk and micellar phases. The above expression may be simplified to $x_{HA}{}^M = M_1\, c_{HA,w}$, since the other terms in equation 12 have experimentally been shown to be constant by Rudin & Wasan, 1992.

Solution Technique

The above system of equations were reduced to 4 equations in 4 variables by variable elimination. Further variable elimination resulted in equations which were impractical for handling. The four equations in four variables were then solved simultaneously. A Newton-Raphson type scheme applicable for 4 variables was applied. This section discusses the solution procedure used for solving the equations.

Applying the pseudo-phase separation approximation along with the mass balances for the acid, surfactant and sodium ions and the charge balance, we get the following four equations in four variables. The independent variables are: X_A (mole fraction of soap in the micellar phase), M (total moles in the micellar phase), C_{HA} (concentration of acid in oil) and C_{Na} (concentration of free sodium ions in water).

$$C_{HA,i} - C_{HA} - 2k_d C_{HA}^2 - \frac{C_{HA}}{V_R K_D} - \frac{Mx_A}{V_o} - \frac{M_2 C_{HA} M}{V_o} - \left[\frac{1}{V_R} + \frac{C_{Na}}{K_{A,D}} g_3\right] C_A = 0 \qquad (2\text{-}33)$$

$$C_{S,i} - \frac{M}{V_w} + \frac{Mx_A}{V_w} + \frac{MC_{HA}M_2}{V_w} - \left[1 + \frac{V_R C_{Na}}{K_S}\right] C_S = 0 \qquad (2\text{-}34)$$

$$C_{S,i} + C_{NaOH,i} + C_{NaCl,i} - C_{Na} - (1-\alpha)\frac{M}{V_W} - V_R\, C_{Na}\, g_3 \left[\frac{C_S}{K_{S,p}} + \frac{C_A}{K_{A,p}}\right] = 0 \qquad (35)$$

$$C_{Na} + \frac{K_A}{K_D}\frac{C_{HA}}{C_A} - \frac{K_w K_D}{K_A}\frac{C_A}{C_{HA}} - C_{Cl} - C_A - C_S - \alpha\frac{M}{V_W} = 0 \qquad (2\text{-}36)$$

where

$$C_A = C_A^P\, X_A \exp\left[\left(\beta_{SA}^m (1-X_A-M_2C_{HA})^2 + \beta_{AH}^m M_2^2 C_{HA}^2 + (\beta_{SA}^m + \beta_{AH}^m - \beta_{SH}^m)\,(1-X_A-M_2C_{HA})M_2C_{HA} \right) - \ln 10 \left(\frac{B\sqrt{I}}{1+\alpha\, A\, \sqrt{I}} + B_{Na-A}C_{Na} \right) \right] \qquad (2\text{-}37)$$

and

$$C_S = C_S^P\ (1 - X_A - M_2 C_{HA})$$
$$\exp\left[\left(\beta^m_{SA} X_A^2 + \beta^m_{SH} M_2^2 C_{HA}^2 + (\beta^m_{SA} + \beta^m_{SH} - \beta^m_{AH})\ X_A M_2 C_{HA}\right)\right. \qquad (2\text{-}38)$$
$$\left. - \ln 10 \left(\frac{B\sqrt{I}}{1+\alpha\ A\ \sqrt{I}} + B_{Na\text{-}S} C_{Na} \right)\right]$$

and

$$g_3 = \exp\left(\ln 10 \left[\frac{B\sqrt{I}}{1+\alpha 0.3\sqrt{I}} + \frac{B\sqrt{I}}{1+\alpha 0.6\sqrt{I}} + 0.055 C_{Cl} + B_{anion\text{-}Na} C_{Na} \right] \right) \qquad (2\text{-}39)$$

and

$$M_2 = \frac{1}{C^m\ K_D} \exp\left[\frac{\Delta G_{mic}}{RT}\right] \qquad (2\text{-}40)$$

The expression for g_3 arises due to partitioning of the sodium salts of the soap and surfactant into the oil phase, which may or may not be significant, but will be accounted for in the proposed model. Earlier we had shown that,

$$\mu^{o}_{NaS,oil} + RT \ln a_{NaS,oil} = \mu^{o}_{Na+} + RT \ln a_{Na+} + \mu^{o}_{S-} + RT \ln a_{S-}$$

$$\exp\left[\frac{\Delta G^{o}}{RT}\right] = \frac{C_{Na} C_{S} \gamma_{Na} \gamma_{S}}{C_{NaS,o}} \qquad (2\text{-}41)$$

The function g_3 is the product of the two activity coefficients.

The search technique used may be represented by the following equation,

$$\begin{bmatrix} x_A^{n+1} \\ M^{n+1} \\ c_{HA}^{n+1} \\ c_{Na}^{n+1} \end{bmatrix} = \begin{bmatrix} x_A^{n} \\ M^{n} \\ c_{HA}^{n} \\ c_{Na}^{n} \end{bmatrix} + \begin{bmatrix} \frac{\partial f_1}{\partial x_A} & \frac{\partial f_1}{\partial M} & \frac{\partial f_1}{\partial c_{HA}} & \frac{\partial f_1}{\partial c_{Na}} \\ \frac{\partial f_2}{\partial x_A} & \frac{\partial f_2}{\partial M} & \frac{\partial f_2}{\partial c_{HA}} & \frac{\partial f_2}{\partial c_{Na}} \\ \frac{\partial f_3}{\partial x_A} & \frac{\partial f_3}{\partial M} & \frac{\partial f_3}{\partial c_{HA}} & \frac{\partial f_3}{\partial c_{Na}} \\ \frac{\partial f_4}{\partial x_A} & \frac{\partial f_4}{\partial M} & \frac{\partial f_4}{\partial c_{HA}} & \frac{\partial f_4}{\partial c_{Na}} \end{bmatrix}^{-1} \times \begin{bmatrix} -f_1^{n} \\ -f_2^{n} \\ -f_3^{n} \\ -f_4^{n} \end{bmatrix} \qquad (2\text{-}42)$$

where the superscripts n and n+1 represent the values of functions at the previous and current iteration. Values of the variables were obtained by generating the expression for the above partial derivatives and programming the above equation on a micro-computer. Iterations were stopped when the all variables from two successive iterations were identical till the 8th significant digit.

Based on the values of the variables obtained the equilibrium pH was computed from the following equation, which is derived from Equation 2-9, where c_{OH} is the equilibrium concentration of OH- ions.

$$c_{OH}^2 - (c_{Na} - c_2 - c_S - c_A - \frac{\alpha M}{V_w})\, c_{OH} - k_w = 0 \qquad (2\text{-}43)$$

Results and Discussion

Figure 2-10 compares predictions for interfacial tension (IFT) based on monolayer and micellar non-ideality, using the pseudo phase separation approximation and experimentally measured IFT data for a model system. The model system contained oleic acid in decane (0.02 M) contacted with an alkaline aqueous solution of Sodium dodecyl benzene sulfonate (0.1 wt %) with an electrolyte concentration (0.1 M). Figure 2-11 shows a comparison of the experimentally measured pH variation over initial aqueous phase pH for a similar experimental system along with predictions from the model. Figure 2-12 shows a comparison of the experimental IFT variation over initial alkali concentrations for two different surfactant (SDBS) concentrations of 0.1 wt % and 0.05 wt % at total counter-ion concentration of 0.1 M and predictions from the model for each. It is observed that decreasing the surfactant concentration from 1000 ppm to 500 ppm produces lower IFTs.

The minima in interfacial tension is produced due to the following reasons. Figure 2-13 shows the predicted decrease in the kinetic contribution to surface pressure (non-electrostatic effects) and the increase in the electrostatic contribution to surface pressure with

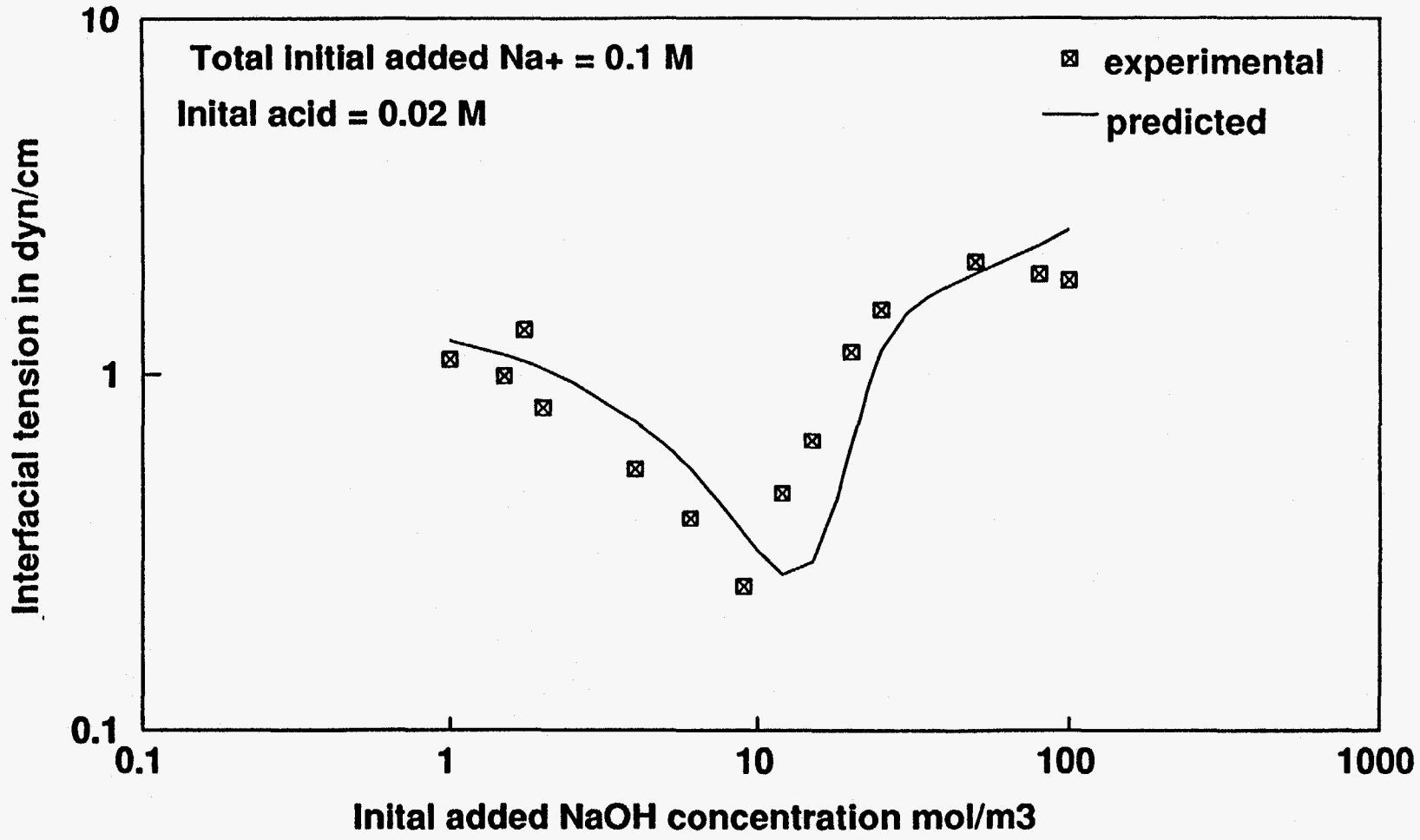

Figure 2-10. Experimental and Computed IFT Based on Monolayer and Micellar non-ideality Theory

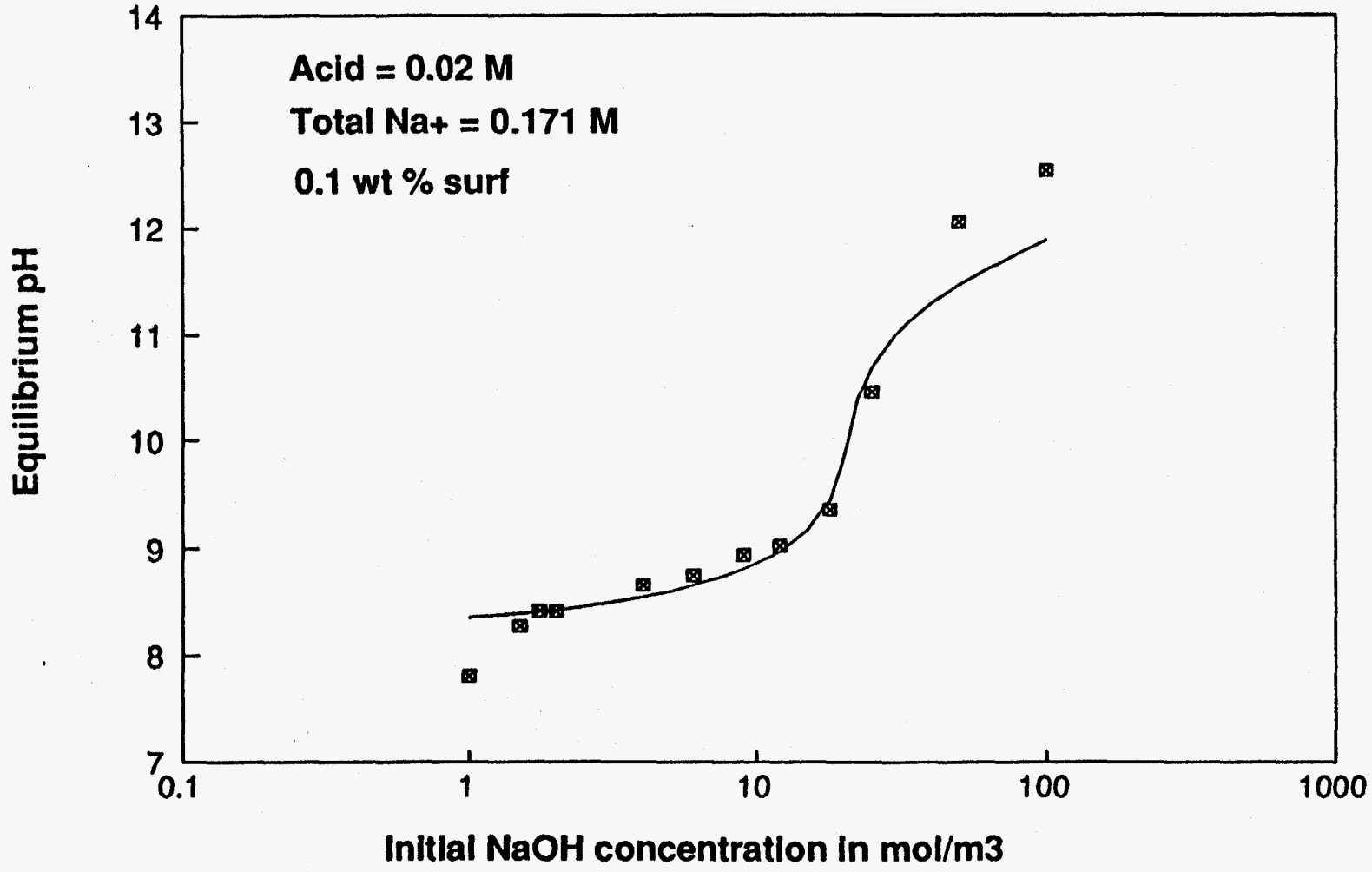

Figure 2-11. Measured and Computed pH Based on Monolayer and Micellar non-ideality Theory

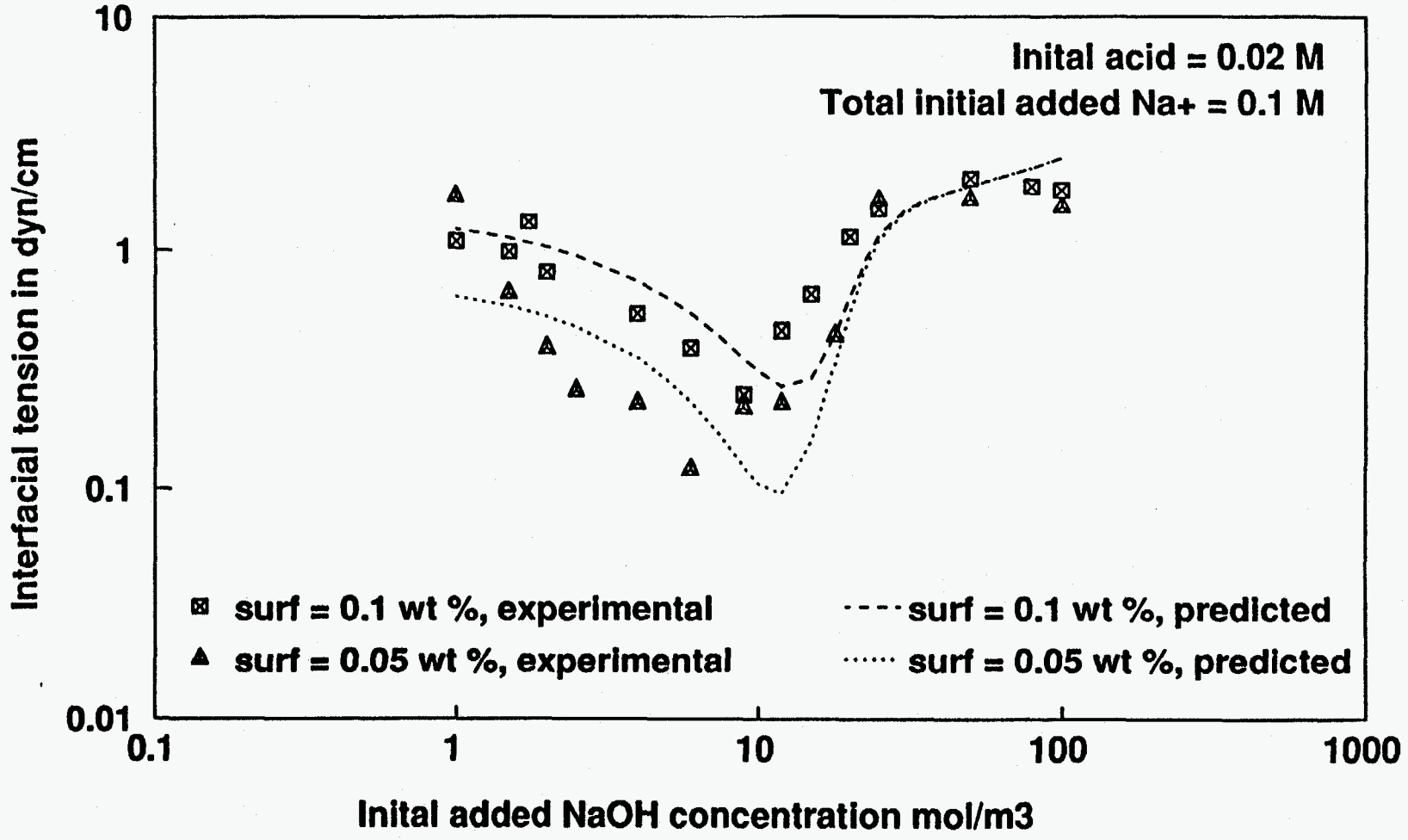

Figure 2-12. Effect of Surfactant Concentration of the position of the IFT Minima, Comparison of the Experimental and Computed Values

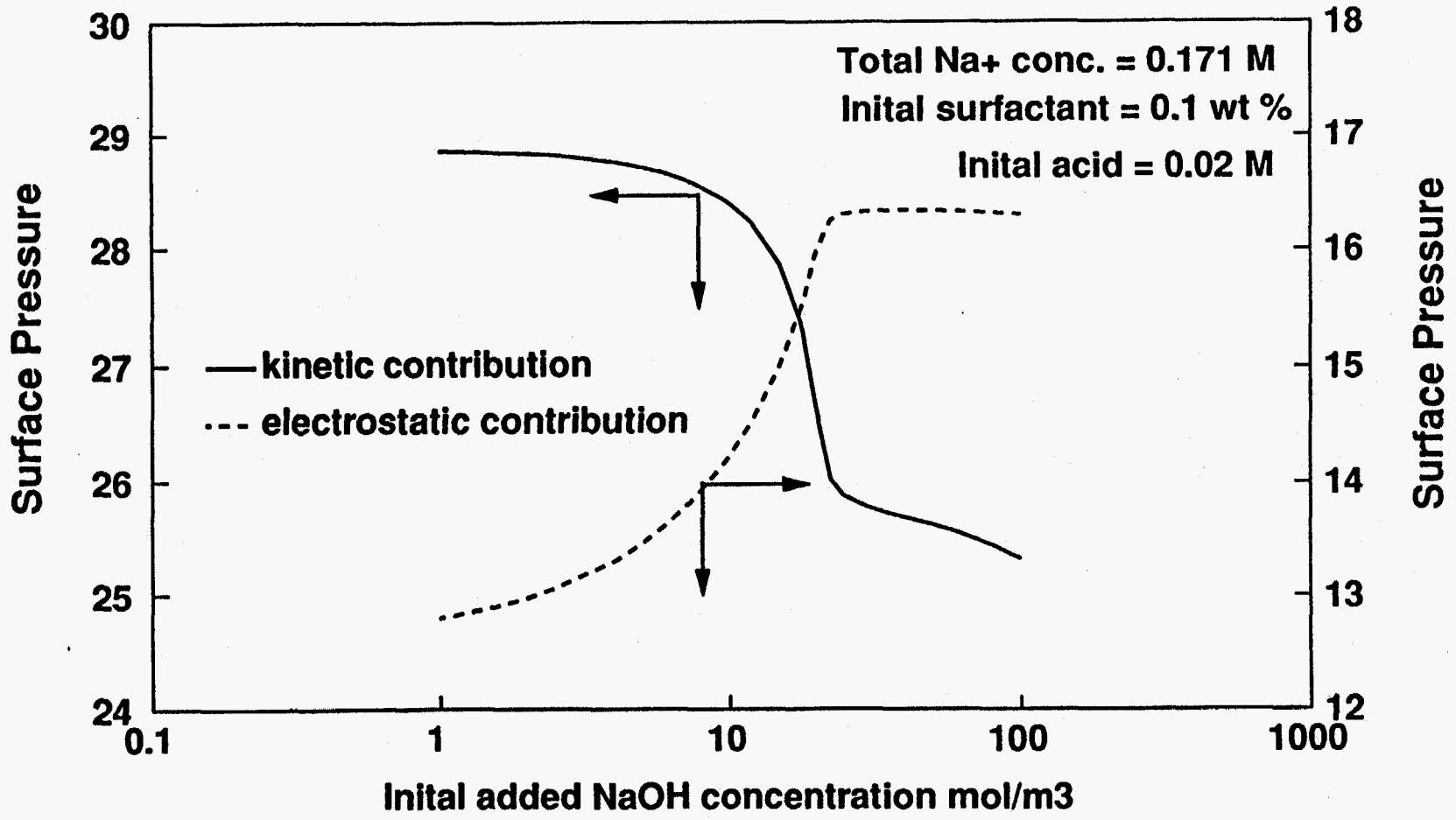

Figure 2-13. IFT Minima - Predicted Cause

increase in initial pH. The kinetic contribution decreases because the total adsorption at the interface decreases even though the adsorption of soap increases. This is due to a larger drop in the acid and surfactant adsorption and is shown in Figure 2-14. The electrostatic contribution increases because the interfacial potential increases with initial pH of the aqueous phase. Figure 2-15 shows the predicted variation of the interfacial potential over the initial alkali concentration of the aqueous phase. Interfacial potential increases because of ionization of the monolayer. Figure 2-16 shows the increase in the fractional ionization with initial alkali concentration of the aqueous phase. Another factor contributing to the increase in interfacial potential is the marginal drop in the free sodium ion contentration as shown in Figure 2-17. The free sodium ion concentration in the bulk drops because of an increase in the micellar phase hold-up which hold sodium ions in their double-layers. Figure 2-18 shows the increase in the micellar phase hold-up with increase in the initial pH of the aqueous phase.

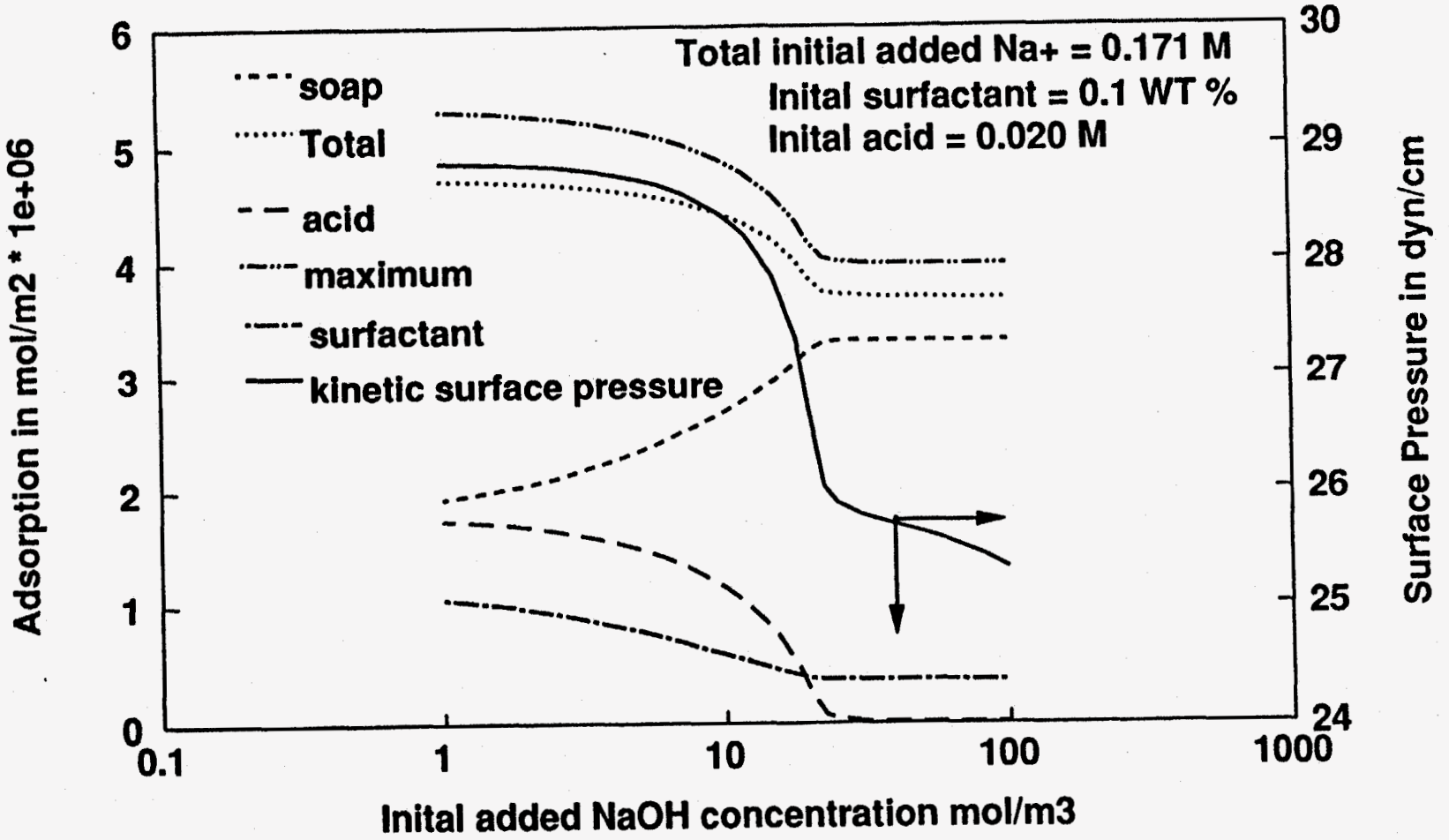

Figure 2-14. Adsorption Variations - Effect on Surface Pressure

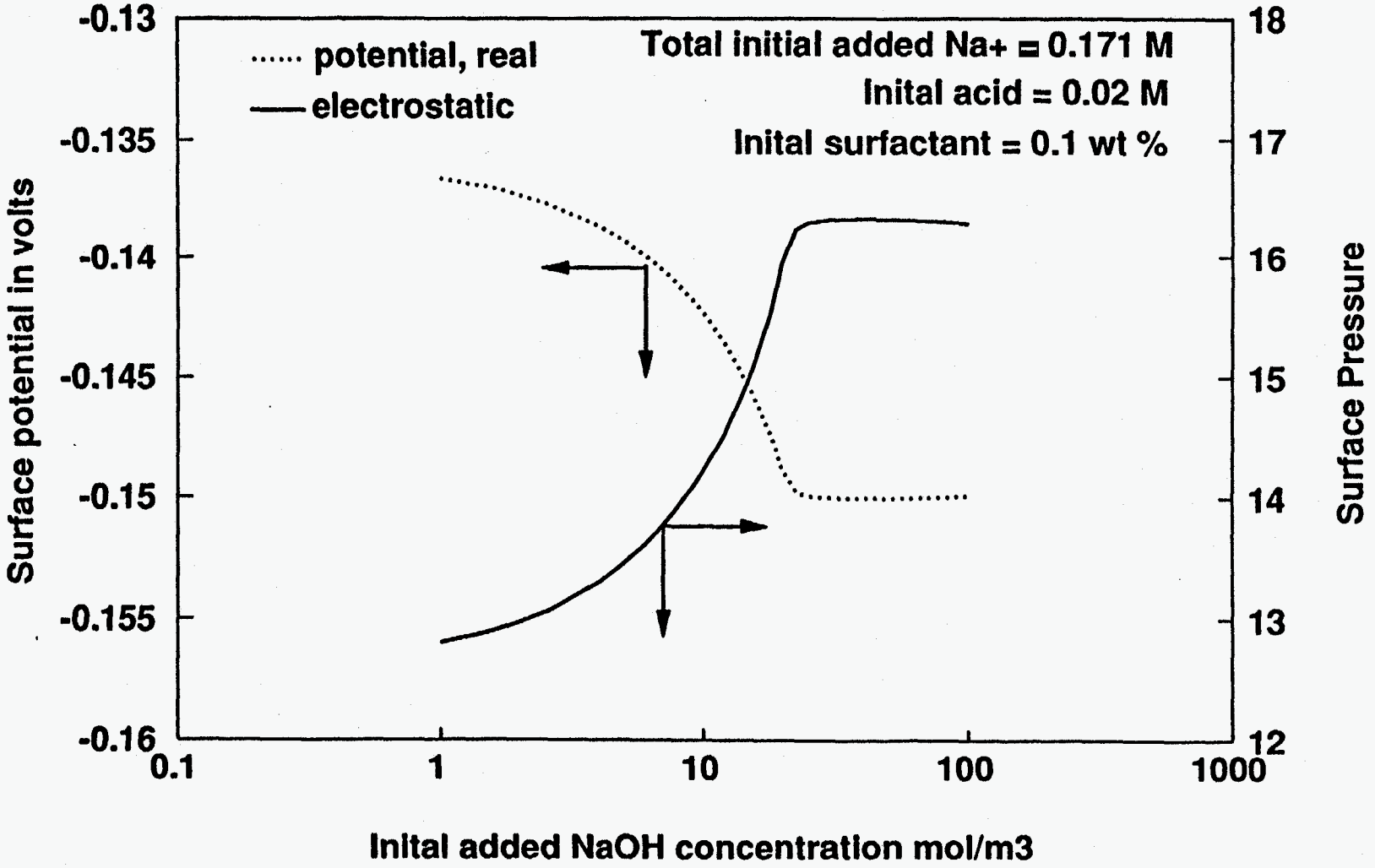

Figure 2-15. Potential Variation - Effect on Electrostatic Surface Pressure

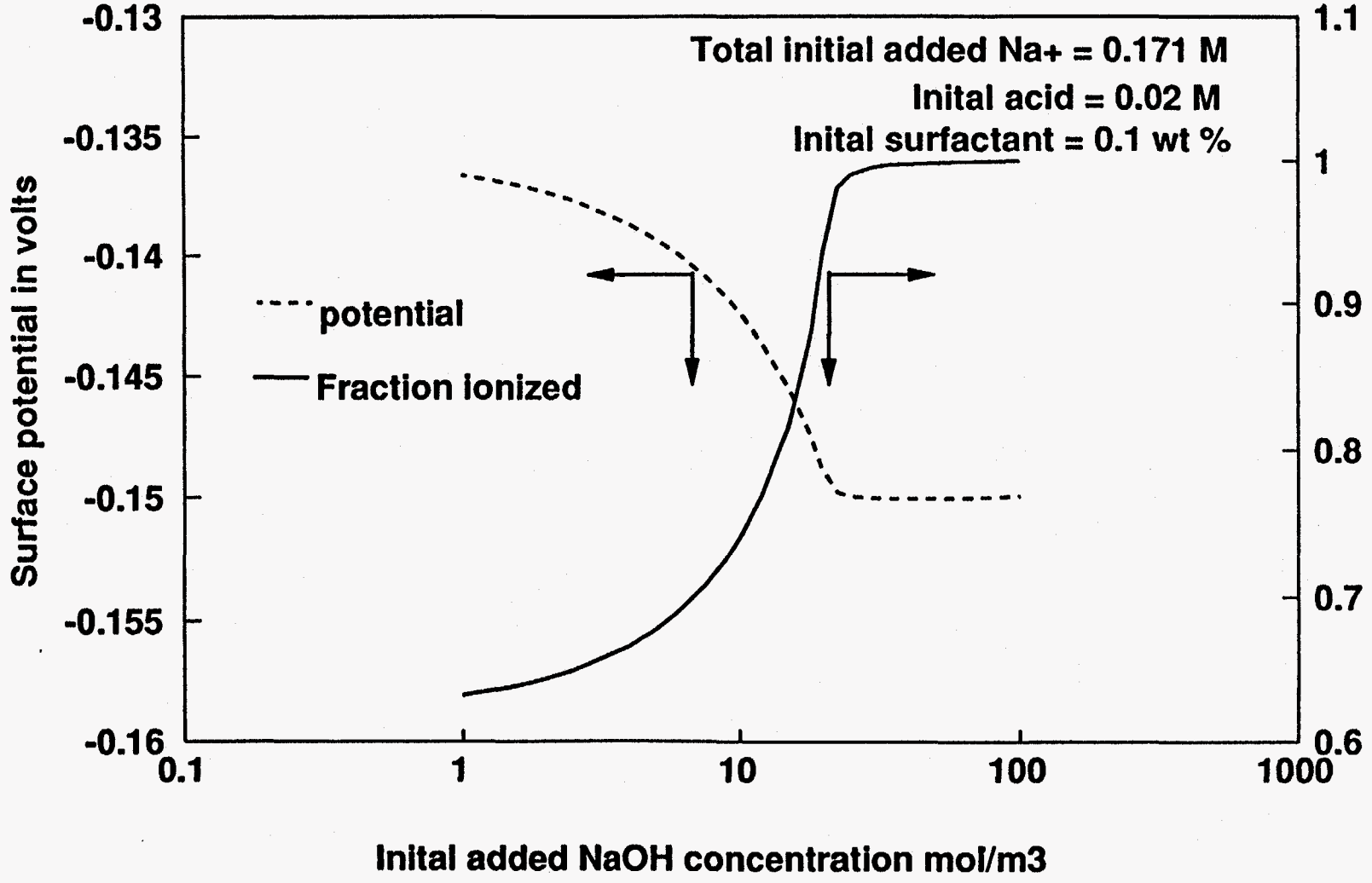

Figure 2-16. Potential Variation - Effect of Monolayer Ionization

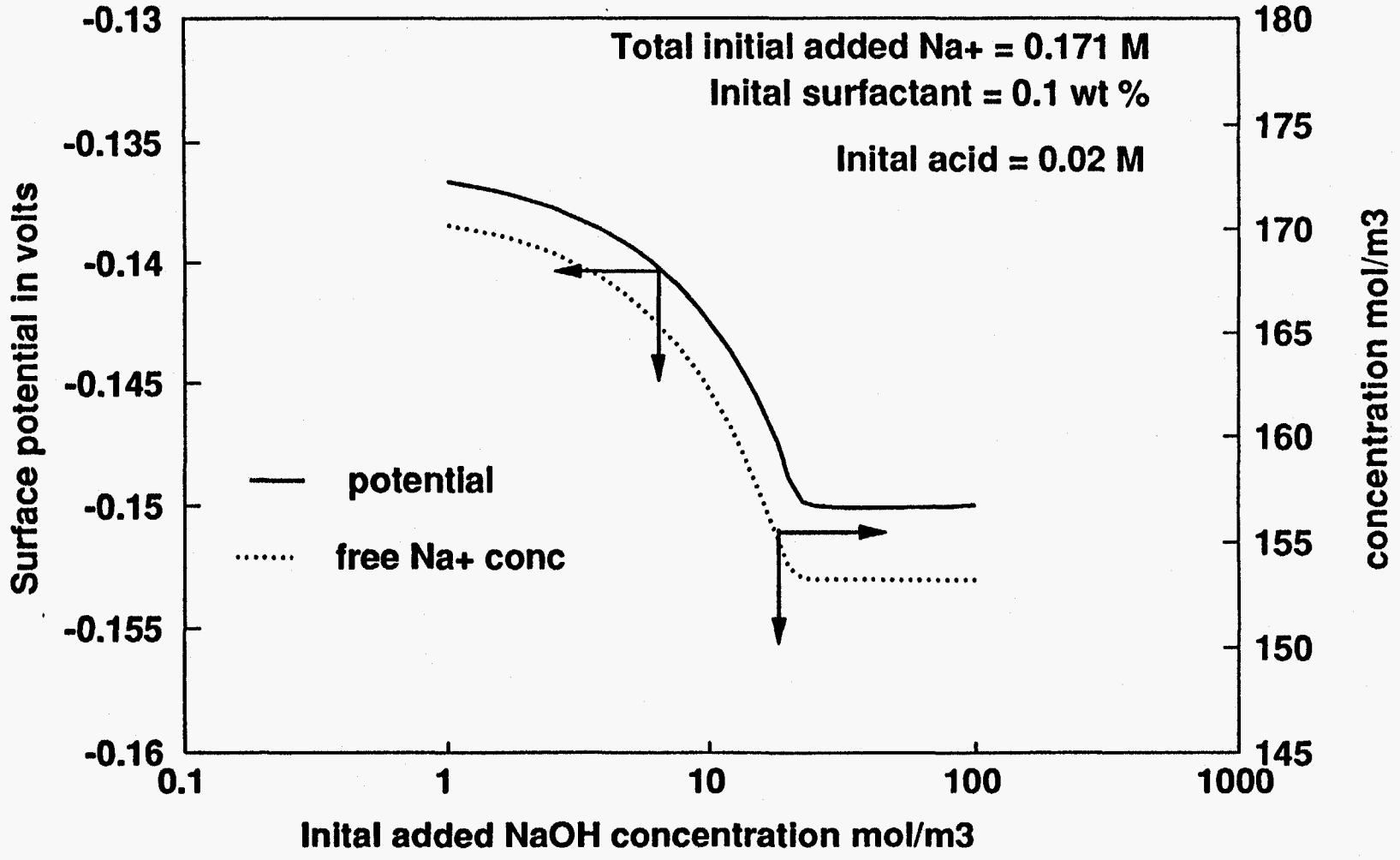

Figure 2-17. Potential Variation - Effect of Free Sodium Ion Concentration

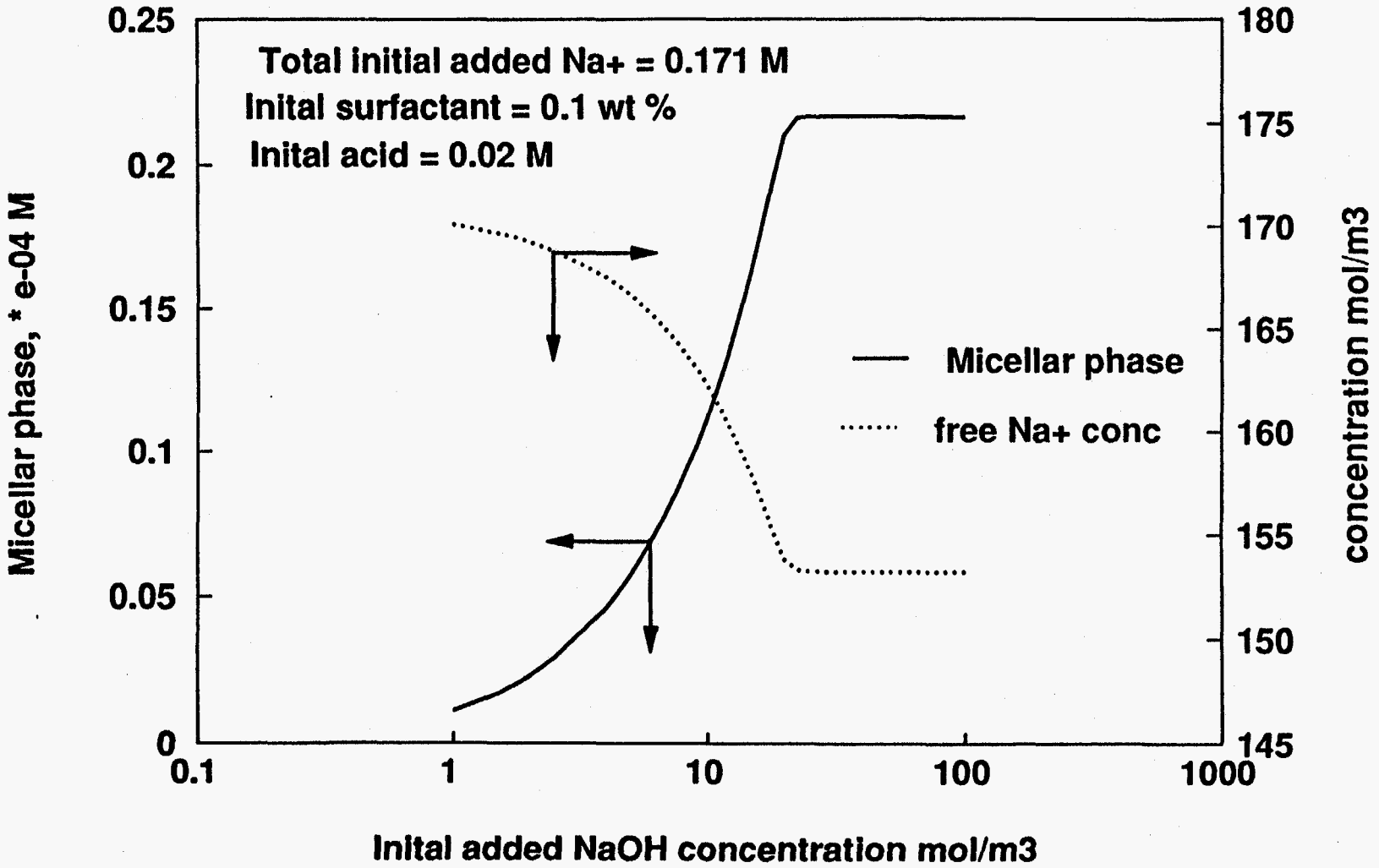

Figure 2-18. Variation in Sodium Ion Concentration - Effect of Micellar Phase Hold-up

References

1. Adamson, Physical Chemistry of Surfaces, 3rd ed, 1982.
2. Bromley L. A., Thermodynamic properties of strong electrolytes in Aqueous Solutions, *AICHE Journal*, **19**, 313 (1973).
3. Chan K. S., Shah D. O., "The molecular mechanism for achieving ultralow interfacial tension in petroleum sulphonate/oil/brine systems." *J. Dispersion Science Tech.*, **1**, 55 (1980).
4. Frumpkin A, *Zeitschr F Physik Chemie*, 466 (1925).
5. Davies J. T., Rideal E. G., Interfacial Phenomena, Academic Press, New York, (1963).
6. Granet R., Khadirian R. D., Piekarski S., Interfacial tension and surfactant distributon in water/oil/Nacl systems containing double tailed sulfonates, *Colloids & Surfaces*, 199-209 (1989).
7. Guggenhiem E A, Turgeon J. C., *Trans. Faraday Soc.*, **51**, 747 (1955).
8. Guggenhiem E A, Thermodynamics, 5th Ed., North Holland Publishing Co., 1967.
9. Hall D. G., Huddleston R. W., "A regular solution treatment of the micelle point in surfactant mixtures of different types.", *Colloids and Surfaces*, **13**, 209-219 (1985).
10. Holland P.M., "Non-ideal mixed monolayer model", ACS Symposium Series, 311, Ed. Scamehorn, 102-115 (1986).
11. Holland P. M., Rubingh D. N., "Nonideal multicomponent mixed micelle model", *J. Phys. Chem.*, **87**, 1984-1990 (1983).
12. Kamrath R.F., Frances E.I.,"Thermodynamics of mixed micellization. Pseudo-phase separation models.", *Ind. Eng. Chem. Fundam.*, **22**, 230-239 (1983).

13. Mukerjee P., Yang A. Y. S., *J. Physical Chem.*, **80**, 1388-1390 (1976).

14. Pitzer K. S., Activity coefficients in electrolyte solutions, *AICHE J.*, **19**, 313 (1973).

15. Ramakrishna T. S., PhD Thesis, Illinois Inst. of Tech., (1985).

16. Rosen M. J., "Surfactants and Interfacial Phenomena", 2nd ed, Wiley, 1988.

17. Rosen M. J., Hua X. Y., *J. Colloid Interface Sci.*, **86**, 164 (1982).

18. Rudin J., Wasan D.T., "Mechanisms for lowering of IFT in alkali/acidic oil systems,2. Theoretical studies.", *Colloids and Surfaces*, **68**, 81-94 (1992).

19. Stainsby G., Alexander A. E., *Trans. of Faraday Soc.*, **46**, 587-597 (1950).

20. Zhao G. X., Chen Y. Z., Ou J. G., Tien B. X., Huang Z. M., Hua Hsueh Pao (*Acta Chimica Sinica*) **38**, 409 (1980).

CHAPTER 3

Effect of Demulsifier on Interfacial and Film Rheological Properties and Stability of Water-in-Crude Oil Emulsions

INTRODUCTION

The emulsification of produced crude oil and brine/water is a common problem in the oilfield industry that is most frequently resolved through the use of chemical demulsifier additives. While this practice is an old and established one which has seen a steady progression of improvements in demulsifier structure and performance, there remains surprisingly little scientific data regarding the details of exactly how demulsifiers work in crude oil emulsions.

As dispersed droplets gravity settle and flocculate in a crude oil emulsion, a bi-liquid foam structure eventually forms (Shetty et al., 1992), with thin films of oil separating the polyhydric cells of water. The formation and eventual rupture of these structures is governed by hydrodynamic forces between the water drops which depends on such factors as drop size and polydispersity, the presence of asphaltene-resin particles and their suspension rheology, and the rheology of the oil-water interface. A complete analysis of the factors governing the hydrodynamic film stability is available (Edwards et al., 1991). It has been observed (Zapryanov et al, 1983; Ivanov, 1980), however, that demulsifiers speed the rate of film thinning and shorten the time it takes for the film rupture, although exactly why this is the case remain unclear. Demulsifiers have been observed to reduce the interfacial viscosity (Berger et al., 1987), although the ability to do so does not always correlate with performance data.

The following study in this chapter attempts to examine the relationship between demulsifier performance, interfacial rheology and dynamic interfacial tension and activity, in

crude oil systems with commercial demulsifiers that are used to treat such emulsions. The film experimental technique is useful in understading the mechanisms which are important to understanding demulsification.

EXPERIMENT

Materials. Demulsifiers used were of the polypropylene oxide type and were obtained from Baker Performance Chemicals, Inc. (BPCI). Molecular weight information for each demulsifier is listed in Table 3-1.

Table 3-1 Demulsifier Molecular Weight

Demulsifier	M_w	M_n
RE-2306	40,067	3,985
RE-2307	56,767	7,143
RE-2308	3,900	3,230
RE-2309	79,547	6,227

Selection of these demulsifiers for study was based on the fact that all were observed in field testing to exhibit some demulsifying activity, to varying degrees, on the subject crude oil emulsion described below.

The oil referred to in all experiments was a heavy black crude oil (API gravity ~21) obtained from Mississippi by BPCI. Extractions with pentane revealed an asphaltene content of 30.5% weight and a resin content of 35.0%. The original sample of oil was emulsified

with 30% by volume of a brine phase found to contain 33,800 ppm sodium chloride. Average drop diameter was 1 μm with ~20% polydispersity. The emulsion was dehydrated by ultra-centrifugation, which also removed a small quantity of finely dispersed solids.

All experiments were performed at 70 °C.

Demulsifier Performance Testing. Water-in-oil emulsions were prepared by manually shaking the centrifuged crude oil with 30% volume of the centrifuged brine phase for several minutes. The emulsion formed readily and was observed with a microscope to possess an average drop diameter of 1 μm, as for the original emulsion.

The demulsification performance test was conducted by placing 25 ml of emulsion into a capped 25 ml graduate cylinder, which was then placed into a water bath and heated to 70 °C. The demulsifier was added from a stock 40% solution in xylene, via microliter syringe, to obtain a concentration in the emulsion of 100 ppm. The cylinder was recapped, manually shaken for several minutes and placed back in the bath. The volume of water which separated from the emulsion was then monitored as a function of time.

Rheology Measurements of an Oil Film. The tensiometer used to measure the rheological properties of an oil emulsion film separating two aqueous brinephasesis described in Figure 3-5 in previous. The capillary possessed an inner radius of 0.32 mm with a wall thickness of 0.05 mm.

Prior to each use, the capillary was rinsed with ultra-pure toluene and heptane, then with ultra-pure water. After cleaning, the capillary was attached to the tensiometer and filled with aqueous brine phase. The capillary tip was then lowered into a cuvette containing a thin

layer of oil on top of additional brine phase. After thermal equilibrium and electrical steady state were reached, a very thin oil film was produced at the tip of the capillary by transfering the tip from the oil phase to the brine phase. This curved film was then expanded by depression of the plunger of the microliter syringe with the computer-controlled linear actuator. After the film reached a constant value, indicating attainment of equilibrium. At this point, two different experiments were performed: 1)dynamic film tension measurement and 2)film stress-relaxation measurement.

1)dynamic film tension measurement. Dynamic film tension measurements were carried out by forming an oil film, as described above, with 100 ppm of demulsifier in the oil phase. After equilibration, the film was expanded at a rate of 2.7×10^{-2} mm^2/sec, which corresponds to the rate of film thinning predicted by the Reynolds equation.

The capillary pressure was recorded as the film was expanded and the film tension calculated from the Laplace equation:

$$P_c = \frac{2\gamma}{R_f} \tag{3-1}$$

where P_c is the capillary pressure, γ is dynamic film tension and R_f is the radius of the film curvature.

The dynamic film elasticity (E) or dilational modulus was calculated from the slope of a plot of the dynamic film tension vs. the normalized film area expansion rate (A/A_o),

$$E = \frac{\partial \gamma}{\partial \ln(A/A_o)} \tag{3-2}$$

where E is the dynamic film elasticity (film modulus), γ is the dynamic film tension, A is

the expanded film area and A_0 is the initial film area at zero time.

2) film stress-relaxation measurement. Film stress-relaxation measurements were carried out by forming an oil film, as described above, with 100 ppm of demulsifier in the oil phase. After equilibration, the film was rapidly expanded and then stopped, whereupon the film capillary pressure was recorded as a function of time and converted to dynamic film tension using Equation 3-1.

Drop-Volume Measurement of Interfacial Tension. Dynamic and static (equilibrium) interfacial tension were measured by the drop-volume method using the apparatus depicted in Figure 3-1. This instrument consists of a tank containing the oil phase, a stainless steel capillary with an outer diameter of 1.6 mm, a syringe pump to control the frequency of water drop formation, and a pressure sensor to measure the frequency of water drop formation observed fluctuations in capillary pressure as the droplets detach. The time interval between droplets (dropping time, t_d) was determined by averaging at least five measured intervals.

Temperature was controlled with circulated water from a constant temperature bath. The tip of the capillary was well polished to ensure good wettability and well-defined contact line with the droplet and external oil phase. The helical nature of the capillary ensures that the liquid inside the capillary will be thermally equilibrated prior to emerging at the tip as a droplet.

Measurements were performed as a function of demulsifier concentration and drop frequency. For each measurement, the oil and aqueous phases were pre-equilibrated. Resultant dropping time, t_d, and drop formation frequencies were used to calculated the dynamic interfacial tension using Equations 3-3 and 3-4, as according to Hunsel et al. (1986),

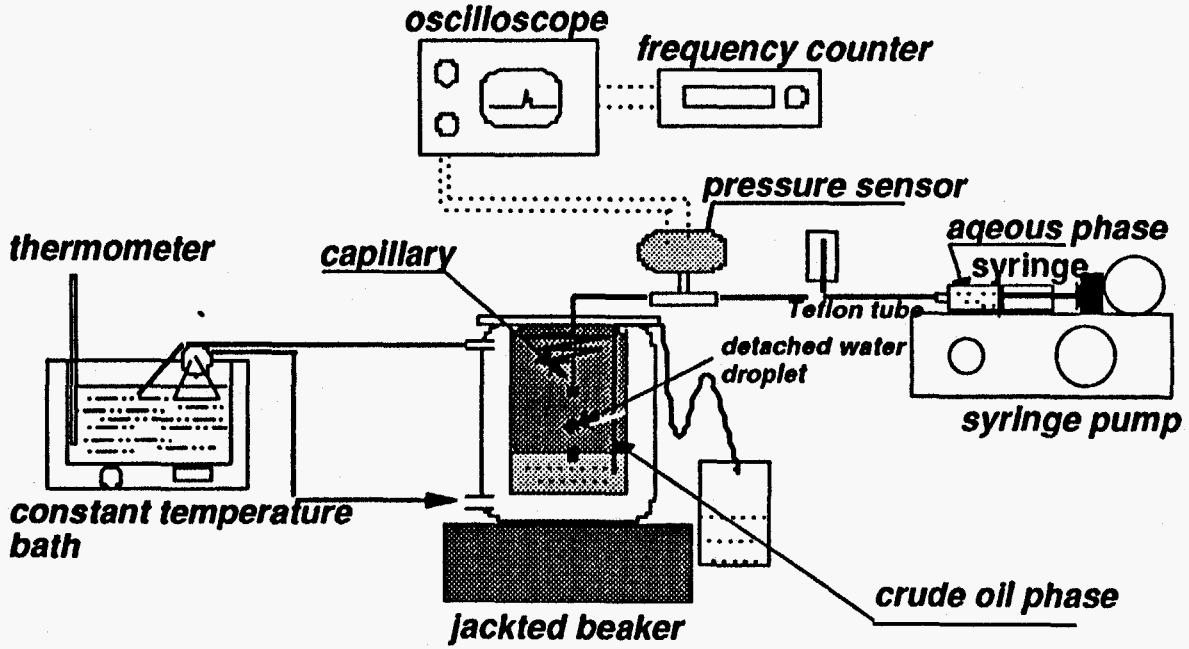

Figure 3-1. **Apparatus for the measurement of dynamic interfacial tension (drop volume method).**

for dynamic conditions,

$$\sigma = \frac{\Delta\rho g V_o}{r} F(V_o/r^3) \qquad (3\text{-}3)$$

$$V_o = \frac{V(t_d) - a t_d^{-3/4}}{1 + b t_d^{-3/4}} \qquad (3\text{-}4)$$

where V_o is the drop volume at infinite dropping time, $V(t_d)$ is the drop volume at dropping time t_d, σ is the interfacial tension, $\Delta\rho$ is the difference in density between phases, g is the gravity constant, r is the radius of the capillary, a and b are constants, and $F(V_o/r^3)$ is a correction coefficient (Wilkinson, 1972). The constant a and b are coefficients which are characteristic of the capillary, and were determined from measurements, in the experimental region of drop frequency, of the interfacial tension of several pure solvent systems, including water/air, toluene/water and hexane/water.

Static interfacial tension was measured by establishing a very low drop frequency (0.01 ~ 0.02 sec^{-1}). The drop volume did not change with further decreases in drop frequency at this point, even in the presence of demulsifier, establishing that an equilibrium condition with the demulsifier existed. The drop volume in this frequency range was used as V_0 to calculate the static interfacial tension from Equation 3-3.

Static or dynamic interfacial activity is defined in Equation 3-5, which represents the slope of a plot of static or dynamic interfacial tension as a function of demulsifier concentration,

$$alph = -\left(\frac{\partial\sigma}{\partial \ln C}\right) \qquad (3\text{-}5)$$

where α is the static or dynamic activity, σ is the static or dynamic interfacial tension, and

C is the bulk concentration of demulsifier.

Adsorption Kinetics Measurements. Dynamic interfacial data obtained from Equations 3-3 and 3-4 as a function of dropping time could be used to study the kinetics of demulsifier adsorption. Since the drop expands continuously during the adsorption process, the dropping time, t_d, must be converted to real adsorption time, as according to Equation 3-6 (Hunsel et al.,1986):

$$t = \left(\frac{3}{7}\right) t_d \tag{3-6}$$

For diffusion-controlled adsorption, a long-time approximation (Rillaerts and Joos, 1982) can be applied, as described by Equation 3-7:

$$\sigma_d = \sigma_e + \frac{RT\Gamma^2}{C}\left(\frac{\pi}{4Dt}\right)^{1/2} \tag{3-7}$$

where Γ is the interfacial concentration, C is the bulk phase demulsifier concentration, σ_e is the equilibrium or static interfacial tension, σ_d is the dynamic interfacial tension, D is the diffusion coefficient, and t is the age of the interface (adsorption time) given by Equation 3-6. Equation 3-7 illustrates that if adsorption is diffusion-controlled, a linear plot σ_d vs. $t^{-1/2}$ should be obtainable. In Equation 3-7, Γ was obtained from the slope of a plot of the static interfacial tension as a function of *ln (C)*, as described by Equation 3-8:

$$\Gamma = -\left(\frac{1}{RT}\right)\frac{d\sigma}{d\ln C} \tag{3-8}$$

RESULTS AND DISCUSSION

Demulsification Performance. Figure 3-2 is a plot of volume percent water separated as a function of time for four demulsifiers and a blank. The speed of separation decreased in the order, RE-2306 > RE-2307 > RE-2309 > RE-2308 > blank. Effectively no separation was observed in the blank sample. Droplet size distribution was observed with a microscope, using a microscopic technique to increase in a manner proportional to the bulk water drop.

Film Rheology. Dynamic film tension measurements for several demulsifiers are presented in Figure 3-3. The slope of the curve in this figure is the dilational modulus or dynamic film elasticity, as defined Equation 3-2. For the demulsifier RE-2306, the film dilational modulus is 14.4 dyn/cm, lowest for the four demulsifiers tested. A good correlation exists between the film dilational modulus and the demulsifier performance depicted in Figure 3-2. Thus the efficiency of a demulsifier seems to be inversely related to the resultant elasticity of the interface.

Experimental results for the film stress-relaxation experiments are presented in Figure 3-4 as a plots of film tension vs. time. The curves exhibit a region of relatively fast relaxation (<0.2 min), followed by a much slower period of relaxation. The steepness of the early, fast section of these curves correlates with the performance data in Figure 3-2. Approximate slopes for these early regions are listed in Table 3-2, along with performance and film dilational modulus data.

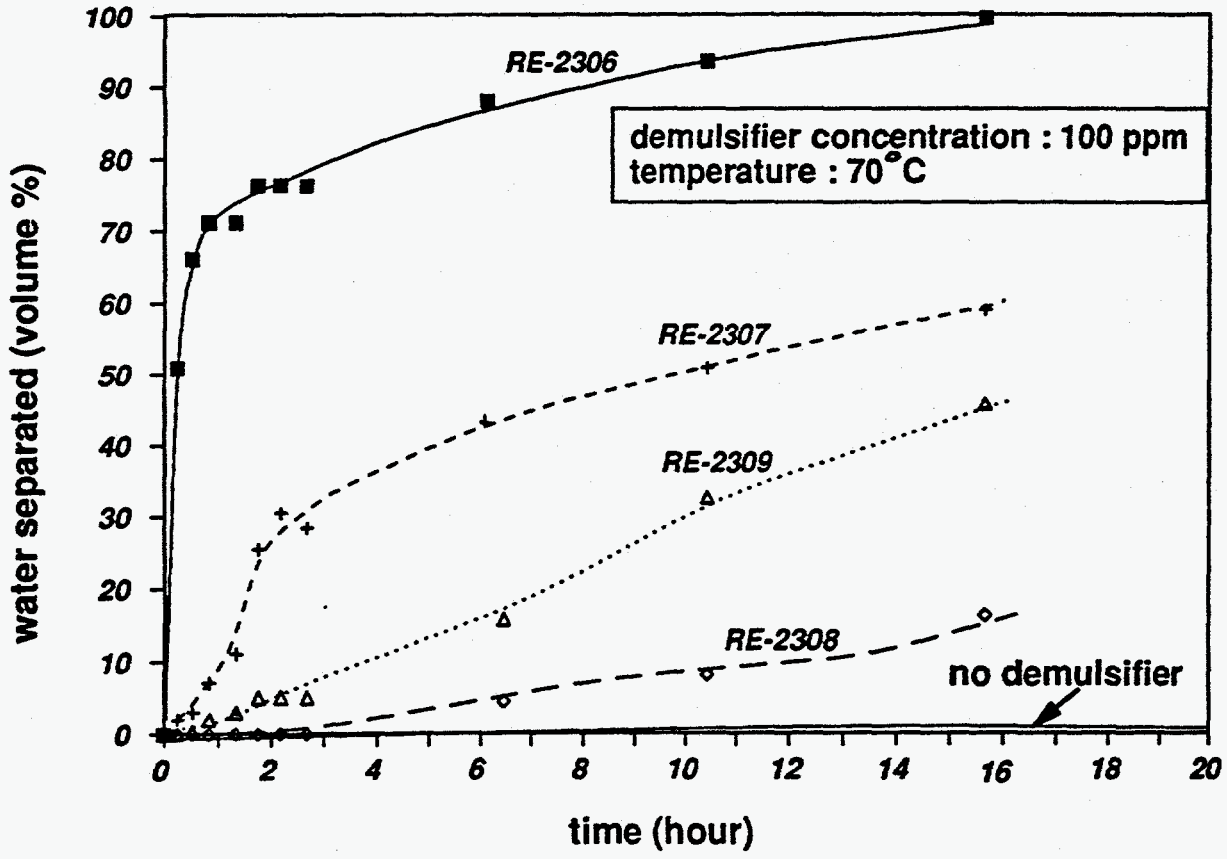

Figure 3-2. **Demulsifier performances: water separation**

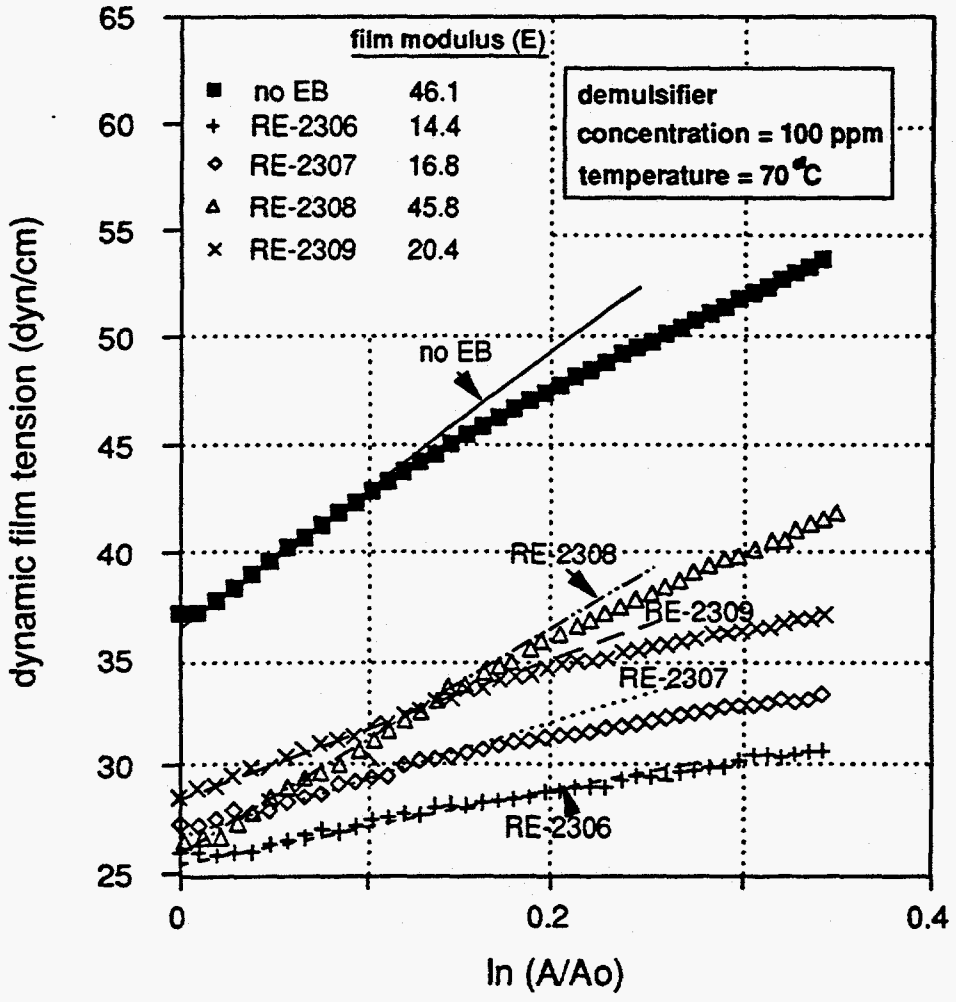

Figure 3-3. **Film tension as a function of film area at 100 ppm demulsifier, 70 °C. The initial slope represents film modulus at 2.7 x 10^{-2} mm^2/sec film expansion rate.**

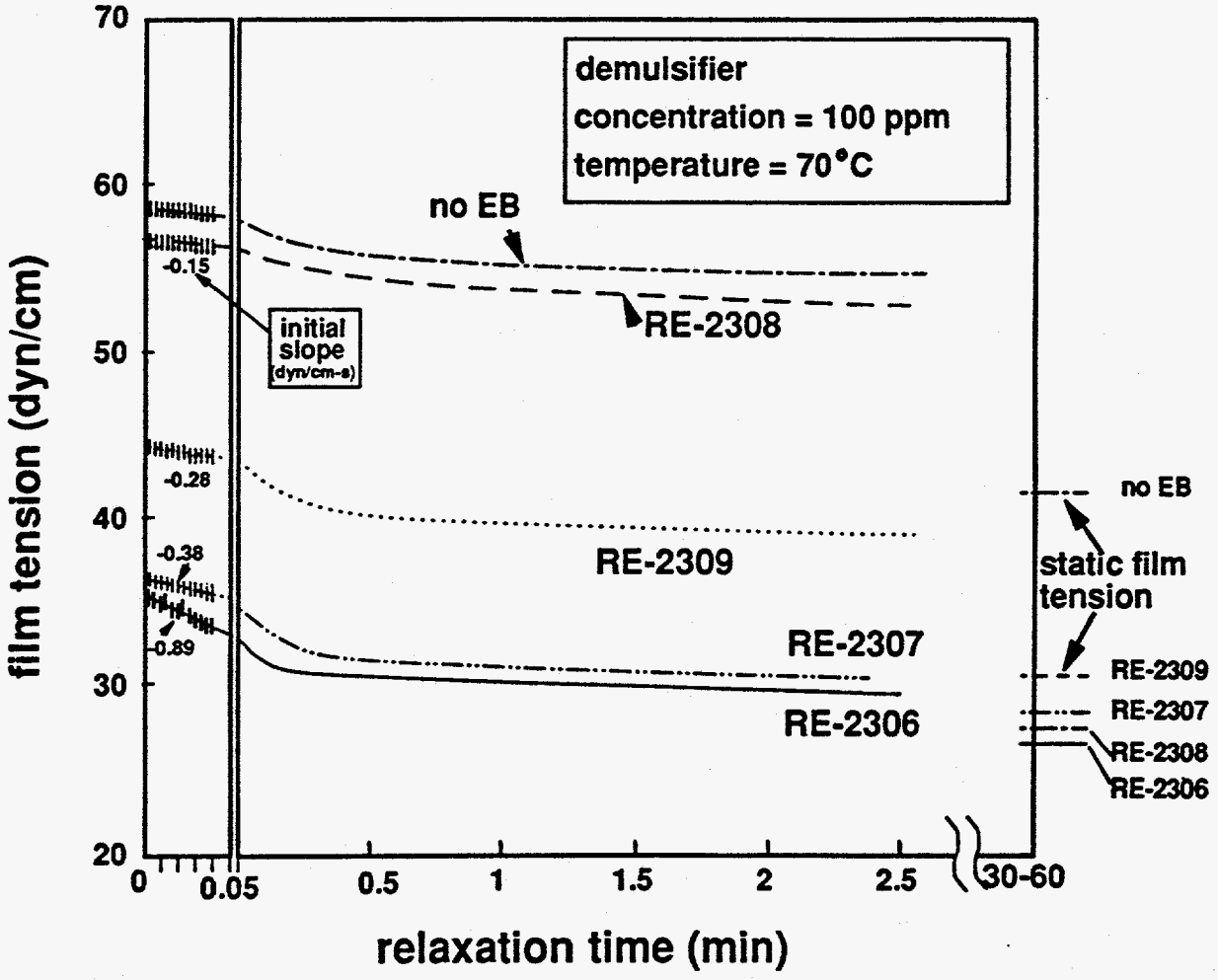

Figure 3-4. **Film relaxation: Film tension as a function of relaxation time at 100 ppm demulsifier concentration, 70°C.**

Table 3-2 Data Summary for Demulsifier Performance, Film Modulus and Initial Slope in Film Stress-Relaxation

Demulsifier	Efficiency* (%)	Film Modulus dyn/cm	Initial Slope** dyn/cm-sec
RE-2306	86	14.4	0.89
RE-2307	42	16.8	0.38
RE-2308	4	45.8	0.15
RE-2309	15	20.4	0.28

* Water separation as volume percent after six hours.
** Initial slope from Figure 3-4.

The data in Table 3-2 clearly illustrates the need for a demulsifier to exhibit fast relaxation kinetics in order to achieve rapid coalescence. This corresponds to a low elasticity of the interface, which should be related to the diffusivity and dynamic interfacial activity of the demulsifier. Fast diffusivity and high dynamic interfacial activity should be especially important for the case of a thinning oil layer between coalescing droplets where demulsifier transport from the bulk will be opposed by the outward drainage (Krawczyk et al., 1991).

Film tensions after 30~60 minutes are treated as static film tensions and are also presented for each demulsifier tested in Figure 3-4. Unlike the dynamic film tension data, a correlation with performance is not apparent. It is interesting to note that, for example, RE-2308 exhibits a relatively low static film tension, yet the dynamic film tension is relatively high, with poor performance being the observed case. The extremely slow relaxation kinetics evident for this demulsifier in Figure 3-4 are indicative of low diffusivity.

Drop Volume Measurements of Interfacial Tension. Low drop frequency (0.01~0.02 sec^{-1}) were used to obtain static interfacial tension as a function of concentration for each demulsifier, and are presented in Figure 3-5. The static interfacial activities, as defined in Equation 3-5, were obtained from the slopes of the interfacial tension vs. *ln C* curves in the 100 ppm region of Figure 3-5 and are presented in Table 3-3. As observed in the film experiments, no correlation is apparent between demulsifier performance and static interfacial tension or activity.

Dynamic interfacial tension as a function of drop frequency for each demulsifier at 50-500 ppm concentration is presented in Figures 3-6 to 3-9. The dynamic interfacial activities, as defined by Equation 3-5, were obtained from the slopes of these

Table 3-3. Static Interfacial Tension and Activity at 100 ppm Demulsifier, 70 °C

Demulsifier	Efficiency %	Static Tension dyn/cm	Static Activity dyn/cm	Dynamic Activity dyn/cm	Diffusivity,D cm^2/sec
RE-2306	86	13.1	1.6	1.6	5.2×10^{-5}
RE-2307	42	13.7	1.9	1.3	5.0×10^{-5}
RE-2308	4	13.4	0.8	0.8	3.2×10^{-9}
RE-2309	15	14.4	1.4	1.2	3.1×10^{-5}

plots in the region of 0.2 sec^{-1} was selected because this value is close to theoretical surface expansion rate calculated for the film thinning process of the emulsion. Table 3-3 illustrates the correlation between demulsifier performance and dynamic interfacial activity, which is consistent with the film rheology results.

As stated previously, a low interfacial activity could result from slow, diffusion-controlled adsorption, which prompted an investigation into the kinetics of demulsifier adsorption, detailed in the following section.

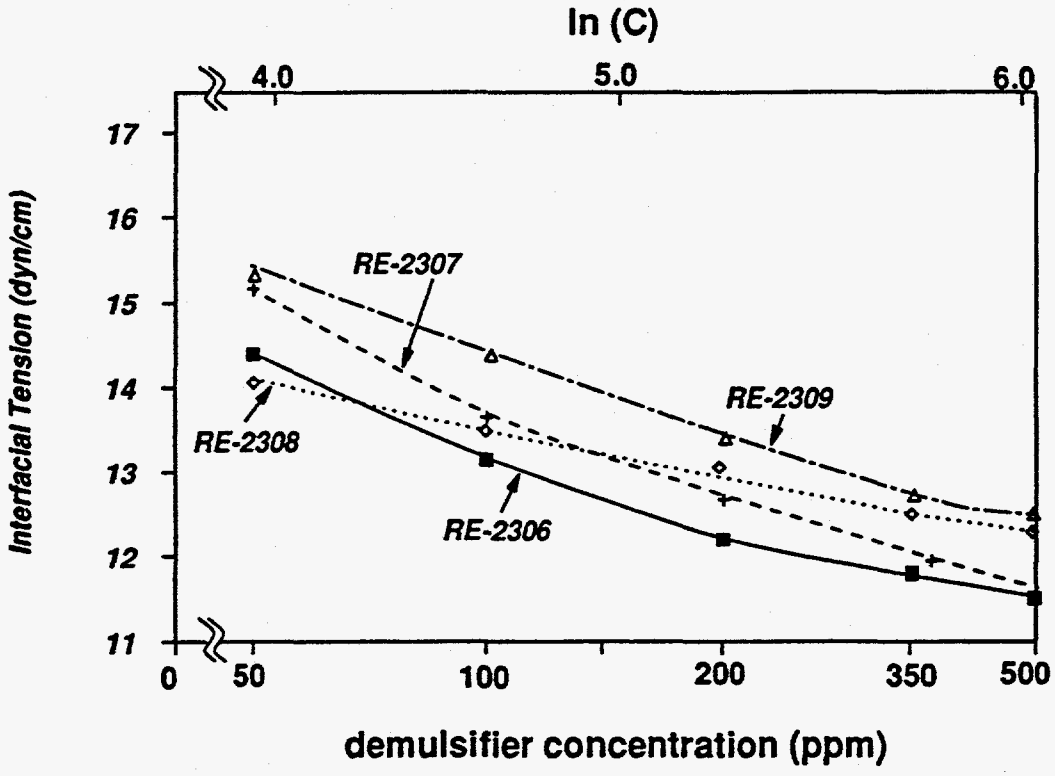

Figure 3-5. **Static (equlibrium) interfacial tension as a function of demulsifier concentration at 70 °C.**

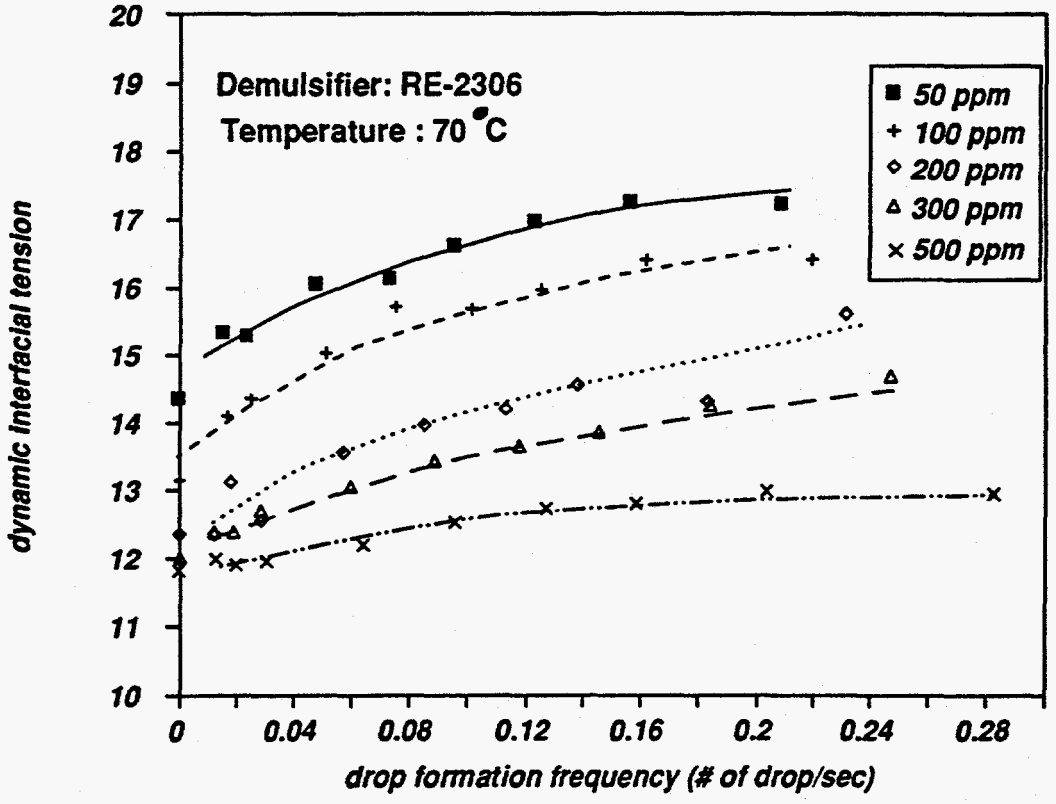

Figure 3-6. **Dynamic interfacial tension as a function of drop frequency for various concentrations of RE-2306.**

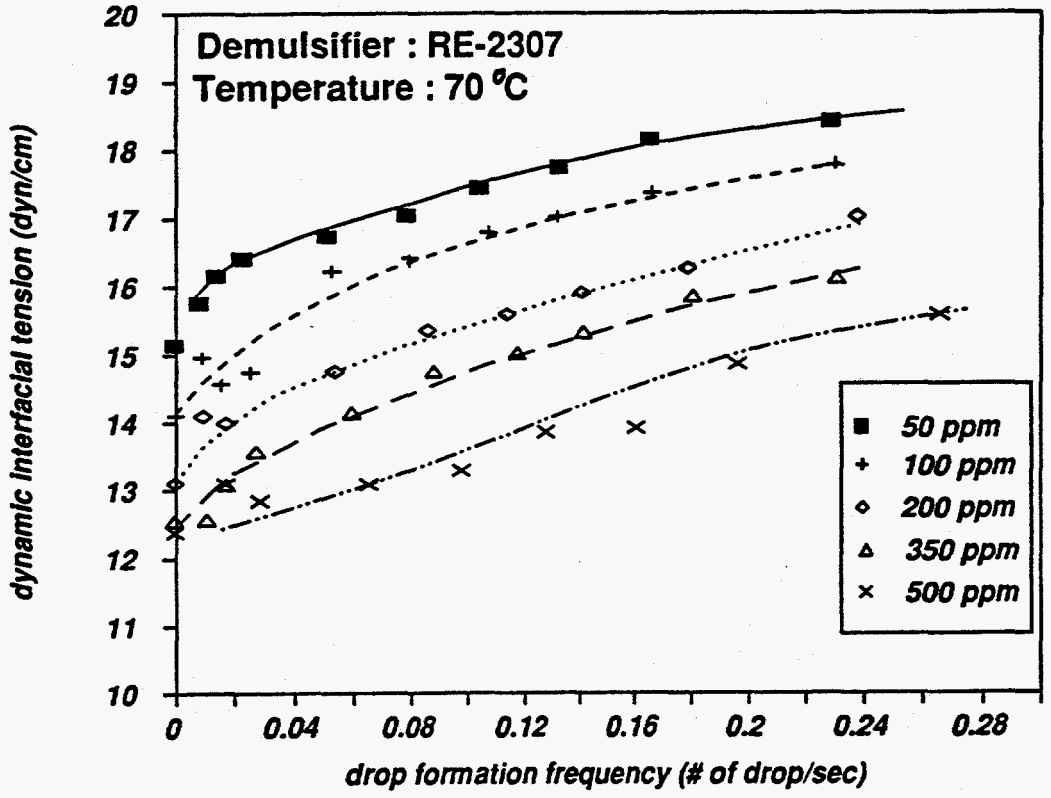

Figure 3-7. **Dynamic interfacial tension as a function of drop frequency for various concentrations of RE-2307.**

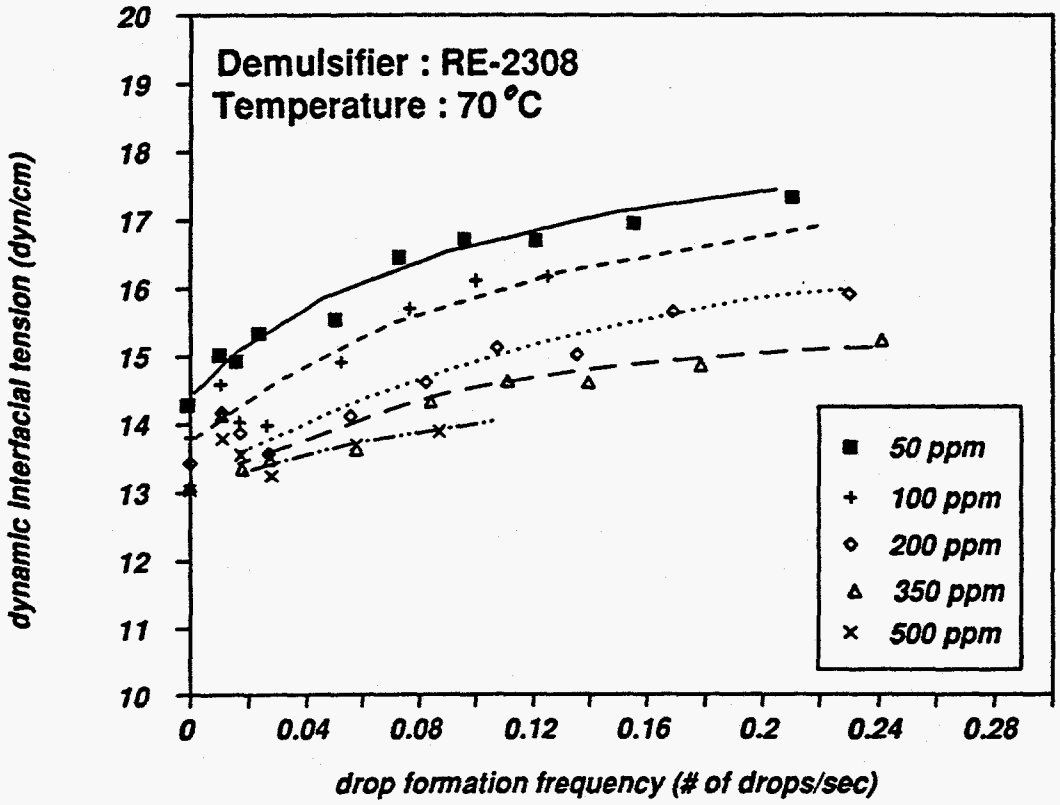

Figure 3-8. **Dynamic interfacial tension as a function of frequency for various concentrations of RE-2308.**

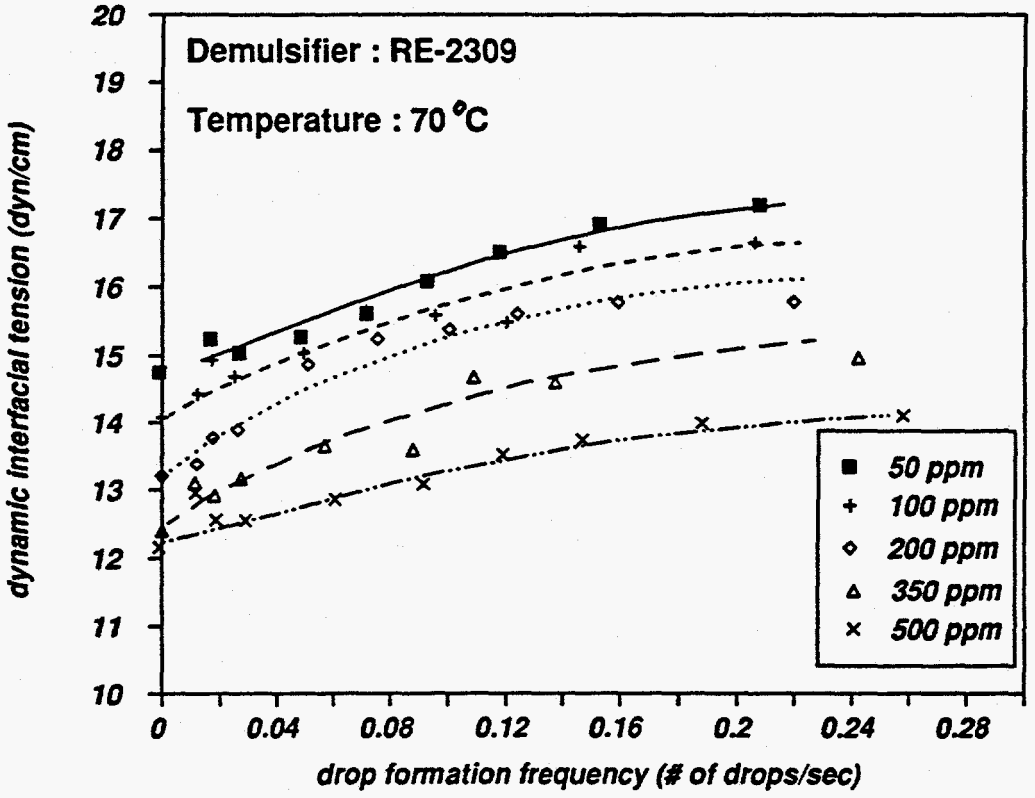

Figure 3-9. **Dynamic interfacial tension as a function of frequency for various concentrations of RE-2309.**

Kinetics of Demulsifier Adsorption. Plots of dynamic interfacial tension as a function of adsorption time (as calculated from Equation 3-6) are illustrated in Figures 3-10 to 3-13 for various concentrations of demulsifier. Figure 3-14 is a plot of the dynamic interfacial tension data, at 100 ppm of demulsifier, as a function of $t^{-1/2}$. The linear nature of these plots indicates that the demulsifier adsorption process is diffusion-controlled. Diffusion coefficients calculated from the slopes of these plots are listed in Table 3-3. The data in Table 3-3 collectively show the connection between low diffusivity, low dynamic interfacial activity and poor performance.

SUMMARY

Demulsifiers commonly used for crude oil demulsification are inevitably polymeric in nature, often tending toward high molecular weight (10,000 - 50,000). High molecular weight has often been seen to increase performance. High molecular weight, however, means low diffusivity, which, in the absence of other variables, should mean lower dynamic interfacial activity and poor performance. Obviously other variables must complicate this picture, especially in system as varied and complex as crude oil emulsions. The work presented in this chapter, however, is valuable in that it demonstrates the important role that rapidly diffusing, low molecular weight components of demulsifiers likely play in demulsification, *i.e.*, maintaining a low dynamic interfacial tension during film drainage. Indeed, low molecular weight (<10,000) components are present in virtually all "high molecular weight" demulsifiers commonly used in the oilfield

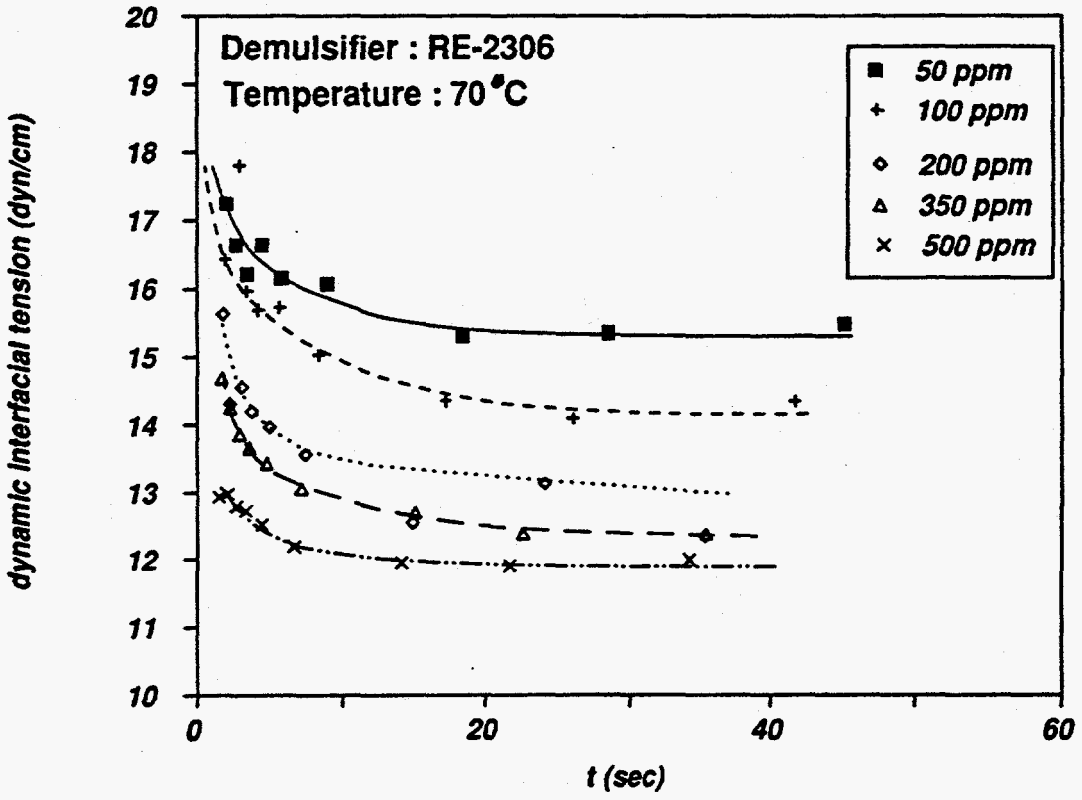

Figure 3-10. **Dynamic interfacial tension vs. diffusion time(t) in the presence of RE-2306 at 70 °C.**

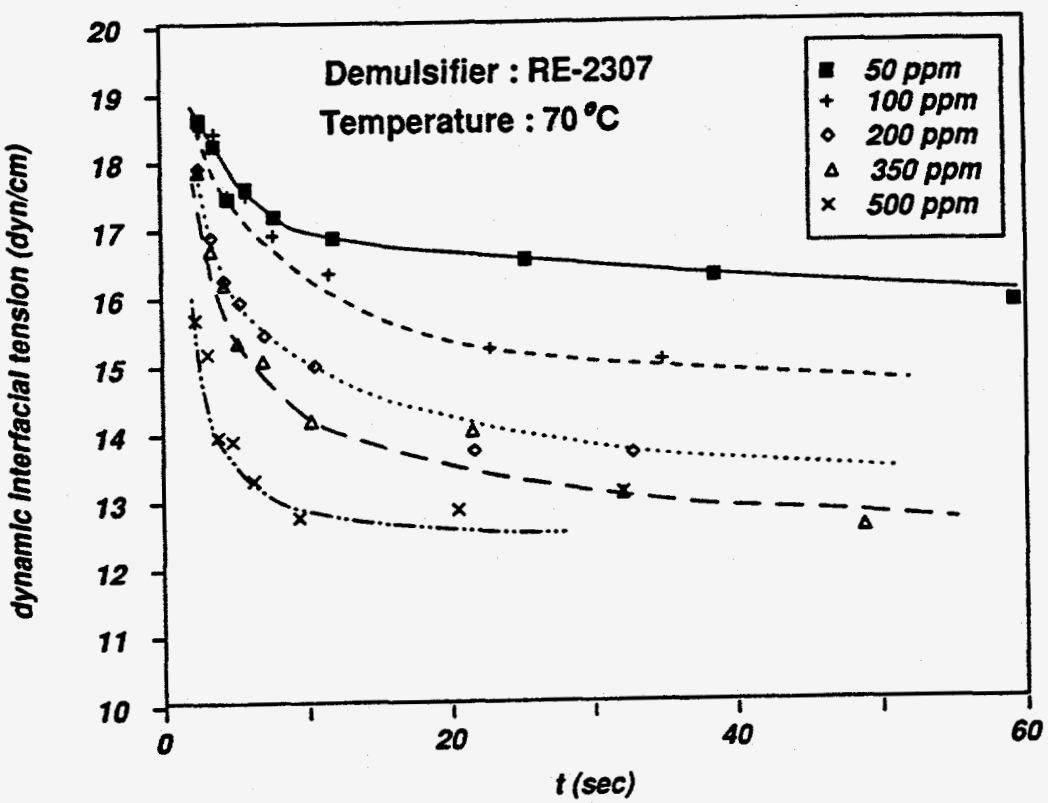

Figure 3-11. **Dynamic interfacial tension vs. diffusion time(t) in the presence of RE-2307 at 70 °C.**

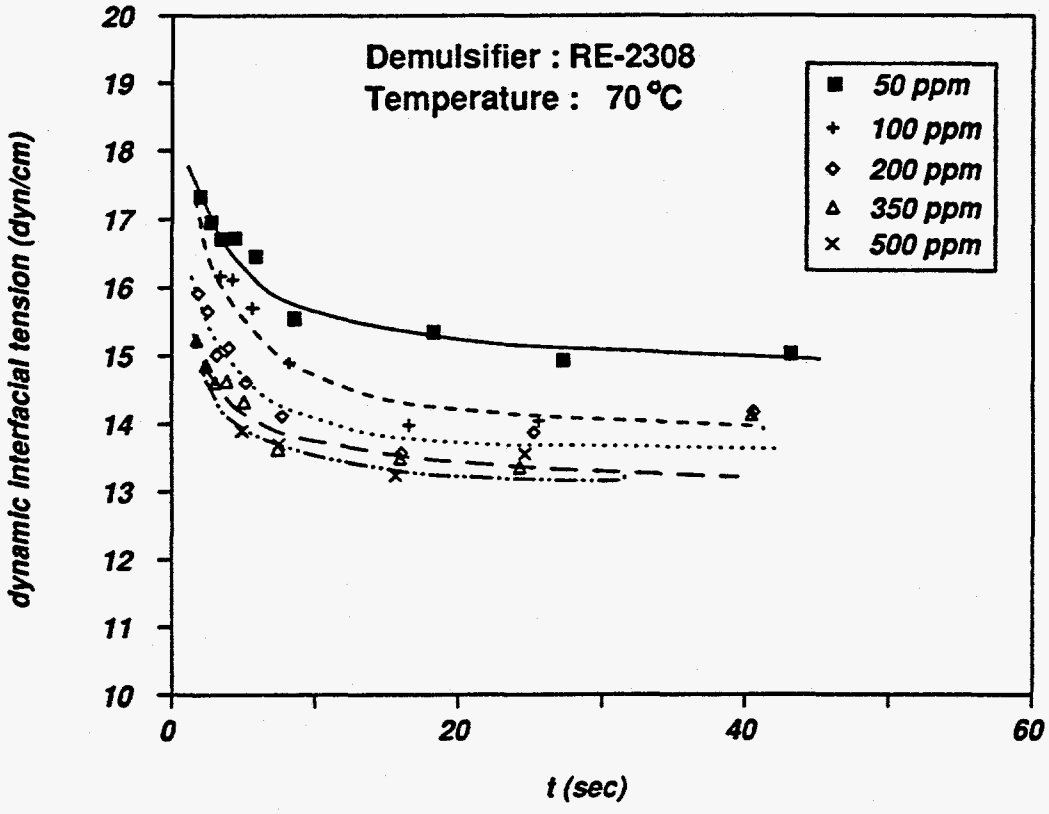

Figure 3-12. **Dynamic interfacial tension vs. diffusion time(t) in the presence of RE-2308 at 70 °C.**

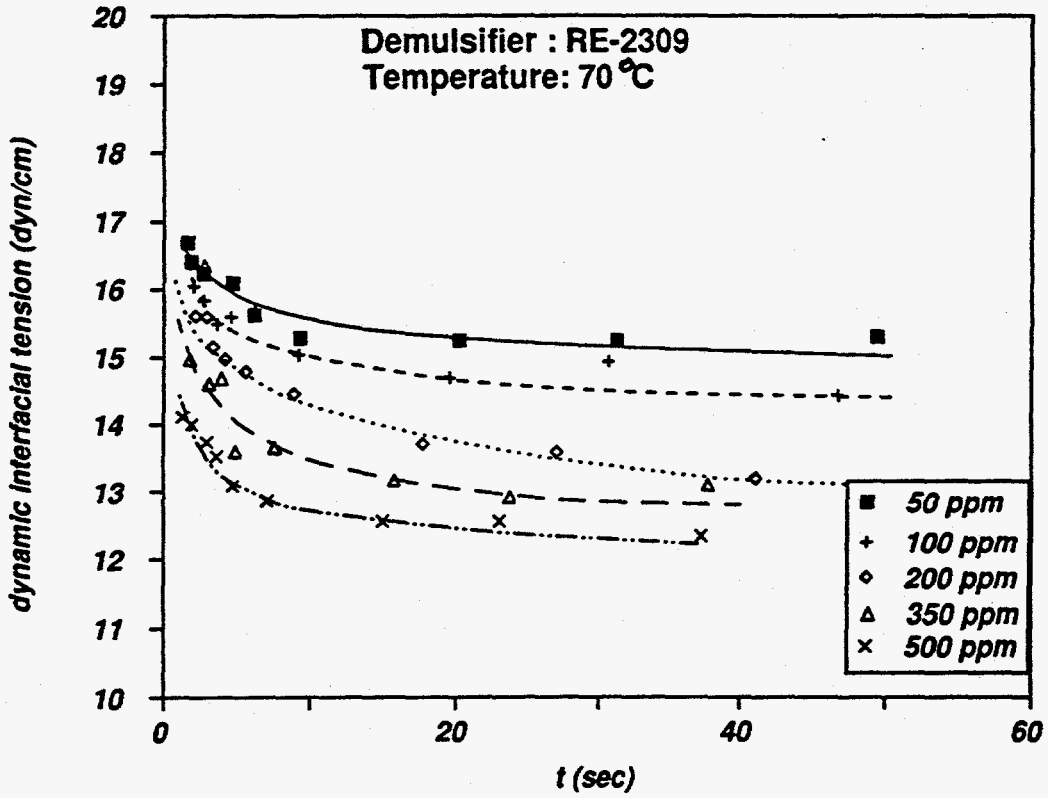

Figure 3-13. **Dynamic interfacial tension vs. diffusion time(t) in the presence of RE-2309 at 70 °C.**

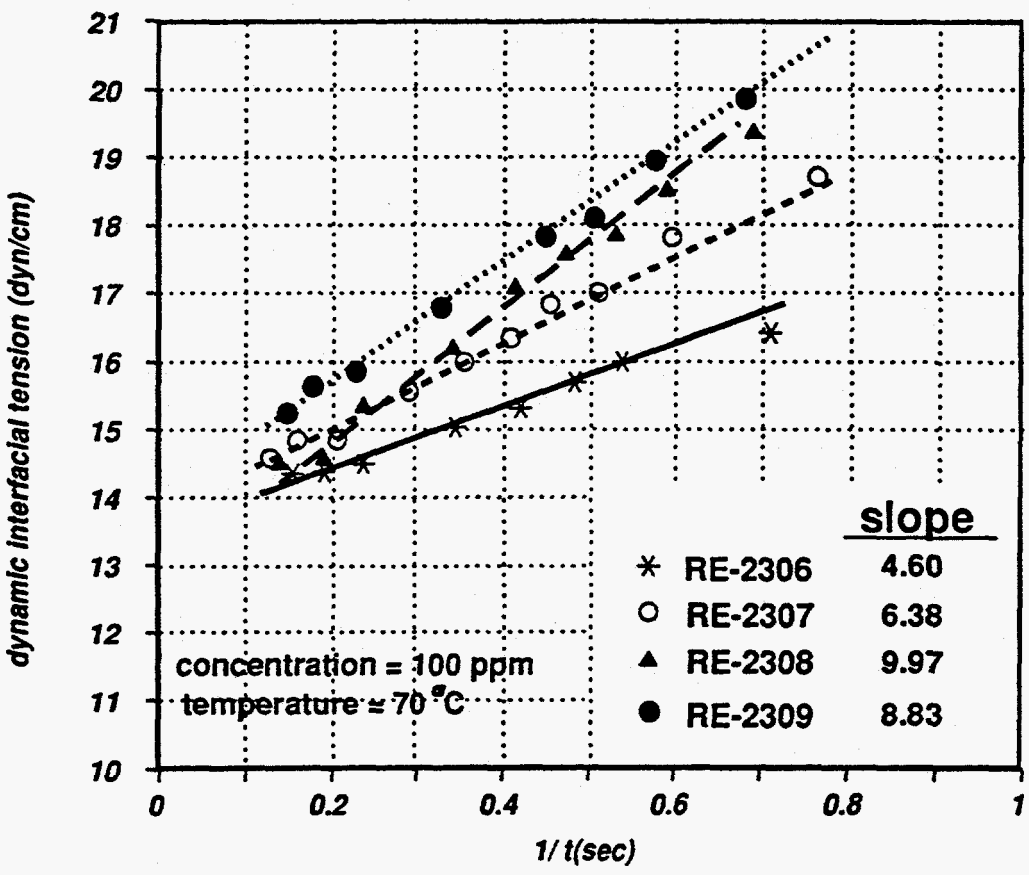

Figure 3-14. **Dynamic interfacial tension vs. 1/ t for 100 ppm demulsifier at 70 °C.**

The novel experimental technique demonstrated in this chapter, in particular those used in studying the rheology of crude oil films, are particularly useful in modeling events leading to coalescence in oilfield emulsions. Additional work is underway to better understand the role in demulsification of high molecular weight demulsifier fractions. Empirical observations from field testing indicate that such fractions often times are necessary to obtain good performance.

NOMENCLATURE

σ : interfacial tension

γ : film tension

R_f : radius of oil film curvature

P_c : capillary pressure

E : film dilational modulus or dynamic film elasticity

A, A_o: expanded film area and initial film area, respectively

t_d : dropping time of a drop

V, V_o: drop volume at any dropping time and at infinite dropping time, respectively

t : adsorption time

R : gas constant

Γ : interfacial concentration of demulsifier

C : bulk concentration of demulsifier

D : demulsifier diffusivity

M_w, M_n: demulsifier molecular weight

REFERENCES

1. Shetty, C.S., Nikolov, A.D., and Wasan, D.T., 1992, *J. Dispersion Sci. Tech.*, **13**, p.121.

2. Edwards, D.A., Brenner, H., and Wasan, D.T., 1991, *Interfacial Transport Process and Rheology*, Butterworth-Heinemann.

3. Zapryanov, Z., Malhotra, A.K., Aderangi, N., and Wasan, D.T., *Int. J. Multiphase Flow*, **9**, p.105 (1983).

4. Ivanov, I.B., *Pure & Appl. Chem.*, **52**, p.1241 (1980).

5. Berger, P.D., Hsu, C., and Arendell, J.P., *Society of Petroleum Engineers*, 457 (1987).

6. Hunsel, J.V., Bleys, G., and Joos, P., *J. Coll. Int. Sci.*, **114**, p.432 (1986).

7. Wilkinson, M.C., *J. Coll. Int. Sci.*, **40**, p.14 (1972).

8. Rillaerts, E. and Joos, P., *J. Phys. Chem.*, **86**, p.3471 (1982).

9 Charles, G.E. and Mason, S.G., *J. Coll. Sci.*, **15**, p.236 (1960).

10. Krawczyk, M.A., Wasan, D.T., and Shetty, C.S., "Chemical Demulsification Petroleum Emulsions using Oil-Soluble Demulsifiers", *Ind. and Eng. Chem. Research*, **30**, p.367 (1991).